

Matériaux pour la Géologie de la Suisse

GEOPHYSIQUE
Nr. 25

Publiés par la Commission Suisse de Géophysique
Organe de la Société Helvétique des Sciences Naturelles,
subventionnée par la Confédération

**AIRBORNE RADIOMETRIC
MAPPING IN SWITZERLAND**

GEORG F. SCHWARZ
EMILE E. KLINGELE
LADISLAUS RYBACH

En Commission
chez Kümmerly & Frey AG, Geographischer Verlag, Berne
1992

Address of authors:

Dr. Georg F. Schwarz

PD. Dr. Emile E. Klingelé

Prof. Dr. Ladislaus Rybach

Institut für Geophysik

ETH-Hönggerberg

CH-8093 Zürich

Preface

The radioactivity maps presented in this volume (No. 25) are the most recent contribution to the "Geophysical Survey of Switzerland". They are an important and valuable supplement to the series of the "Geophysical Maps of Switzerland" published by the Swiss Geophysical Commission. This series includes surveys of the magnetic and gravity fields, the seismicity and earthquake hazard, and the surface heat flow density in Switzerland.

Mainly because of financial limitations only selected regions of Switzerland could be covered by the originally planned airborne radiometric survey. The measurements carried out so far were primarily concentrating on the central part of the Swiss Alps where large areas of crystalline rocks with highly contrasting lithologies are exposed. In addition the main extra-Alpine geological units, i.e. the Jura Mountains, the Molasse Basin and the Quaternary have also been covered with smaller surveys.

The methodological aspects of the data acquisition, the data processing and the calibration procedure have already been treated extensively in the Publication No. 23, entitled "Methodische Entwicklungen zur Aerogammaspektrometrie" by G. Schwarz (1991).

The maps presented in this volume display only that part of the dose rate which is due to the distribution of natural radioactive sources in the Earth's crust. They can, however, serve as an important input information for the compilation of a dose rate map for all of Switzerland which eventually will include cosmic radiation and artificial radioactivity from fallout, such as the Chernobyl event, etc.

Thanks for financial support are due to the Swiss Federal Office of Education and Science, the Swiss National Science Foundation, The Swiss Academy of Science, The Swiss Federal Institute of Technology and in particular to the Swiss Federal Nuclear Safety Inspectorate. They all have contributed in one way or another making it possible to obtain the results contained in this publication.

On behalf of the Swiss Geophysical Commission



Prof. Dr. Stephan Mueller
President

Table of contents

Table of contents	i
List of figures	iii
List of tables	iv
Abstract	v
1 Introduction	1
1.1 Starting base, Framework	1
1.2 Project aim	2
1.3 Other projects	4
2 Data acquisition	6
2.1 Measuring instrument	6
2.2 Flight planning	8
2.3 Installation	9
2.4 Survey	10
2.5 Quality control	12
3 Data processing	13
3.1 Overview	13
3.2 Spectrum equalization	15
3.3 Background and cosmic radiation	18
3.4 Spectral stripping	20
3.5 Atmospheric radiation	23
3.6 Altitude correction	25
3.7 Topographical correction	27
3.8 Conversion to general units	30
4 Data presentation and errors	35
4.1 Map generation	35
4.2 Significance and errors	37
4.3 Digital processing of airborne radiometric maps	40

5 Flights	43
5.1 Selection of the survey areas	43
5.2 Flight statistics	44
6 Geological Overview	46
6.1 Jura	
6.1.1 Aargau Jura	46
6.1.2 Vaud Jura	46
6.2 Molasse Basin	46
6.3 Alps/Crystalline units	47
6.3.1 Aar Massif	47
6.3.2 Gotthard Massif/Tavetsch Massif	48
6.3.3 Aiguilles-Rouges Massif	49
6.3.4 Bernhard Nappe	49
6.4 Alps/Sediments	50
6.4.1 Helvetic belt	50
6.4.2 Sediment cover of the Gotthard Massif and the Penninic nappes	50 51
6.5 Quaternary	51
7 Maps	52
7.1 Map captions	53
8 Characteristic geological settings	55
8.1 Jura	55
8.2 Molasse basin	55
8.3 Alps/Crystalline units	56
8.4 Alps/Sediments	58
8.5 Quaternary	59
9 Concluding remarks	60
10 References	62
Acknowledgments	66

List of figures

Figure 2.1: Scheme of the measuring instrument	7
Figure 2.2: Field of view of a gamma-ray detector	8
Figure 3.1: Measuring situation	13
Figure 3.2: Spectrum	17
Figure 3.3: Determination of attenuation coefficients	26
Figure 3.4: Topography correction	30
Figure 3.5: Experimentally determined detector sensitivities	33
Figure 4.1: Grid and Flight path	36
Figure 4.2: Scatterogram	41
Figure 4.3: Color diagramm for ternary radioelement maps	42
Figure 5.1: Overview of the surveyed areas	43
Figure 6.1: Geological map of the Central Massifs	47

List of tables

Tab 2.1: Flight parameters	9
Tab 2.2: Technical data of the helicopters	10
Tab 3.1: Energy windows	17
Tab 3.2: Helicopter background and cosmic stripping factors	19
Tab 3.3: Stripping factors of a point source	21
Tab 3.4: Correction of the stripping factors	22
Tab 3.5: Comparison of the stripping factors	23
Tab 3.6: Attenuation coefficients	27
Tab 3.7: Detector efficiency determination	31
Tab 3.8: Detector efficiency	32
Tab 3.9: Detector sensitivity	34
Tab 4.1: Relative errors	39
Tab 5.1: Compilation of the flight data	44
Tab 8.1: Rock of activities of the Jura	55
Tab 8.2: Rock of activities of the Molasse Baisin	56
Tab 8.3: Rock of activities of the Alps/Crystalline units	57
Tab 8.4: Rock of activities of the Alps/Sediments	59

Abstract

In the years 1986 to 1991 an airborne radioactivity survey was flown by the Swiss Geophysical Commission in selected regions of Switzerland with high level natural radioactivity. The main survey area was a 150 x 20 km NW-SE strip in the Swiss Alps.

All data were sampled at one second intervals using a 256 channel spectrometer, with a 16.8 liter NaI detector. The survey was carried out with helicopters at a mean terrain clearance of 120 m. The survey grid was flown with a north-south flight line direction and 500 m line spacing.

Commonly used calibration and reduction procedures can only be used with several modifications and additional correction steps in the extreme topographic conditions of the Swiss Alps. The data processing procedures adopted in this project in reducing effects of topography on airborne gamma-ray spectrometry measurements are described.

The results are presented as a set of color maps at 1:500'000 and 1:200'000 scale. The natural terrestrial dose rates (cosmic background subtracted) of all the surveyed areas are compiled on three maps. For the main survey area ("Central Massifs") three isotope maps (K^{40} , Bi^{214} und Tl^{208}), three ratio maps (Bi^{214}/Tl^{208} , Bi^{214}/K^{40} und Tl^{208}/K^{40}) and a ternary radioelement map is added. To facilitate the comparison of the airborne radiometric data with geology the boundaries of the geologic units of the survey area "Central Massifs" are shown on an overlay transparency.

1 Introduction

1.1 Starting base, Framework

The radioactive radiation is part of our physical environment. The largest contribution to the radiation field is of natural origin. This contribution is generated by the cosmic radiation, the natural radioactivity of the ground as well as by the radioactive decay products of radon in the air. Artificial radioactivity is emitted by nuclear power plants, industrial plants and research institutes. These emissions are very low in normal operation. Through accidents however large amounts of radioactivity can be released to the environment.

The NADAM system (Net for Automatic Dose Alert and Measurement), a network of 51 stationary dose measuring installations with remote data transfer monitors the radioactivity level in Switzerland continuously since 1986. The measuring instruments are coupled to the weather observation stations of the Swiss meteorological survey. The Branch for Radioactivity Surveillance of the Federal Office of Public Health (SUEP) monitors the environmental radioactivity particularly the surroundings of nuclear installations and factories handling, processing or producing radioactive material. In addition it executes spot checks and measurement series on samples of air, rain, food and so on. A further authority, the Swiss Federal Nuclear Safety Inspectorate (HSK) supervises the nuclear power plants and the nuclear research facility Paul Scherrer Institut (PSI).

Besides these punctual routine measurements regional measurements of the terrestrial radiation (using ionization chambers) were carried out already in 1961 (Halm et al., 1962). The measuring point density of this survey however, is not sufficient for modern requirements.

For a better evaluation of the natural radiation level, the Swiss Geophysical Commission (SGPK) decided to map selected regions of Switzerland by means of airborne gamma ray spectrometry. These maps form a meaningful complement to the several

geophysical maps of Switzerland on the scale of 1:500'000 that have already been completed by the SGPK: gravity, magnetics, seismicity, heat flow and aeromagnetics.

After an evaluation phase, the aerogammaspectrometric measuring system was purchased 1985 in cooperation with the Federal Commission for Radioactivity Surveillance (KUeR). The methodology developments (Schwarz, 1991) as well as the measurements were carried out by the Institute of Geophysics of the Swiss Federal Institute of Technology (Zürich) within the framework of the Swiss Geophysical Survey in the following years.

1.2 Project aim

The airborne radioactivity survey of Switzerland aims at 1:200'000 scale maps of gamma radiation in selected regions with elevated natural radioactivity. Regional and local gamma-ray radiation maps are of key importance for a variety of purposes: location and monitoring of contamination, basic data for radiation biology (width of variation of natural exposure in the context of the effects of low doses), information relevant to prospecting for raw materials (for example potassium alteration) and geological mapping. The investigation artificial radiation was not part of this project, but is examined in two additional projects (see chapter 1.3).

The main attention was given to the crystalline rocks of the Central Massifs of the Swiss Alps because of their relatively high natural radioactivity. Additionally regions with previously known uranium mineralizations have also been surveyed (Verrucano, Aiguilles Rouges massif). The area covered by this survey is about 3000 km² and lies between the Lötschental and the Walensee. Beside of the main area several regions with characteristic lithology have been covered like the Quarternary gravel terraces, the Tertiary of Molasse Basin, the limestones of the Jura and the meta-sedimentary cover of the central massifs.

Since areal radiometric surveys are very expensive and time consuming, they are advantageously carried out airborne. The main advantages of airborne measurements as compared to ground measurements are (IAEA, 1979):

- **Speed:** Airborne surveys permit rapid evaluation of radiation levels of large areas. In inaccessible regions (topography, development), as for example the Swiss Alps, surveys with complete areal coverage are only possible from the air. Because of the larger ground clearance and the higher speed, the yield of an airborne system is about 2'500 times larger than of a comparable ground system. This is of key importance in radiological accidents.
- **Cost effective:** Although the costs for the measuring instruments and for the flights are relatively high, the resulting cost per surveyed area is clearly lower than for a comparable terrestrial survey.
- **Representative:** The determined radionuclide concentrations respectively dose rates represent an average value for an area of 300 m x 300 m (at a flight altitude of 120 m). They hence provide representative sampling.

Most of the limitations are imposed by the relatively short travel range of gamma rays in the air respectively in the ground.

- **Poor penetration depth:** The detected gamma radiation originates from the top 20 cm to 40 cm layer of the surface, and therefore the method does not detect gamma rays emitted by buried sources. This limitation affects also ground measurements.
- **Dangerous:** Since the measurements have to be carried out at very low flight altitudes (ideally less than 120 m), areas of high topographic relief are often difficult to survey because of aircraft limitations and flight obstacles. Surveys in such regions can only be carried out by means of costly helicopter flights.
- **Poor spatial resolution:** The obtainable spatial resolution is limited by the relatively broad field of view of the detector. Furthermore the method is not very sensitive to point sources because the gamma intensity, measured at the detector, represents an average intensity for a broad area.

With the aid of airborne gamma-ray spectrometric measurement the radioisotope concentration of the ground as well as the radiation field (dose rate) can be determined. Radioisotope concentration and dose rate are important parameters for geological studies and environmental applications. The main applications of airborne radiometric measurements are:

- **Exploration:** Airborne radiometric methods are mainly used for uranium exploration on a world wide scale. However the method is not restricted to the search for the radioactive uranium and thorium ores. Hydrothermal alteration, often closely related to ore deposits (zinc, copper, lead), can be detected due to the potassium enrichment (Ward, 1981).
- **Geological overview mapping:** The determination of the concentration of the natural radioisotopes K^{40} , Bi^{214} and Tl^{208} give hints to the chemical composition of the rocks (potassium, uranium and thorium content). This allows distinction of lithological units, especially in crystalline milieu.
- **Radiation protection:** Dose rate maps allow an estimation of the variability and the regional distribution of the terrestrial radiation, which is important in radiobiology particularly on the discussion on the effect of low radiation doses.

1.3 Other projects

The surrounding regions (approx. 50 km²) of the four nuclear power plants (Beznau, Gösgen, Leibstadt and Mühleberg) and the Swiss nuclear research facility (Paul Scherrer Institute) are surveyed annually with the same equipment since 1989. The airborne measurements are financed by the Swiss Federal Nuclear Safety Inspectorate and aim to monitor the dose-rate distribution and to provide a documented reference base (Schwarz et al., 1989, 1990 and 1991). To quantify artificial radioactivity the MMGC-ratio (ratio of the lower to the higher energy part of the spectrum) is used.

Airborne radiometric measurements are without doubt the most efficient tool to locate lost radioactive sources. In case of accidents with radioactive material (transport and industry accidents) or contamination with debris of nuclear-powered satellites the system can be used to locate the radioactive sources or to get an overview of the

contamination situation. These measurements can help decision makers for measures like stay limitations for the population in contaminated areas or missions of recovery teams. In an emergency situation the measurements will be done by military helicopters under the control of the Swiss National Emergency Operation Center (NAZ). Training flights are made each year in order to deploy measuring system optimally.

2 Data acquisition

2.1 Measuring instrument

The equipment used for the survey consists of the following components:

- **A detector package** (Geometrics DET-1024) consisting of four 4"x4"x16" sized prismatic thallium doped sodium iodide crystals. Each crystal is equipped with its own photomultiplier tube (PMT). The whole package is heat isolated and contains a controlled heater, which allows to keep the temperature constant within a range of $\pm 0.1^{\circ}\text{C}$.
- **A detector interface** (Geometrics GR-900) controlling the detector heating. Furthermore it includes the high voltage power supplies and controls for the PMT's.
- **A multi channel spectrometer** (Geometrics GR-800) covering the gamma ray energy range of 400 keV to 3000 keV with 255 channels. An additional channel is used for the registration of high energy cosmic radiation.
- **A data acquisition system** (Geometrics G-714). The system synchronizes and controls the measurements. The spectrometer data are collected together with time, fiducial, and flight number and submitted to the tape drive. During operation the system is controlled by a remote control console. Additional peripheral devices can be added to the system using one of the eight available analog digital converters.
- **A camera** (Automax 35 mm) for flight path recovery. The camera is vertically mounted and takes a picture of the ground every three seconds. The corresponding fiducial number is lighted up on the film. The actually flown flight path is reconstructed comparing these pictures with a topographical map.

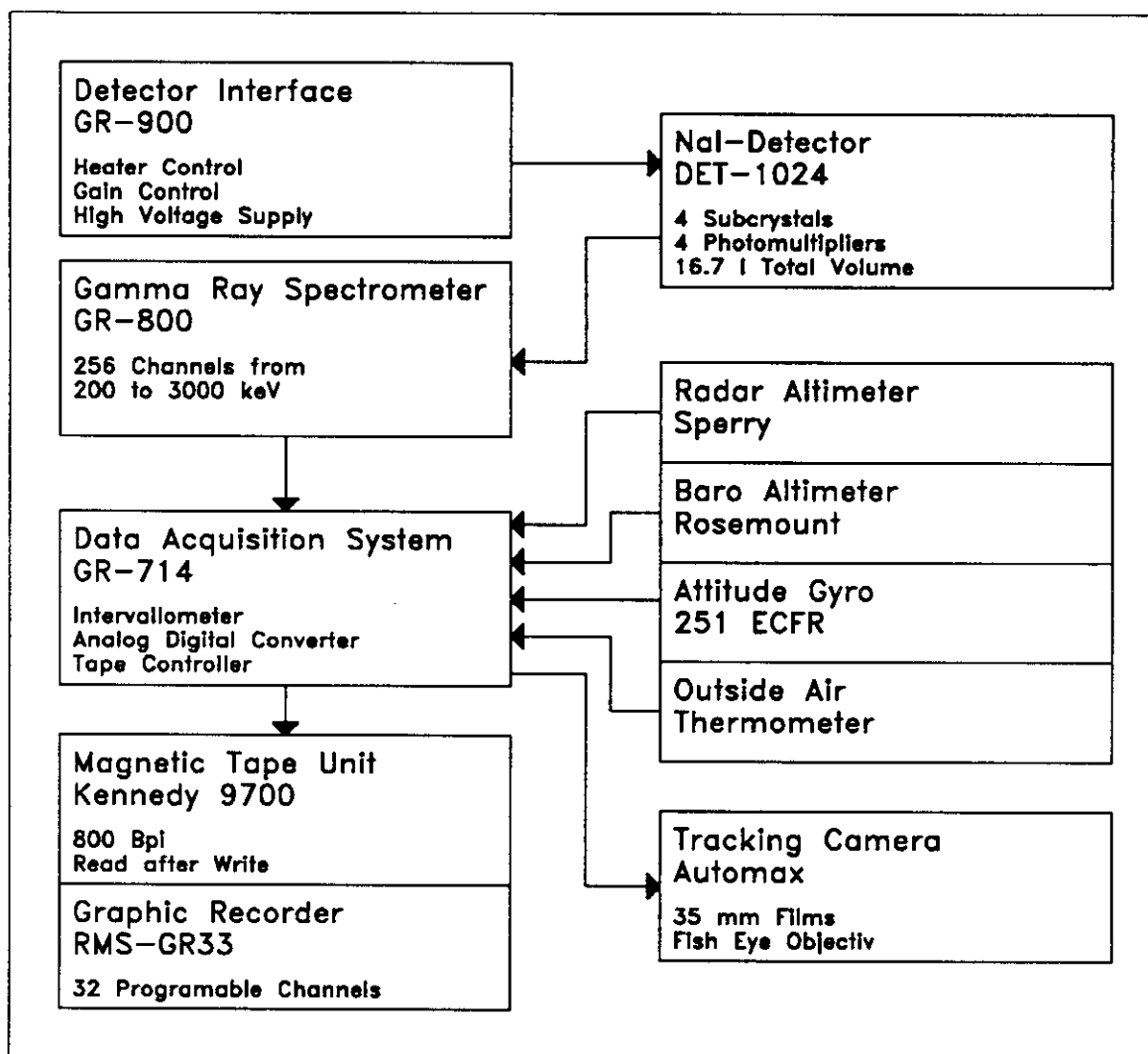


Figure 2.1: Scheme of the measuring instrument

- **A tape drive** (Kennedy-9700) for data recording.
- **A chart recorder** (RMS GR-33) for viewing the recorded data during the flight.
- Additionally **radar altitude** (Sperry AA-200), **barometric pressure** (Rosemount 1241), **outside air temperature** (Davtron 301C) and **pitch and roll angles** of the helicopter (AIM 251 CFR) are recorded continuously.

At a base station barometric pressure, temperature and humidity are recorded simultaneously with the flights.

2.2 Flight planning

In order to achieve uniform coverage of the surveyed area the flights are carried out in a regular grid of flight lines. The flight line spacing depends on the detector sensitivity and on the desired ground coverage. Unlike a camera, a gamma-ray detector does not have a fixed field of view since it can receive radiation from any angle. The ground coverage of airborne measurements is therefore not determined exactly.

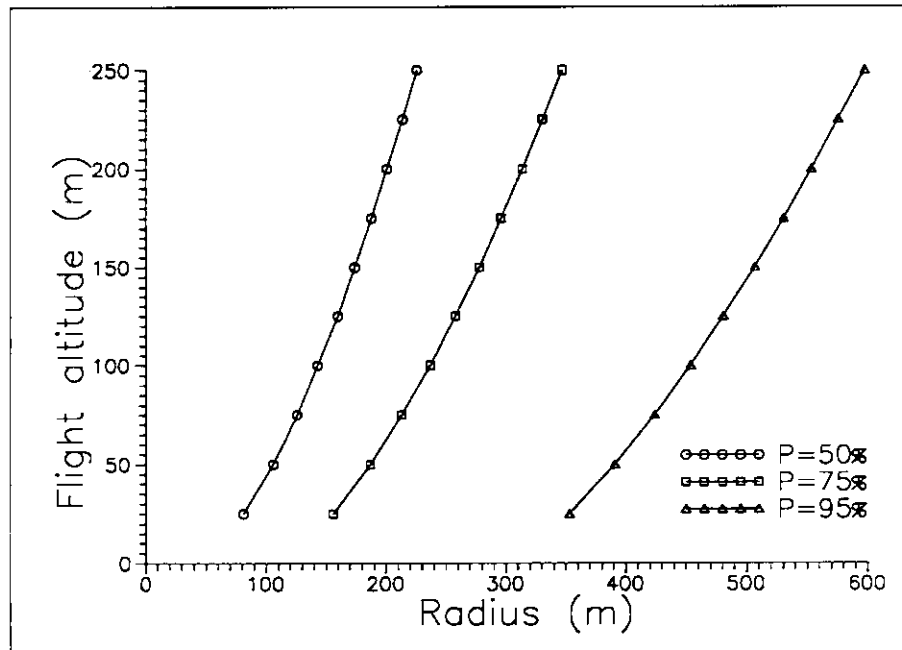


Figure 2.2 : Field of view of a gamma-ray detector over a homogeneous infinite source (K^{40}) in dependence on the flight altitude. The three curves indicate the radius of the area beneath the detector contributing 50%, 75% resp. 95% of the total radiation.

For airborne gamma-ray observations, the field of view of a detector is commonly thought as the circular area beneath the aircraft contributing to a fixed percentage P of the total detected radiation (generally $P=75\%$). The area contributing 75% of the total radiation corresponds approximately to the area of the smallest resolvable structure (Pitkin und Duval, 1980). However, the relative contribution of different areas on the ground depends on the activity distribution in the ground. A strongly radioactive source can be detected even if it is outside of some nominal field of view. Only over a homogeneous infinite source the field of view of the detector is defined precisely. Nevertheless this concept provides important hints on the relative contribution of the area beneath the detector and therefore on the spatial resolution of the detector even at inhomogeneous activity distribution.

The area covered by the field of view of the detector depends strongly on the flight altitude as can be seen from figure 2.2. It is desirable to fly as low as possible because of the absorption of gamma-rays by the air. For safety reasons (flight obstacles, flight limitations) the flight altitude can not be lower than 92 m (300 ft) in flat terrain resp. 122 m (400 ft) in mountainous areas. The measurements for the Swiss airborne radiometric survey were therefore carried out at a reference altitude of 122 m (400 ft). According to figure 2.2 the radius of the corresponding area covering 75% of the field of view is about 250 m. The flight line spacing was therefore fixed to 500 m.

Table 2.1: Flight parameters

Flight line spacing	500 m
Heading	N-S
Flight altitude	122 m
Ground speed	25 m/s
Sample rate	1 s

The ground speed is only of minor importance if the measurements are carried out with helicopters which always fly relatively slow. It has only to be considered during search for point sources. A summary of the flight parameters is given in table 2.1.

2.3 Installation

The previously described equipment can be installed into two different kinds of helicopters. Normally an AS350B1 Ecureuil helicopter of Heliswiss AG (Belp/BE) is used for routine surveys. Emergency flights are accomplished with Swiss army Alouette-III helicopters. Table 2.2 summarizes the technical data of both helicopters.

Table 2.2: Technical data of the helicopters used for survey flights

	Ecureuil AS350B	Alouette-III AS316B
Company	Aérospatiale	Aérospatiale
Turbine type	Turboméca Arriel	Artouste-III B
Turbine power	523 PS	550 PS
Fuel consumption	165 l/h	200 l/h
Rotor diameter	10.65 m	11.02 m
Length overall	12.99 m	12.87 m
Cabin width	2.53 m	2.85 m
Height overall	3.08 m	2.97 m
Empty weight	990 kg	1300 kg
Gross weight	1950 kg	2100 kg
Max. flight time	3 h	2.5 h
Cruise speed	220 km/h	180 km/h
Certified altitude	4875 m/M	6500 m/M
Max. mission range	660 km	450 km

The detector and the rack are mounted behind the two front seats, in place of the passenger's seats. For the installation of the equipment no modifications to the helicopter are needed. The whole equipment can be fixed to standard attach points.

2.4 Survey

Airborne gamma spectrometric surveys were executed mostly during summer and early autumn because of the stable meteorological conditions.

Because of the complexity of the measuring system a permanent surveying and careful calibration of the instruments is very important. With the energy calibration procedure the spectra of the four detectors are adjusted to the same gain. Energy calibration is done before every flight using a 370 kBq (10 μ Ci) Cs¹³⁷ source. An individual gain control potentiometer is provided for each detector PMT. Using these potentiometers the spectrum of every crystal can be adjusted very precisely to the gamma ray energy of cesium (661 keV). Finally a thorium spectrum is recorded to check the quality of the calibration using the Th²⁰⁸ peak at 2615 keV.

To check the function of the measuring system a test is carried out at the beginning and the end of every flight. For this the system is run for about 30 s at ground. The data acquired in that way also can be used for a subsequent energy calibration. The second test provides information about the radon content of the atmosphere. A flight line is flown at an altitude of 305 m (1000 ft) above ground always at the same place. Measurements that vary heavily from the average of all test lines at this site indicate an increase of radon concentration. Flights carried out during such a period should be advantageously repeated.

During the measurements the incoming gamma rays are accumulated during one second by the spectrometer. The resulting spectrum is written together with the fiducial number, the outside air temperature, the radar altitude, the barometric pressure and the actual time to the magnetic tape. Totally 652 Bytes of information are stored every second. Every third second a picture of the overflown ground is taken by the flight path recovery camera. These pictures are used to reconstruct the actual flight path.

Navigation was done visually using flight maps of 1:25'000 scale. It is aimed to follow the planned flight lines (see chapter 5) as precise as possible at a very low flight altitude (less than 120 m), which makes high demands to the pilot, the navigator and the helicopter, especially in mountainous regions. The heading is followed using typical terrain points. The biggest problem flying in the Swiss Alps are flight obstacles like cable cars and power lines. Some areas contain as much as one flight obstacle (with ground clearance up to 300 m) per kilometer flight line. For security reasons the position of the helicopter must always be known with a precision of ± 100 m.

The characteristic data of each flight line (fiducial of line start and line end, heading and time) are noted on a flight protocol for control purposes. Furthermore the coordinates of the line start and the line end are marked on the flight map.

One fueling lasts out for about 120-150 minutes of flight. The effective measuring time during a flight is around 70 minutes, which corresponds to 100 km flight line.

2.5 Quality control

The quality check takes place directly after landing. The processing computer has therefore to be transportable. The computer used for this purpose is an IBM compatible personal computer with a magnetic tape drive connected to it.

For the field processing of the airborne radiometric data an integrated program package has been developed. It allows not only the quality control but also a complete processing of the data including map generation (Schwarz, 1990). The software is menu driven and easy to use and easy to learn even for non computer specialists.

For the first quality control the field tapes are read into the computer and checked for tape errors. Energy calibration and energy resolution of the spectrometer are checked as well. Faulty spots are erased, and operator errors, like wrong line numbers are corrected. The checked and corrected tapes are backed up for later use.

3 Data processing

3.1 Overview

The gamma radiation registered by the detector in a helicopter is composed of the contributions from soil, atmosphere, aircraft and cosmic radiation (see figure 3.1):

- **Cosmic radiation:** During the absorption process of the cosmic high energy particle radiation gamma radiation is produced, which is registered by the spectrometer.

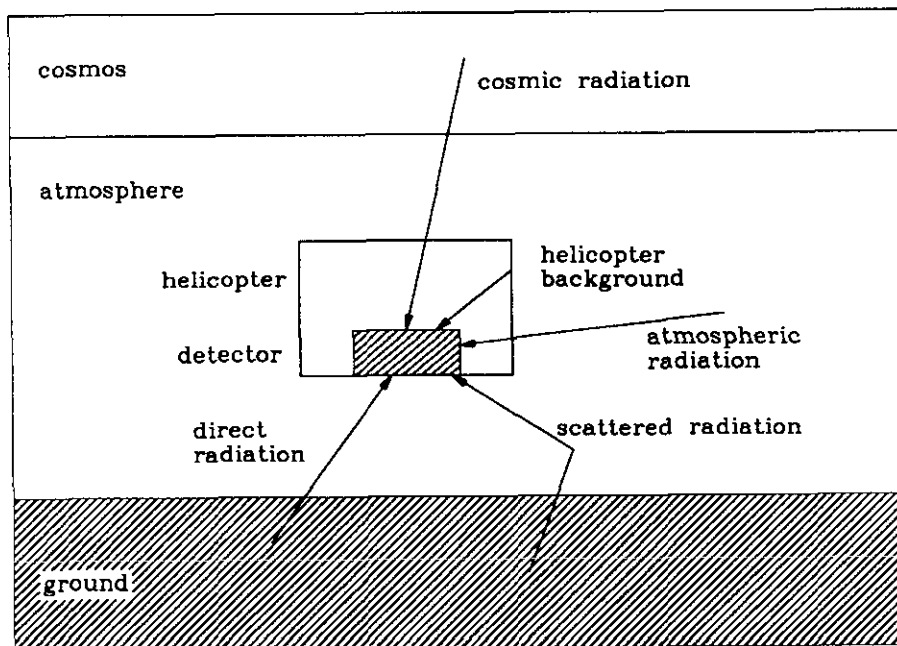


Figure 3.1: Situation encountered during airborne radiometric measurements

- **Atmospheric radiation:** The most important radiation source in the atmosphere is the isotope Rn^{222} of the inert gas radon. It originates from the decay of uranium. The concentration of radon in the air depends on meteorological conditions and is strongly variable (Kogan et al., 1969).
- **Background radiation from aircraft and detector:** In the aircraft as well as in the detector material itself small amounts of radioactive material are present. Their radiation are registered during the measurements.

- **Scattered radiation:** Gamma rays are scattered in the detector crystals, in the air and also in the soil. The scattering changes the energy of the radiation and therefore the original spectrum.
- **Terrestrial radiation:** Terrestrial radiation is mostly produced by the decay of the four natural radio isotopes U^{235} , U^{238} , Th^{232} and K^{40} . Sometimes contributions of long living decay- and activation-products from nuclear weapon tests and/or nuclear facilities as Cs^{137} and Co^{60} add to the natural contributions.

The aim of airborne radiometric measurements is the determination of the radio-nuclide content of ground using the information of the direct terrestrial gamma radiation. All other contributions are perturbing and have to be removed. This is done with a set of corrections called background corrections. The background corrections depend neither on the ground geometry nor on the soil activity distribution. They are therefore location independent and can be performed on every application. Generally the background corrections are carried out in four steps:

- **Spectrum equalization:** Correction of the perturbation originating in the measuring instrument itself, especially drift and dead time of the spectrometer. Afterwards the spectrum is reduced to spectral windows.
- **Aircraft background/cosmic radiation:** Removal of the contributions of aircraft- and detector background as well as of the cosmic radiation.
- **Spectral stripping:** Reduction to the primary (direct) radiation contribution by removing the effects of scattering and contributions from other isotopes.
- **Atmospheric radiation:** Correction of the contributions of radon in the air.

To reduce the radiation intensities measured from the air to the ground activity a second set of corrections is needed. These corrections are called normalization corrections and are carried out applying the following steps:

- **Altitude correction:** The effects of a varying flight altitude are removed with the altitude correction. These variations represent the most significant perturbation to airborne radiometric measurements. The gamma ray intensity decreases rapidly with increasing ground clearance because of absorption of gamma rays in the air. Nearly no ground radiation is registered at flight altitudes higher than 300 m to 400 m. Actually measured flight profiles show a strong negative correlation between flight altitude and count rate.

- **Topographical correction:** The effects of topographic relief can be neglected in flat or slightly hilly areas. In narrow valleys, which are abundant in the Swiss Alps, topography can produce a strong increase of the count rates by as much as 100%. Over mountain peaks the count rate decreases by 10% to 30%. These effects can be corrected adequately in most practical circumstances with the topographical correction.
- **Conversion to general units:** In a last step the detector specific count rates are converted to the corresponding soil activity or radionuclide concentrations.

Contrary to the background corrections, the normalization corrections need assumptions on the distribution of the radioactive source(s). The topographical and the altitude corrections as well as the conversion to general units can only be carried out when the activity distribution is known. Normally the natural radioisotopes are homogeneously distributed in the ground. Their activity distribution can therefore be considered as known, which is not the case regarding artificial isotopes. This is the reason why the normalization corrections with exception of the altitude correction generally apply only to the natural isotopes.

All correction steps are described in detail in the following chapters.

3.2 Spectrum equalization

With the help of the spectrum equalization correction the errors originating in the measuring instrument itself, especially drift and dead time of the spectrometer are removed.

- **Drift:** The output signal of the detector crystal and the photo multiplier tube is temperature dependent. Although the detector crystals are placed in a heated isolated case, the temperature stabilization can fail especially under direct sun exposition. The result is a change of the energy-channel relation.
- **Dead time:** When the spectrometer is processing a pulse, no other incoming gamma quantum may be processed. The system is "Dead" during this period and registers a too small count rate especially at high intensities.

With the energy calibration done by hardware (see chapter 2.4) all the detectors are normalized to a common gain. Since a too strong or asynchronic drift of single PMT's can completely perturb the data their quality has to be carefully checked already in the field, so that erroneous data can be rejected early.

Sometimes a subsequent energy calibration (Schwarz, 1991) using the natural gamma peaks at 1460 keV (K^{40}), 1765 keV (Bi^{214}) and 2615 keV (Tl^{208}) (see figure 3.2) can be carried out.

If the dead time of the spectrometer is independent of the count rate (which is true for NaI detectors), the correction factor for the dead time correction is (Adams and Gasparini, 1970):

$$I_{corr} = I_{raw} \cdot \frac{1}{1 - I_{tot} \cdot \tau} \quad (3.1)$$

I_{corr}	Corrected count rate	[cps]
I_{raw}	Raw count rate	[cps]
I_{tot}	Total count rate of the spectrometer	[cps]
τ	Dead time	[s]

The dead time τ of the GR-800 spectrometer is 5 μ s (EG&G Geometrics, 1985).

The whole spectral information is recorded during the measurement flights (figure 3.2). For the further processing these spectra can be compressed to eight energy windows. The compression reduces the mass storage requirements to one sixteenth of the original amount of data. In addition the count statistics can be improved.

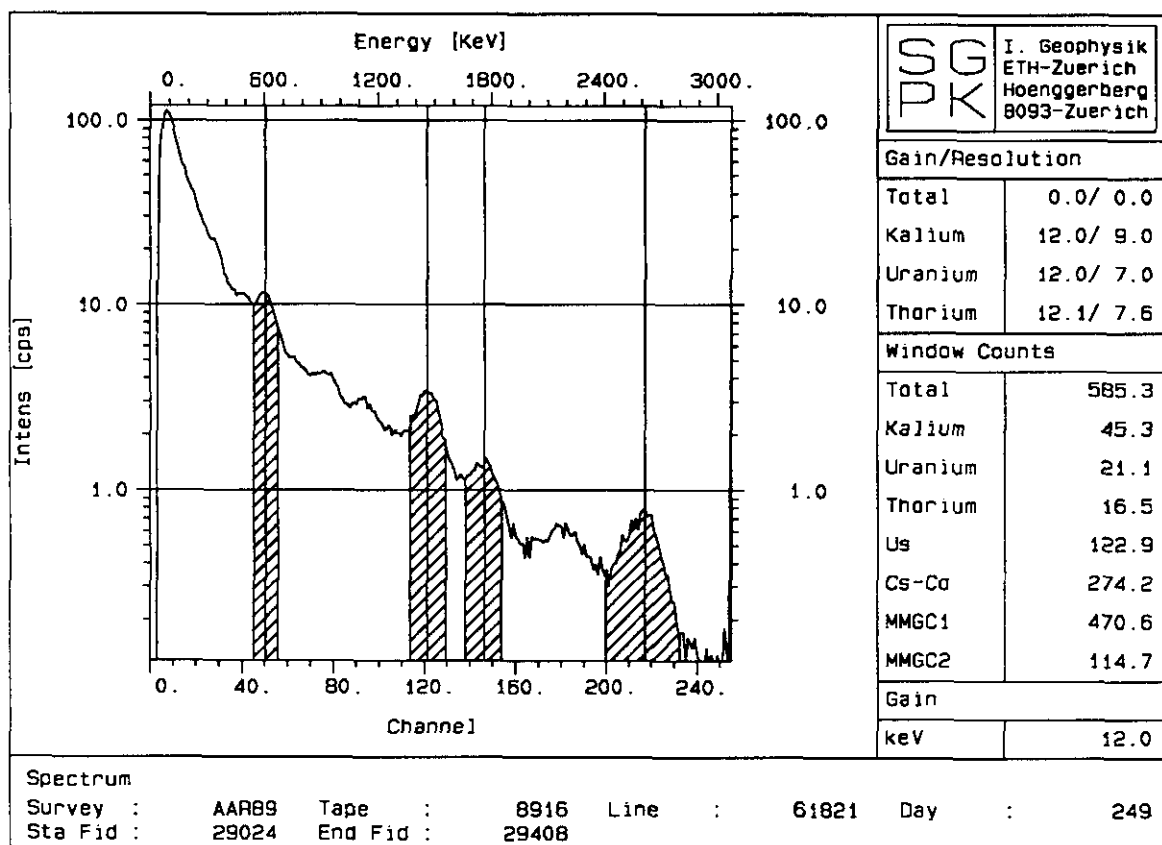


Figure 3.2 : Example of a spectrum

Table 3.1 : Energy windows used for airborne gamma ray spectrometry.

Window name	Isotope	γ -Peak energy [keV]	Lower bound [keV]	Upper bound [keV]
Total	-	-	400	3000
Potassium	K ⁴⁰	1460	1360	1560
Uranium	Bi ²¹⁴	1765	1665	1865
Thorium	Tl ²⁰⁸	2615	2415	2815
Us	Bi ²¹⁴	609	543	673

The energy windows are centered on spectral regions of special interest (table 3.1). The region centered at the 1460 keV peak of K⁴⁰ is used for the determination of the potassium content. Uranium is detected using the 1765 keV line of the daughter product Bi²¹⁴. For thorium the 2615 keV line of Tl²⁰⁸ is used. The energy windows are located at higher gamma ray energies where the absorption by air is less important. Furthermore they are sufficiently separated from each other to keep interactions small. The total count window covers the complete spectrum of natural

gamma radiation and is representative for the total amount of gamma radiation. Additionally a window centered at the 609 keV line of Bi^{214} (Us) is recorded for some special applications .

3.3 Background and cosmic radiation

The intensity of the cosmic radiation depends mainly on the thickness of the atmosphere above the measurement location and therefore on air pressure and altitude above sea level. Since the primary particles are electrically charged they are deflected by the earth's magnetic field. There is also a relation between the cosmic radiation intensity and the geographical latitude.

The helicopter background radiation is mainly generated by dust in the cabin and sometime radioactive luminous paint on the flight instruments (only in elder helicopters). The contribution from radioactive contaminations in the detector material (mainly K^{40}) is regarded as a part of the helicopter background, which is assumed to be constant.

The cosmic spectrum covers the complete energy range of gamma radiation. Since the highest energy of terrestrial gamma radiation is around 3000 keV, all radiation recorded above 3000 keV will have a cosmic source. The spectrometer records the energy range between 3000 keV and 6000 keV in a special channel, the so called "cosmic window".

Although the cosmic radiation intensity varies, the shape of the spectrum does not change. This fact is used for the determination of the helicopter and cosmic background. The calibration data are taken above large lakes, where the soil radiation is completely absorbed by water. Lake Geneva and Lake Constance were chosen for the Swiss survey. The flights were carried out at altitudes of 1830 m, 2440 m, 3050 m, 3660 m and 4270 m (6000 ft, 8000 ft, 10000 ft, 12000 ft and 14000 ft) above sea level.

Whereas the helicopter background is constant, the contribution of the cosmic radiation increases with increasing height. After Purvance and Novak (1983) there is a linear relation between the count rate in each spectrometer channel and the cosmic window:

$$I = I_B + S_C \cdot I_C \quad (3.2)$$

with:

I	Measured count rate	[cps]
I_B	Helicopter background	[cps]
S_C	Cosmic stripping factor	
I_C	Count rate in the cosmic window	[cps]

Using linear regression the constants I_B and S_C and their errors ΔI_B ΔS_C can be determined for every window. The results from the calibration flight on the 31.8.1989 above the Lake Constance are listed in table 3.2.

Table 3.2 : Helicopter background and cosmic stripping factors (calibration flight on the 31.8.1989, Lake Constance). The cosmic stripping factors in the fourth column were determined on the same detector type (Lama1 and Lama2, EG&G Geomterics, 1980) by the manufacturer.

Energy window	Helicopter background [cps]		Cosmic stripping factors ETH		Cosmic stripping factors EG&G	
	I_B	ΔI_B	S_C	ΔS_C	S_C (Lama1)	S_C (Lama2)
Total	118.0	1.9	2.58	0.022	3.02	3.32
Potassium	9.0	0.6	0.13	0.007	0.17	0.18
Uranium	3.3	1.3	0.12	0.015	0.14	0.15
Thorium	1.7	0.6	0.18	0.007	0.19	0.20
Us	27.6	2.2	0.23	0.025	-	-

The correction constants mainly depend on the helicopter and the detector type. The calibration should be repeated once a year or after changing the helicopter.

The correction for helicopter and cosmic background is carried out using the following formula:

$$I_{corr} = I_{raw} - (I_B + S_C \cdot I_C) \quad (3.3)$$

where:

I_{corr}	Corrected count rate	[cps]
I_{raw}	Raw count rate	[cps]
I_B	Helicopter background	[cps]
S_C	Cosmic stripping factor	
I_C	Count rate in the cosmic window	[cps]

3.4 Spectral stripping

The gamma ray spectrum received during field measurements is very complex. It is composed of the contributions of several radio isotopes. The spectrum is further complicated by scattering, which can occur in the ground, in the air and in the detector itself. The counts in the uranium window for example originate not only from primary Bi^{214} photons, but also from scattered or incompletely absorbed 2615 keV quanta from Tl^{208} .

The spectral stripping correction removes the contributions of scattered photons and from other isotopes, so that the window only contains counts from the direct primary radiation (component of the 'photo peak') of the corresponding isotope. The correction of course only applies to windows representing a "photo peak". For total count windows this correction is of course meaningless.

The stripping factors are determined ideally on concrete calibration pads (size: 8 x 8 m, thickness: 50 cm) with a precisely known potassium, uranium and thorium content (Ward, 1978; Killeen, 1979). Unfortunately there are no calibration pads available in central Europe. The stripping factors had to be therefore determined using radioactive point sources with activities around 37 kBq (1 μCi). The precise

activity of the calibration sources have not to be known, since only ratios are used in the calculations. For each energy window the corresponding calibration source is needed. In our case a potassium, uranium and a thorium source were necessary.

If the calibration sources are not contaminated by other radio isotopes, the count rate in any window can be expressed as follows:

$$I_i^j = I_j^j \cdot f_{ji}^* \quad (3.4)$$

I_i^j Count rate in window i using source j [cps]
 f_{ji}^* Stripping factors

The stripping factors respectively their error will be therefore:

$$f_{ji}^* = \frac{I_i^j}{I_j^j} \quad \Delta f_{ji}^* = \sqrt{f_{ji}^* \cdot \frac{I_i^j + I_j^j}{I_j^{j^2}}} \quad (3.5)$$

The calibration measurements were carried out in winter 1988. The sources were positioned at a distance of 1 m from the detector. The measuring time was 100 s. The laboratory background was determined and removed from the calibration spectra.

Table 3.3 : Stripping factors determined using point sources.

Source→ Window↓	Potassium		Uranium		Thorium	
	f_{ji}^*	Δf_{ji}^*	f_{ji}^*	Δf_{ji}^*	f_{ji}^*	Δf_{ji}^*
Potassium	1.00	-	0.72	0.04	0.37	0.02
Uranium	0.00	0.00	1.00	-	0.24	0.02
Thorium	0.00	0.00	0.07	0.01	1.00	-

Since no scattering occurs within a point source, the stripping factors found in the previous paragraph are not the same as the ones encountered during the measurements. They have to be corrected for the scattering in the ground and the air. The change of a stripping factor by scattering (g) is given by Grasty (1975) or Schwarz (1991) (for the detector used in this survey). It can be approximated by a straight

line ($g=g_{int}+g_{slp}\cdot h$) in the altitude range of airborne measurements (50 m to 250 m). The intercepts g_{int} and the slopes g_{slp} of this approximation line are listed in the following table.

Table 3.4 : Change of the stripping factors due to scattered radiation in the ground and the air.

Source→ Window↓	Potassium		Uranium		Thorium	
	g_{int}	g_{slp}	g_{int}	g_{slp}	g_{int}	g_{slp}
Potassium	-	-	0.14	0.0006	0.11	0.0003
Uranium	-	-	-	-	0.10	0.0003
Thorium	-	-	-	-	-	-

To obtain the definitive stripping factors f the change due to scattering (g , see table 3.4) is added to the factors determined by point sources (f' , see table 3.3) giving $f=f'+g_{int}+g_{slp}\cdot h$. The measured count rate I_{raw} in the energy windows is given by the following formula:

$$\vec{I}_{raw} = \mathbf{f} \cdot \vec{I}_{corr} \quad (3.6)$$

\vec{I}_{corr}	Vector consisting of the direct (unscattered) count rates	[cps]
\vec{I}_{raw}	Vector consisting of the raw count rates	[cps]
\mathbf{f}	Stripping factor matrix	

Since the contribution of the direct unscattered radiation I_{corr} is the wanted parameter after the spectral stripping correction, the stripping factors f cannot be used directly for the correction. The matrix \mathbf{f} consisting of the stripping factors has first to be inverted to lead to the final correction formula:

$$\vec{I}_{corr} = \mathbf{s} \cdot \vec{I}_{raw} \quad (3.7)$$

\mathbf{s}	Inverse stripping factor matrix ($\mathbf{s}=\mathbf{f}^{-1}$)
--------------	--

Table 3.5 lists the correction factors (s). For comparison the factors determined on calibration pads of the same detector type are listed on the second column (EG&G Geometrics, 1980).

Table 3.5 : Comparison of the stripping factors determined with point sources and corrected for scattering (ETH) to the factors determined on calibration pads of the same detector type (Lama1 and Lama2, from EG&G Geomterics, 1980).

Detector→ Stripping factors↓	ETH	EG&G Lama1	EG&G Lama2
S _{UK}	-0.83	-0.82	-0.82
S _{TU}	-0.32	-0.28	-0.28
S _{TK}	-0.19	-0.18	-0.17
S _{KU}	0.00	0.00	0.00
S _{UT}	-0.07	-0.07	-0.07
S _{KT}	0.00	0.00	0.00

The stripping factors are mainly determined by the size and the shape of the detector. The helicopter has only a minor influence.

3.5 Atmospheric radiation

The atmospheric radiation is mainly produced by radon (Rn^{222}) diffusing out of soil. This radioactive inert gas is a daughter product of the uranium (U^{238}) decay series. It influences therefore especially the uranium window. Although the half time of radon is only four days, radon is always present in the atmosphere, since it is reproduced in the soil steadily.

The radon concentration in the atmosphere is extremely variable, the daily variation being the most prominent. Further correlation between radon content and air pressure, temperature and soil humidity have been reported (Kogan et al., 1969). Because of the complexity of the emanation, diffusion and transport of radon, the mechanisms causing these variations are partially unknown.

The standard solution for the radon content determination is a shielded upward looking detector, registering only atmospheric and cosmic radiation (Purvance and Novak, 1983). Since the Swiss detection system contains no upward looking detector the atmospheric contribution has to be determined differently. Two methods are possible:

- **Flights over water:** The ground radiation is absorbed by the water, so that over a lake or a large river only the atmospheric contribution will be registered (Darnley and Grasty, 1970). This method can be applied at reasonable costs, only if the lake is located near the surveyed area.
- **Climbing flights:** The atmospheric radiation can approximately estimated from the decrease of the radiation intensity with increasing flight altitude (Schwarz, 1991). This method can be applied in every environment but its results are less precise than results from flights over water.

Because of the fluctuations of the radon concentration the determination has to be carried out several times a day. This will cause a lot of additional survey costs whichever of the methods used. If only a qualitative monitoring of the radon concentration is needed a much simpler method can be used:

- **Radon lines:** A same flight line of 3 km length (flight altitude 305 m (1000 ft)) is measured several times a day. An elevated radon concentration is indicated when the measured count rate of a flight differs strongly from the average count rate of all radon line measurements.

The combination of climbing flights and radon lines allows an efficient monitoring of the radon concentration of the atmosphere. The radon determinations during the Swiss survey always showed relatively low values. The reason for the low radon concentrations could be attributed to a good air circulation in the Alps during summer time.

A second fact indicates that the radon concentrations were very low. After Green (1987) areas surveyed during periods of high radon concentrations should show a typical banding in the uranium data, because of the daily radon fluctuations. This banding cannot be observed on the Swiss data. Furthermore all methods described in this section do not allow the determination of the lateral radon distribution. Therefore no radon correction was applied.

3.6 Altitude correction

With the altitude correction the data are normalized to a common reference altitude. It is assumed that the radiation intensity depends only on the flight altitude. This corresponds to the condition that at every measurement the overflown terrain can be approximated by a halfspace.

The correction function is given by the decrease of the count rate over a halfspace with a homogeneous activity distribution:

$$I(h) = I_0 \cdot E_2(\mu_a \cdot h) \quad (3.8)$$

h	Flight altitude	[m]
$I(h)$	Count rate at altitude h	[cps]
I_0	Count rate at ground	[cps]
μ_a	Attenuation coefficient of the air	[m ⁻¹]
E_2	Exponential integral of second order (Abramowitz and Stegun, 1972, p.228)	

The natural radioactivity of soil can be used for the experimental determination of the attenuation coefficients of the air. For that, calibration flights were carried out over flat homogeneous terrain at flight altitudes of 30.5 m, 61 m, 91.5 m, 122 m, 152.5 m, 229 m and 305 m (100 s each). The data were reduced to direct ground radiation using the background corrections. Formula 3.7 was then least square fitted to the data set using the Levenberg-Marquart method (Press et al., 1986). The resulting parameters are the attenuation coefficient μ_a and the count rate at ground I_0 . Figure 3.3 shows an example for such a determination.

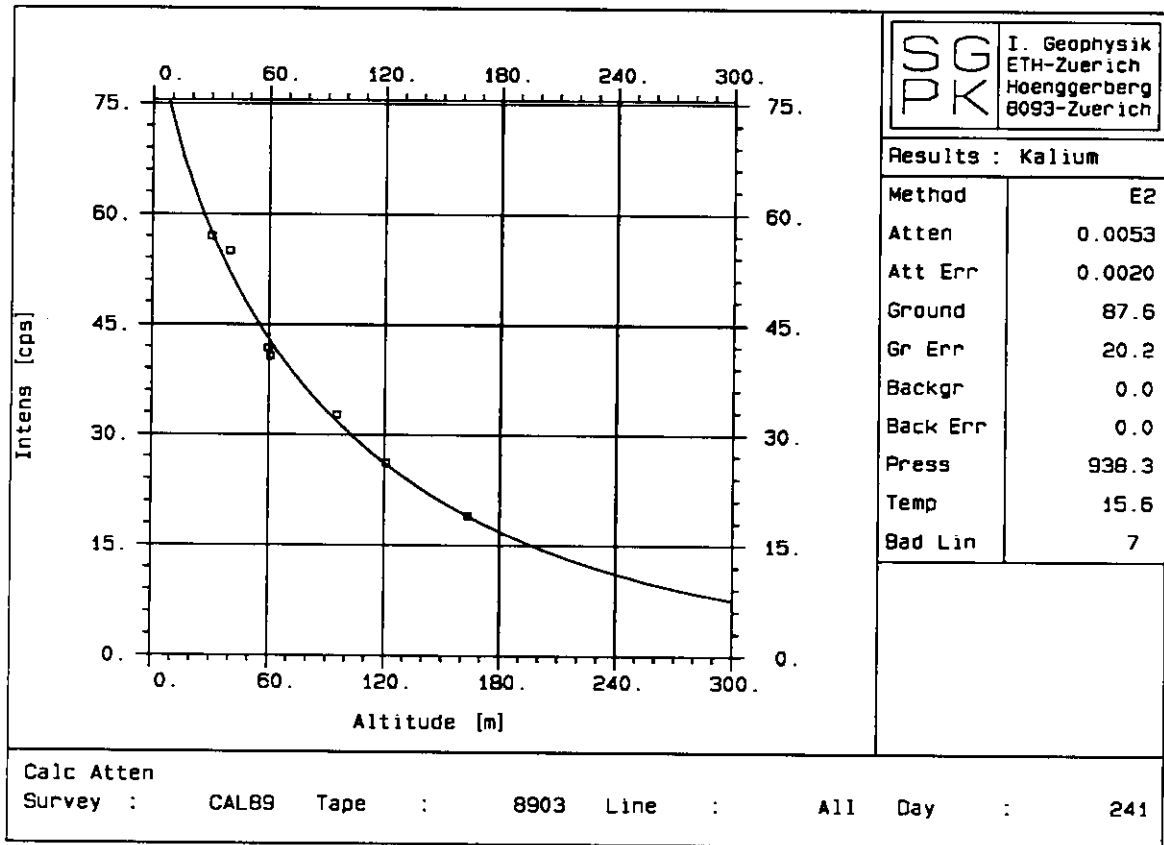


Figure 3.3 : Determination of the attenuation coefficient of air in the potassium window.

Since the attenuation coefficient depends on the energy of the radiation the determination has to be carried out for every energy window. The attenuation coefficients also depend on the density of the absorber. In the case of air the density is temperature and pressure dependent. The coefficients have therefore to be normalized to standard atmospheric conditions with the following formula:

$$\mu_{ref} = \mu_{raw} \cdot \frac{T_{mes}}{273.15} \cdot \frac{1013.25}{P_{mes}} \quad (3.9)$$

μ_{ref}	Corrected attenuation coefficient at 0°C and 1013.25 hPa (standard atmosphere)	[m ⁻¹]
μ_{raw}	Measured attenuation coefficient	[m ⁻¹]
T_{mes}	Temperature	[°C]
P_{mes}	Air pressure	[hPa]

The experimentally determined attenuation coefficients (table 3.6) are generally lower than the coefficients published in literature (Adams and Gasparini, 1970). This difference could be caused by the anisotropic detector response, which was not taken

into account for the determination of the coefficients. To take this effect into account the experimentally determined attenuation coefficients are used in the following calculations.

Table 3.6 : Results of the attenuation coefficient determination of the 29.8.1989 in Spiez(BE). The first column contains the experimentally determined values. The reference values are taken from Adams and Gasparini, 1970

Window	μ_{ETH} [m ⁻¹]	$\Delta\mu_{ETH}$ [m ⁻¹]	$\mu_{Literature}$ [m ⁻¹]
Total	.0050	.0003	-
Potassium	.0060	.0008	.0068
Uranium	.0046	.0114	.0061
Thorium	.0049	.0044	.0051

The correction formula for the altitude correction is given by:

$$I_{corr} = I_{raw} \cdot \frac{E_2(\mu_{ref} \cdot h_{ref})}{E_2(\mu \cdot h)} \quad (3.10)$$

I_{corr}	Corrected count rate	[cps]
I_{raw}	Raw count rate	[cps]
μ_{ref}	Attenuation coefficient at 0°C and 1013 hPa	[m ⁻¹]
h_{ref}	Reference altitude	[m]
μ_a	Attenuation coefficient at measurement conditions	[m ⁻¹]
h	Flight altitude	[m]

3.7 Topographical correction

The difficulties of processing data acquired in areas with high topographic relief are twofold. First, it is impossible to maintain the desired survey altitude constant because of the limited flight capabilities of the aircraft. Furthermore, the measurements are strongly influenced by ground geometry.

It is evident that a detector entirely surrounded by radioactive material (4 π -geometry) measures a higher count rate than over a half space of the same activity. In flat terrain the overflow area in a first approximation can be considered as a half space

(2π -geometry). This approximation is not valid in the mountains. In a narrow valley the solid angle seen by the detector is obviously higher than 2π . As a result, the measured count rate will be higher than over a half space of the same ground activity. On the other hand the count rate over a mountain peak or ridge (solid angle $< 2\pi$) will be lower.

In order to estimate the influence of topographic irregularities the gamma-ray field has been modelled above real topography in both two and three dimensions (Schwarz et al., 1992). The calculations demonstrate a strong increase of the count rates by as much as 100% in narrow valleys, which are abundant in the Swiss Alps. Over mountain peaks the count rate decreases by 10% to 30%. In flat or slightly hilly regions the topographic effects can be neglected.

The correction procedure for topography and flight altitude variations is based on the same method as used for the model calculations. The modelled radiation intensity J_{mod} is calculated using either 2D-models or 3D-models described in Schwarz et al. (1992), assuming that the radioisotopes are uniformly distributed ($q=\text{constant}$) over the field of view of the detector. The radiation intensity over flat topography (half-space) at reference flight altitude (h_{ref}) is given by Kogan et al. (1969):

$$J_{\text{hfsp}} = \frac{q}{2\mu_s} \cdot E_2(\mu_a h_{\text{ref}}) \quad (3.11)$$

J_{hfsp}	Radiation intensity of a halfspace	
q	Soil activity	[Bq·m ⁻³]
μ_a, μ_s	Attenuation coefficient of air resp. of soil	[m ⁻¹]
h_{ref}	Reference flight altitude	[m]
E_2	Exponential integral of second order	

The relative contribution of topography (N) is then the ratio of the radiation intensity of the halfspace J_{hfsp} to the modelled radiation intensity J_{mod} . The unknown factor q/μ_s in formula 3.8 does not affect the relative contribution of topography (N), since it appears both in J_{mod} and J_{hfsp} . The count rate over an irregular surface is then reduced to $I_{\text{corr}} = I_{\text{raw}} \cdot N$.

The error of the correction factor N is given in first approximation by:

$$\Delta N = N \cdot \sqrt{\mu^2 \cdot \Delta h^2 + \Delta \mu^2 \cdot (h_{ref} - h)^2} \quad (3.12)$$

ΔN	Error of correction factor
$\Delta \mu$	Error of attenuation coefficient
Δh	Error of flight altitude

The errors of attenuation coefficients are listed in table 3.6. The error of the altitude measurement is typically less than 10 m. In airborne radiometric applications ΔN will therefore be usually less than $N/10$.

In principle a single measurement can only determine the mean activity q in the field of view of the detector (one measurement = one parameter). Lateral and vertical inhomogeneities inside the field of view of the detector cannot be resolved. The assumption of a homogeneous radionuclide distribution in developing the topographic correction method is therefore justifiable.

Figure 3.4 shows the result of topography correction applied on flight line 11091 (survey Marecottes). The topography-caused anomalies at 1000 m, 1600 m and 4300 m over the narrow valleys are effectively removed. The remaining peaks at 1600 m and 4300 m are located exactly over rivers. Usually river sediments show higher count rates possibly due to heavy mineral accumulation. To eliminate these peaks an unreasonable attenuation coefficient of air (far from tabulated values) would be needed for the topographic correction, which will cause overcorrection in other parts of the profile.

To calculate the model radiation intensity digital terrain data are needed. In regions where no DTM data are available the topography can be constructed using the difference between barometric altitude (altitude above sea level) and radar altitude (altitude above ground) both continuously recorded during measurements. Both methods show very similar results, so in our opinion the fast 2D correction based on barometric altitude data is sufficient for practical applications. In addition the 2D method allows topographic correction in surveys even where no digital terrain data are available.

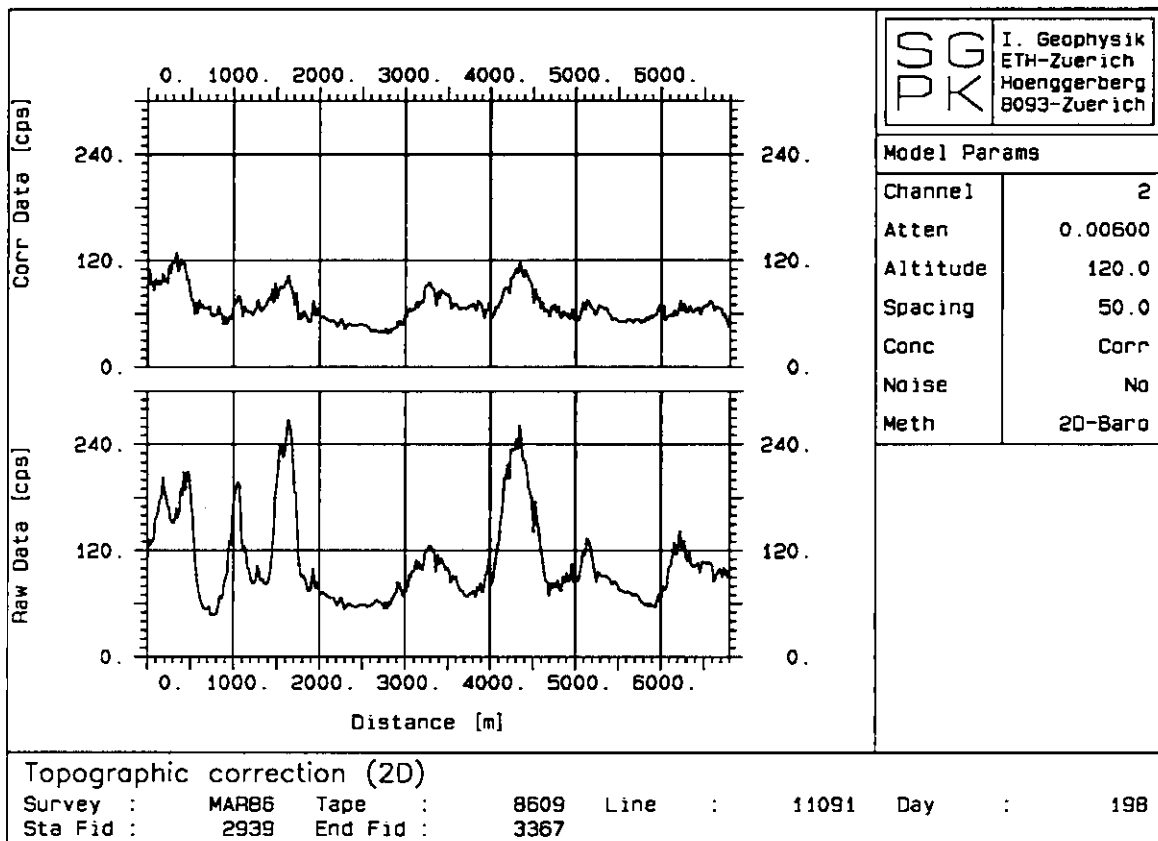


Figure 3.4 : Topography correction (2D) of flight line 11091 (survey Marecottes) calculated from terrain data based on radar- and barometric-altitude. The upper chart shows corrected count rate in the potassium window (1.37-1.57 MeV), the bottom chart the corresponding uncorrected data. The peaks at 1600 m and 4300 m are located over rivers, see text.

3.8 Conversion to general units

The conversion of the measured detector-specific count rates to commonly used units needs two parameters: the detector efficiency and the detector sensitivity. The detector efficiency is defined as the ratio incoming gamma photons/registered photons. The detector sensitivity is the actual conversion coefficient. Both parameters are energy dependent and have to be determined for every window. The detector sensitivity is depends also on the activity distribution and the geometry of the source.

Like the stripping factors, the detector sensitivity is ideally determined with calibration pads. Since the radioisotope content in the pads is precisely known, the detector sensitivity can directly be determined. The determination without pads is based on the detector efficiency and model calculation of the gamma ray flux.

For detector efficiency determination a Cs^{137} and a Co^{60} source each of an activity of 1.8 GBq (50 mCi) were used. The measurements were carried out at distances of 30.5 m, 61 m, 91.5 m, 122 m and 152.5 m (180 s each). Additionally the natural background was recorded at every altitude.

The count rate of a point source at a distance x after removal of the background is given by:

$$I(x) = \frac{Q \cdot \varepsilon \cdot s}{4\pi \cdot x^2} \cdot e^{-\mu_a \cdot x} \quad (3.13)$$

$I(x)$	Count rate	[cps]
ε	Detector efficiency	[counts/ γ]
s	Detector cross section	[m ²]
μ_a	Attenuation coefficient of air	[m ⁻¹]
Q	Specific gamma activity of the source	[γ /s]

The detector efficiency ε and the attenuation coefficient μ_a are determined with linear regression.

Table 3.7 : Results of the determination of the detector efficiency ε at the energies 660 keV and 1330 keV (Measurements with a Cs^{137} and a Co^{60} calibration source on the 29.8.1989 in Spiez/BE)

Nuclide	Energy [keV]	Q [γ /s]	ε [counts/ γ]	μ_a [m ⁻¹]
Cs^{137}	660	1.57E9	0.43	.0092
Co^{60}	1330	1.81E9	0.29	.0075

The detector efficiency in the potassium, uranium and thorium window can be derived from the experimentally determined detector efficiencies at 660 keV and 1330 keV using the following approximation of the efficiency curve of sodium iodide detectors (Grasty, 1975):

$$\varepsilon(E) = D \cdot E^c \quad (3.14)$$

$\varepsilon(E)$	Efficiency curve	[counts/ γ]
E	Gamma energy	[keV]
D, c	Detector constants	

Introducing the experimentally determined efficiencies from table 3.7 in equation 3.13 we get $D=16.3$ and $c=-0.56$ for the detector constants. The detector efficiency for every window can now be calculated (Table 3.8).

Table 3.8 : Detector efficiency in the energy windows.

Window	Energy [keV]	ε [cnt/ γ]
Potassium	1460	0.28
Uranium	1765	0.25
Thorium	2615	0.20

The detector sensitivity at flight altitude can be calculated from the detector efficiency using the following formula:

$$z_h = F_\gamma \cdot s \cdot \varepsilon \cdot E_2(h \cdot \mu_a) \quad (3.15)$$

z_h	Detector sensitivity at flight altitude h	[cps·kg/Bq]
F_γ	Gamma ray flux (per concentration unit)	[γ ·kg/Bq/s/m ²]
ε	Detector efficiency	[counts/ γ]
s	Detector cross section	[m ²]

The gamma ray flux F_γ at ground level, was taken from model calculations of Løvborg et al. (1975) (fourth column, table 3.9). The sixth column of table 3.9 contains the detector sensitivities determined that way for a flight altitude of 120 m.

A second method for determining the detector sensitivity is given by ground measurements. High precision in-situ gamma spectrometric measurements were made at several locations around the nuclear power plant Beznau and the Paul Scherrer

institute (Leupin, 1990 and Murith et al., 1990). Furthermore the radionuclide activities of several rock types in the surveyed areas have previously been determined by gamma spectrometric measurements on rock samples (Kissling, 1976; Labhart and Rybach, 1971; Schärli, 1989).

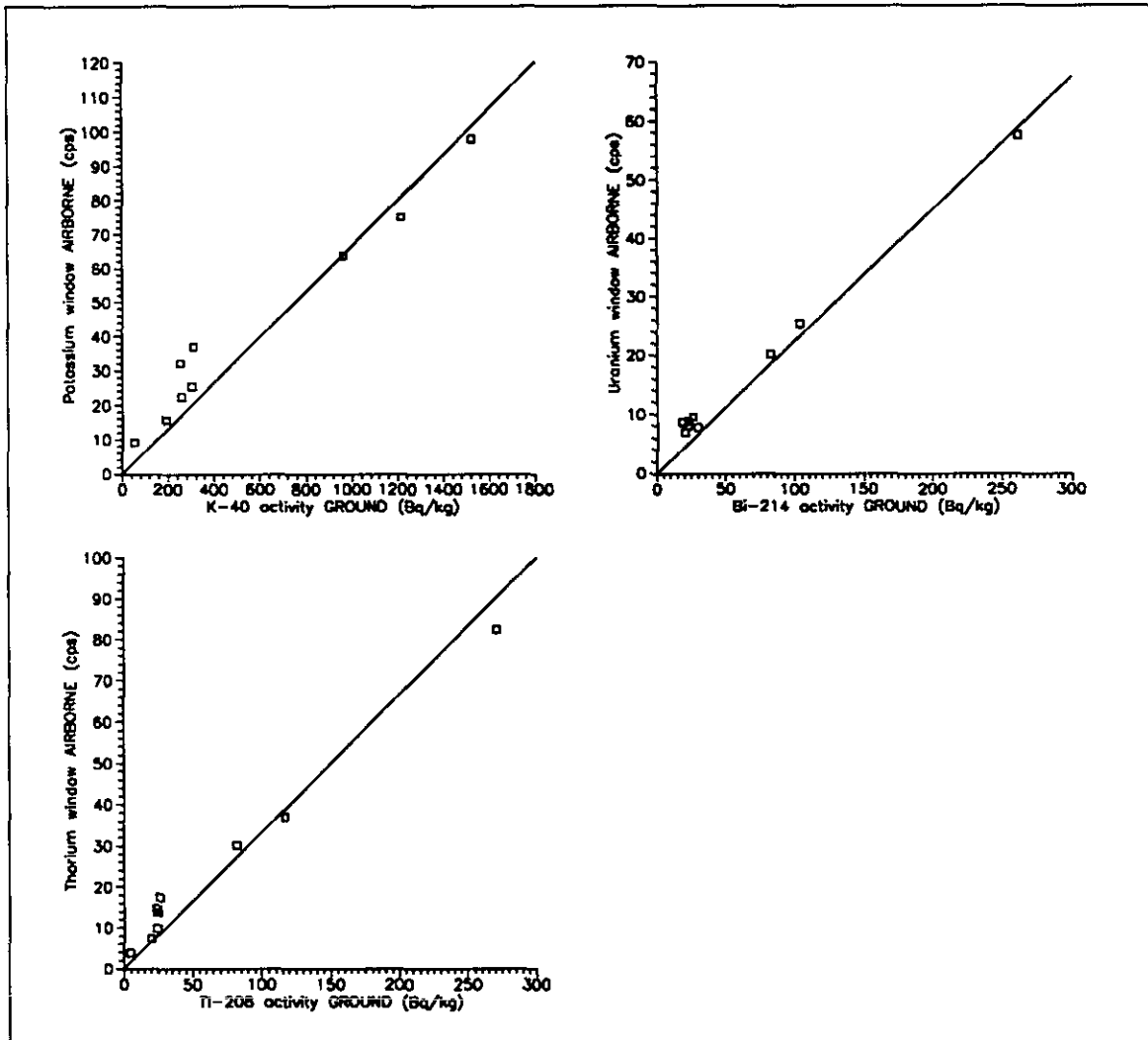


Figure 3.5 : Experimentally determined detector sensitivities

The count rates measured with the airborne system are plotted against the activity determinations at ground in figure 3.5. The ratio of count rate and ground activity gives the detector sensitivity for the specific flight altitude. The data plotted in figure 3.5 were recorded at a flight altitude of 120 m. The detector sensitivities for this altitude can be determined from the charts. Their values are: 7 cps in the potassium window per 100 Bq/kg K^{40} , 23 cps in the uranium window per 100 Bq/kg Bi^{214} and 33 cps in the thorium window per 100 Bq/kg Th^{232} .

The straight lines in figure 3.5 represent the average detector sensitivities for every window.

Table 3.9 :Summary of the detector sensitivity determinations (120 m above ground).

Window	Radio nuclide	Activity [Bq/kg]	γ -Flux [$\gamma/s/m^2$]	Dose rate [nSv/h]	Z_{ETH} Model [cps]	Z_{ETH} Exp. [cps]	$Z_{EG\&G}$ Lit. [cps]
Potassium	K^{40}	100	850	5	9	7	9
Uranium	Bi^{214}	100	2220	52	28	23	28
Thorium	Tl^{208}	100	4510	73	41	33	48

Table 3.9 shows that the experimentally determined detector sensitivities (Z_{ETH} -Exp.) are generally smaller than the detector sensitivities derived from the detector efficiency (Z_{ETH} -Model). The reference values in the last column were determined by the detector manufacturer on a system of the same type (EG&G Geometrics, 1980).

Using the tabulated detector sensitivities, the count rates can easily be converted to the equivalent ground activities. The values listed in the fifth column allow the calculation of the dose rate.

4 Data presentation and errors

4.1 Map generation

The flight maps used for navigation are of 1:25'000 scale. The planned flight path and the flight obstacles are marked on the maps. The navigation was done visually based on these flight maps, trying to follow the planned path as precisely as possible. The deviation from the planned flight path is generally less than 100 m. The nominal flight altitude of 120 m is controlled by the radar altimeter.

The flight camera takes a picture of the overflown ground every three seconds. The fiducial number is lighted up on the film so that the picture later can be identified. The flight path is reconstructed using these pictures, by comparing the pictures to topographic maps. Striking objects like houses, rivers, roads can be localized with a precision of 10 m to 50 m. The position of the center of the picture is marked on the map together with its fiducial number. This time consuming process is called spotting. The reconstructed flight path is digitized afterwards and assigned to the measured data. Examples of flight path maps are shown in chapter 5.

The density of the measurement points varies strongly within a surveyed area. Along the flight lines a measurement is taken every second, which corresponds to a distance of 25 m between two measurements at a flight speed of 90 km/h. The spacing between the flight lines is with 500 m much wider.

For the data representation on maps the data should be available in form of regular grids. The interpolation cannot be performed with standard methods (as used in aeromagnetism for example) for two reasons:

- The special behavior of the gamma ray field cannot be approximated by a smooth function, because it contains abrupt steps at rock boundaries for example.
- The statistical error of airborne radiometric data is very large, so that the value of a single measurement point is not significant.

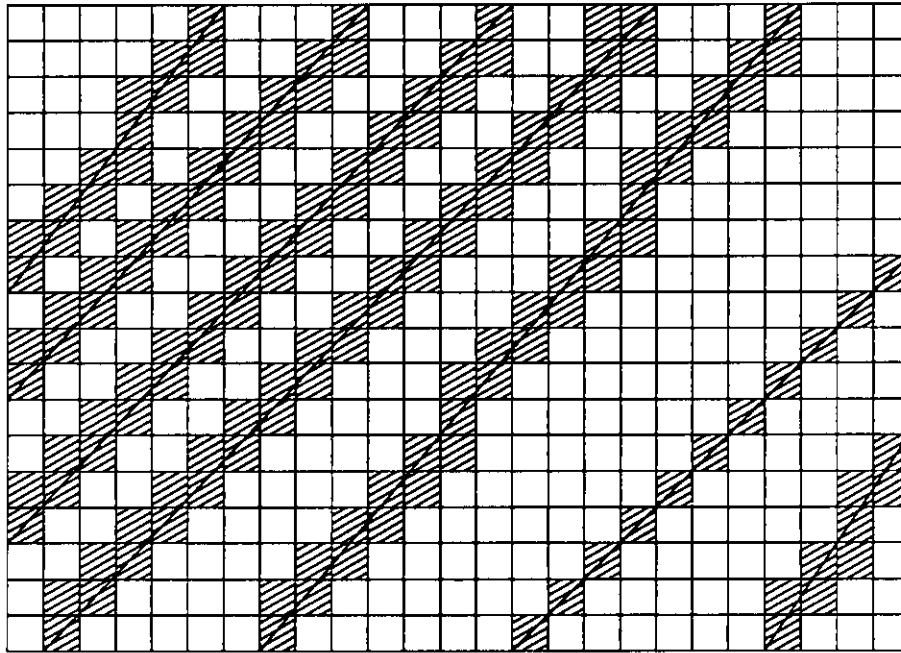


Figure 4.1: Grid and flight path

A simple method also used in image processing was therefore chosen for the interpolation (Green, 1987). The surveyed area was subdivided into squares of equal size (pixels). To every pixel is assigned the average of all values contained in it. The pixel size is 250 x 250 m which corresponds roughly to the field of view of the detector at a flight altitude of 120 m (see fig 2.2).

Since the line spacing is 500 m, only half of the pixels will contain data without interpolation (see figure 4.1). The remaining pixels are filled with the average of the surrounding neighbors if they have at least three already assigned neighbors. This procedure is repeated until the grid is completely filled. It has to be mentioned that the original values are not changed by this interpolation procedure.

Because of the large errors of airborne radiometric data (see chapter 4.2) it is difficult to perform a grid equalization. The cross lines are therefore not used for the map generation, but they serve for the control of data quality. The map was smoothed using a 3 x 3 running average box filter. The error of localization (+/- 50 m) is small compared to the pixel sizes and can therefore be neglected. The deviations from the planned flight path should nevertheless be kept small, otherwise the coverage will not be constant.

For the representation of the data in form of maps there are three different possibilities:

- **Isoline maps:** This classical representation form is not very well suited for airborne radiometric data since the values show large scattering, so that the data have to be smoothed strongly before plotting. To increase readability of the maps colored isolines should be used to code the intensities.
- **Pixel maps:** Pixel maps use colored boxes to display the data. Pixel maps are especially suited for the presentation of unsmoothed data, since rough errors are less perturbing in this form of map.
- **Surface representation:** The data are displayed as a three dimensional surface. The surface can likewise be colored. The surface representation allows a good visual overview over a region. It is especially suited for the display of large activity contrasts. The surface diagrams were made with the help of the "SURFER" program of Golden Software Inc. (Golden, Col.).

4.2 Significance and errors

Radiometric measurements always show a large statistical scattering. The total error is composed of numerous sources. The four most important are:

- **Error of the measurement:** The values of radiometric measurements follow a Poisson distribution. Even a measurement on a perfect instrument will have an error corresponding to the square root of its value. Especially at low count rates the relative error will be very large.
- **Errors of correction factors:** The correction factors themselves are experimentally determined with the aid of radiometric measurements and have therefore errors. The errors of the correction factors are listed in the corresponding sections.
- **Simplified correction methods:** In the derivation of the correction methods some simplifications were made, that do not necessarily correspond to reality. The normalization corrections (see chapter 3.1) for example depend on a homogeneous activity distribution in the ground. Other perturbations like soil humidity or atmospheric radon is not corrected at all.

- **Systematical errors:** Systematical errors can occur for example when the measuring equipment is not working properly.

The error of the measurement itself and the influence of imprecisely determined correction factors can be determined with the error propagation equation. The error introduced by simplified correction methods can only be estimated roughly since the relevant parameters generally are not known. Systematical errors also cannot be quantified. Nevertheless the precision error as calculated with the error propagation equation gives a good indication on the data quality. If the data is already inadequate with the precision error it will be definitely inadequate with the larger absolute error.

Instead of using the complete error propagation equation a simpler empirical approximation formula proposed by EG&G Geometrics (1980) can be used. The difference between the approximation formula and the complete error propagation equation is usually less than 10% (Schwarz, 1991). The error of a corrected measurement is given by:

$$\Delta I_{corr} = 1.5 \cdot \sqrt{I_{corr} + \sum |I_{CT}|} \quad (4.1)$$

ΔI_{corr}	Error of the corrected measurement
I_{corr}	Corrected count rate
$\sum I_{CT} $	Sum of the corrections applied

As expected, the error of single measurements is very large especially in windows with low count rates. As can be seen from formula 4.1 the corrections applied to a measurement contribute essentially to the error. The relative contribution of the helicopter background, the cosmic and the altitude correction is approximately equal for all windows. But there are great differences regarding the stripping corrections. The largest stripping corrections apply to the uranium window, so that this window shows the largest errors.

The data displayed on radiometric maps normally represent an average of several single measurements. With a pixel size of 250 x 250 m and a measurement taken every 25 m a pixel represents the mean of ten measurements, which reduces the error of the displayed pixel considerably. Of course the error also reduces with increasing count rate.

Table 4.1 : Relative errors of airborne measurements (example from Swiss Molasse basin)

Window	Relative error of a single measurement [%]	Relative error of five averaged measurements [%]	Relative error of ten averaged measurements [%]
Total	8	4	3
Potassium	28	13	9
Uranium	56	22	17
Thorium	33	13	10

If the relative error of a pixel map is less than 30%, it is considered as statistically significant (Purvance and Novak, 1983). Table 4.1 shows that this limit is normally achieved after averaging five samples. The choice of the significance level is of course disputable and depends on the specific application.

Only the error of the count rate has been discussed until now. When converting the airborne count rates to ground activities additional perturbing effects have to be considered.

For a constant ground activity a lower count rate is measured over forests than over meadows due to the additional absorption by trees. For a simple approximation one can estimate the influence of trees by replacing them by a homogeneous layer having the same biomass. The attenuation of such a layer is given by the expression $I = I_0 \cdot e^{-\mu \cdot d}$, where I is the measured count rate, I_0 is the count rate without additional absorber, μ is the attenuation coefficient and d is the thickness of the absorber.

The biomass of a forest can be derived roughly from its wood stock volume (ignoring the contributions from leaves and bushes). The wood stock volume in the Swiss Mittelland is around 300 m³/ha and 500 m³/ha (EAFV, 1988). In the Alps these values are something lower (100 m³/ha to 300 m³/ha). Therefore the resulting equivalent layer has a thickness of 1 cm to 5 cm. The attenuation of such a layer varies between 5% and 25% (using an attenuation coefficient of $\mu = 5 \text{ m}^{-1}$ (Adams and Gasparini, 1970)).

Soil humidity and rain also influence the measurements. Additional water increases the soil density and therefore the self absorption. Kogan et al. (1969) estimate the effect of soil humidity to be 5% to 10%. This effect is especially troublesome because the soil humidity varies with time.

The repeated measurements in the regions surrounding the Swiss nuclear installations (Schwarz et al., 1989, 1990, 1991) allow a first estimation of the reproducibility of airborne radiometric measurements. The comparison of the results from 1989, 1990, 1991 show that the relative activity distribution can be reproduced very well in every window. But the results show a more or less constant deviation from the mean values over the whole areas. The deviation is about 10% for the total count window, 20% for the potassium window and 30% for the uranium and thorium window.

This deviation could have several reasons like: differences in the soil humidity, fluctuations of the radon concentration, systematic errors and so on.

4.3 Digital processing of airborne radiometric maps

In this section some post-processing methods for digital radiometric maps will be described. The aim of these methods is to simplify the visual interpretation of the maps. The processing techniques are used to suppress undesirable or redundant information and to enhance the important features. Applying these methods it has to be considered that they already represent a kind of an interpretation of the map content.

Activity distribution maps are tainted with large incertitudes as demonstrated in section 4.2. The effects of forests and soil humidity but also uncompletely removed topographic effects are especially annoying. These effects can distinctly reduced with the aid of ratios. The ratio of two windows is less affected by an additional absorber than the single window values, since the ratio is only affected by the difference of the attenuation coefficients of the two windows. Ratios are especially suited for representation of uncorrected raw data. For the representation of natural radioactivity the potassium/total, the uranium/total and the thorium/total ratios are used.

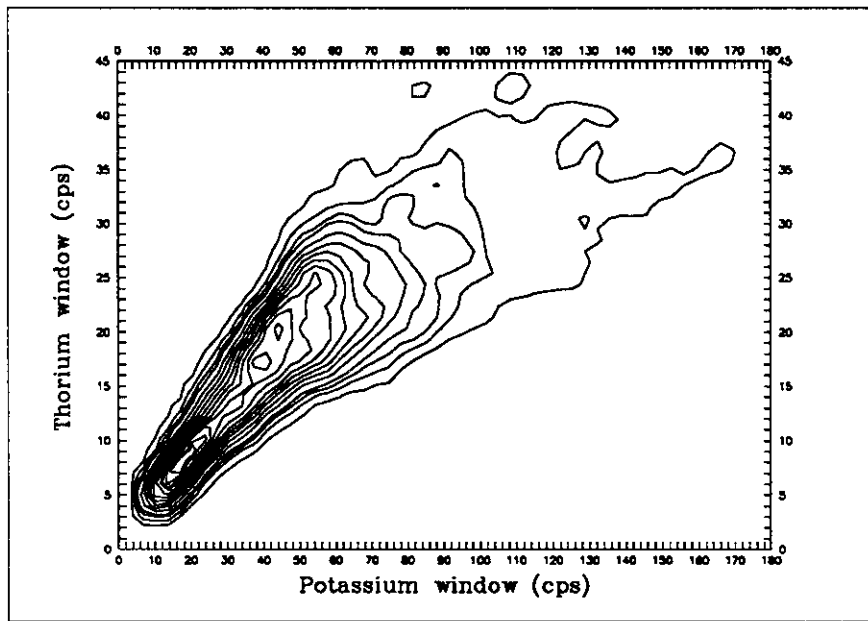


Figure 4.2: Scattergram of the potassium and the thorium window. The isolines represent lines of equal relative incidence.

The maps of the natural radioisotopes are all very similar because of the strong correlation between the radioelements due to geochemical reasons. An example for this fact is shown in figure 4.2. It is the scattergram of the potassium and the thorium window. The isolines represent lines of equal relative incidence and show the strong correlation of the two windows. The high correlation has been observed not only in a variety of airborne surveys (Saunders et al., 1987; Green, 1987) but also by radiometric laboratory measurements on Swiss rocks (Rybach and Labhart, 1973).

Working with ratios will therefore not only reduce disturbing effects, but also reduce the contrast of the image. A very good method to increase the contrast and with it the interpretability of an image is called histogram equalization (Haberäcker, 1985). After histogram equalization every color covers the same area on the map. The visual impression of such a representation is optimal. As a consequence the color scale becomes nonlinear.

Ternary maps are used for geological purposes. In this representation the maps of potassium, uranium and thorium are merged into a single map. The color red is assigned to the potassium window. Uranium and thorium are colored green and blue respectively. The three colors are added like in the additive color model (Smith, 1978). Regions with a high relative potassium content will appear in red color shades on the map. Correspondingly areas with a high relative uranium or thorium content

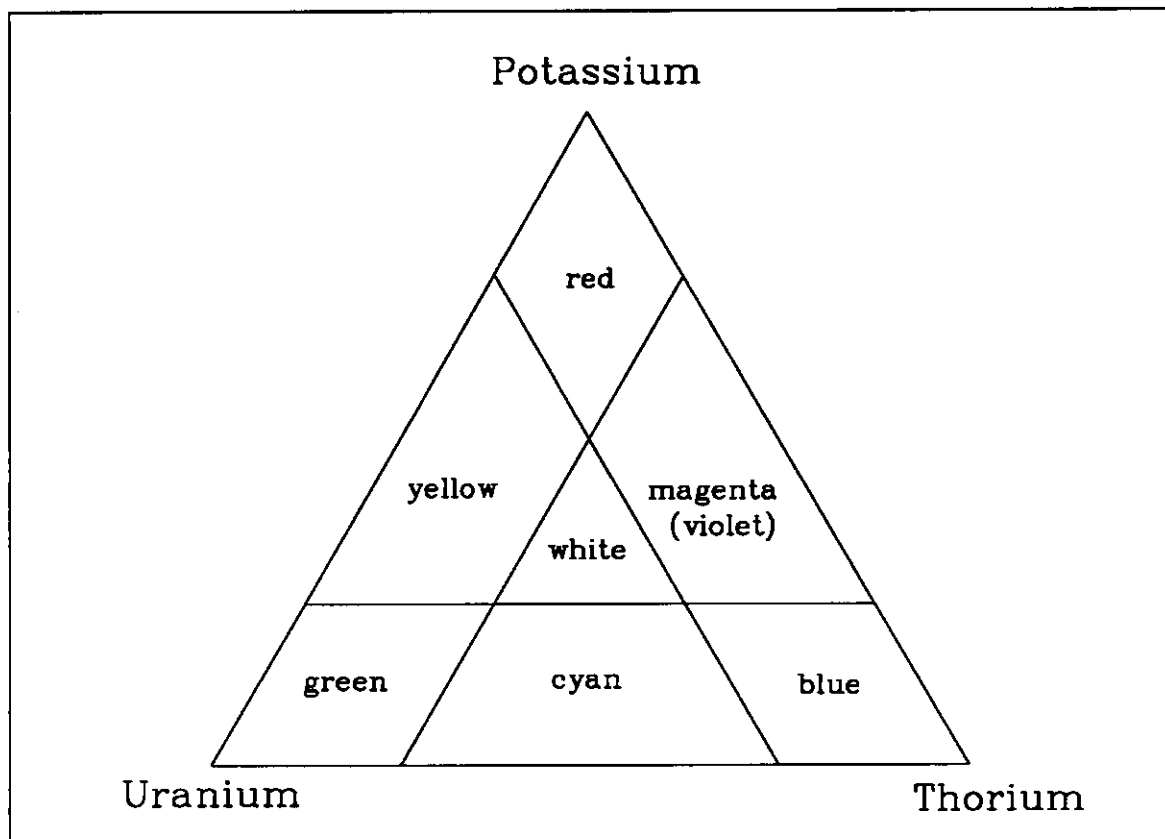


Figure 4.3: Color diagram for ternary radioelement maps.

will appear in green or blue shades. Regions with equally balanced radioisotopes will be plotted as gray or white shades depending on the total activity (see figure 4.3).

5.1 Selection of the survey areas

Since it was not possible to cover the entire area of Switzerland by the airborne measurements due to financial limitations the main attention was focused on the crystalline rocks of the Central Massifs of the Swiss Alps because of their relatively high natural radioactivity. Figure 5.1 gives an overview of the surveyed regions.

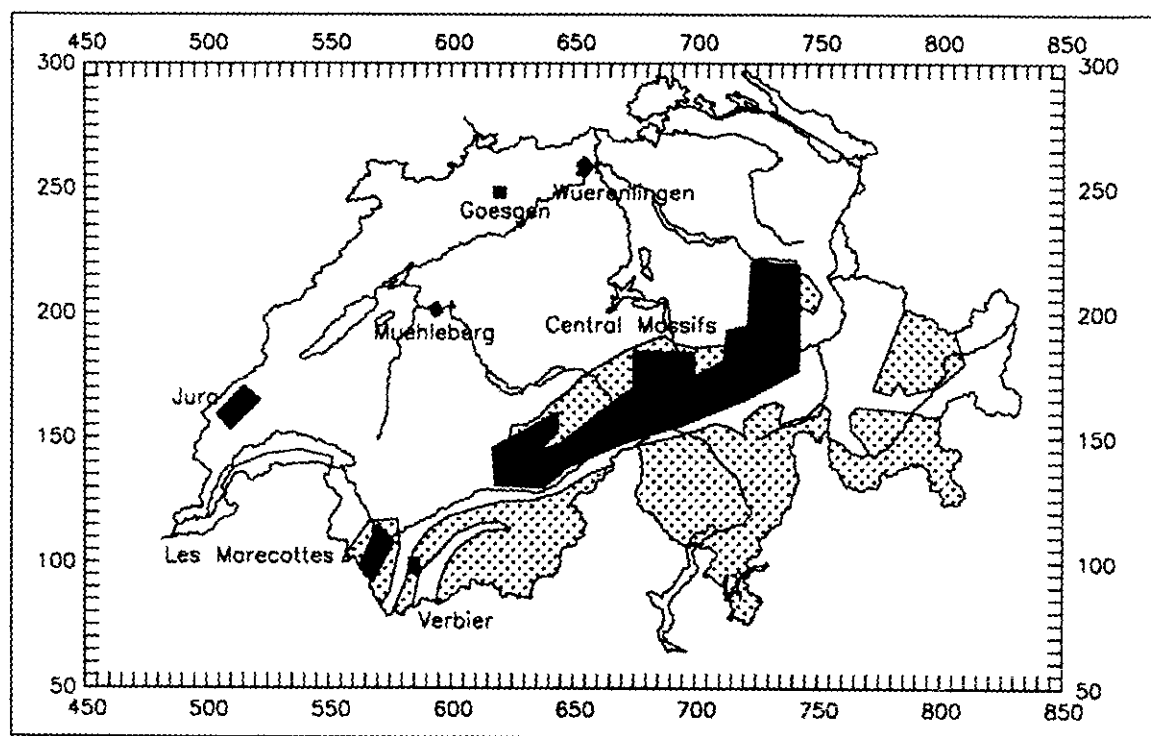


Figure 5.1: Overview of the surveyed areas (black). Stippled areas; crystalline rocks.

The main survey area (Central Massifs area) extends from the valley of Lötschental to the Walensee lake in a strip of a width of 10 to 30 km. The area of this survey is about 2800 km² and covers the major part of the Central Massifs. To the north of the Central Massifs also alpine sediments with previously known uranium mineralizations (Verrucano) have been surveyed as well as the metasedimentary cover of the massifs to the south.

Besides the main area several regions with characteristic lithology of Switzerland have been covered with smaller surveys. The Quaternary gravel terraces, the Tertiary of Molasse Basin (area "Mühleberg") and the limestones of the Jura (areas "Würenlingen", "Gösgen" and "Lac de Joux") where surveyed in connection with the project for the surveillance of the Swiss nuclear installations (see 1.3).

Also the regions "Les Marecottes" and "Verbier" (Aiguilles Rouges massif, Bernhard Nappe) with previously known uranium mineralizations have been surveyed. A geological overview of all the surveyed regions is be given in chapter 6.

5.2 Flight statistics

After some instrumental tests the production survey started in 1986. The measurements where carried out during summer or early autumn because of more stable meteorological conditions in these periods. Furthermore there lies less signal absorbing snow in the mountains at that time.

The complete project lasted from 1986 to 1991. The measurements started with two pilot surveys at "Les Marecottes" and "Verbier" in 1986. In the same year the systematic survey of the "Central Massifs" was started.

Table 5.1: Compilation of the flight data

Year	Survey areas	Flight time [h]	Flight line [km]	Covered area [km ²]
1986	Central Massifs, Les Marecottes, Verbier	37	920	460
1987	Central Massifs	37	1'160	580
1988	Central Massifs	27	950	480
1989	Central Massifs	24	800	400
1990	Central Massifs	24	940	470
1991	Central Massifs, Lac de Joux	37	1'340	670
Total		186	6'110	3'060

The region between Sion and the pass of Grimsel was surveyed in the period of 1986 to 1987. Supported by the Swiss air force the region of Murgtal/Weisstannental was measured in the same years. 950 km of flight lines were measured in the Gotthard area in 1988. This was followed in 1989 by the survey in the Vorderrhein valley between Flims and Brigels. In summer 1990 the remaining part between Brigels and the Gotthard pass could be covered (800 km flight lines). The measurements of 1991 concentrated on the region north of the Gotthard pass (between the village of Erstfeld and the Gotthard pass) and on the region south of the Lac de Joux in the Swiss Jura. Remaining gaps in the area of Murgtal/Weisstannental could also be covered.

A compilation of the flight data can be found in table 5.1. Totally over 6000 km of flight lines have been flown which corresponds to a surveyed area of 3000 km².

6 Geological Overview

The three main geological units of Switzerland are, from north to south, the Jura, the Molasse Basin and the Alps.

6.1 Jura

The Jura mountains form the north-western boundary of Switzerland. The radio-metrically surveyed areas are located at the eastern (Aargau Jura) and the western end (Vaud Jura) of the Swiss Jura.

6.1.1 Aargau Jura

The Aargau Jura is situated at the easternmost part of the Jura mountains, where it terminates as a single fold underneath the Molasse. The outcropping sediments mainly originate from the Upper Jurassic (Malm, Dogger). They consist mainly of marl shales with a few layers of limestone and black clays (Wildeggen-formation, Opalinus clay). Limestones can only be found in the Upper Dogger (Hauptrogenstein).

6.1.2 Vaud Jura

In the Vaud Jura Malm- and Cretaceous-limestones are dominating at the surface. On the southern border of the survey area "Lac de Joux" also a part of the Molasse Basin was surveyed.

6.2 Molasse Basin

The Molasse Basin lies between the Jura and the Alps. The radiometrically surveyed regions belong all to the Lower Freshwater Molasse. It consists essentially of Tertiary detrital formations (sandstones, conglomerates), mainly derived from granitic units from the uplifting Alps.

6.3 Alps/Crystalline units

The main survey area covers the major part of the Central Massifs of the Swiss Alps, which are the Aar Massif in the north and the Gotthard Massif in the South. In between the two large massifs lies the smaller Tavetsch massif somewhat more to the east. Figure 6.1 shows a simplified geological map of the Central Massifs and the adjacent sediments.

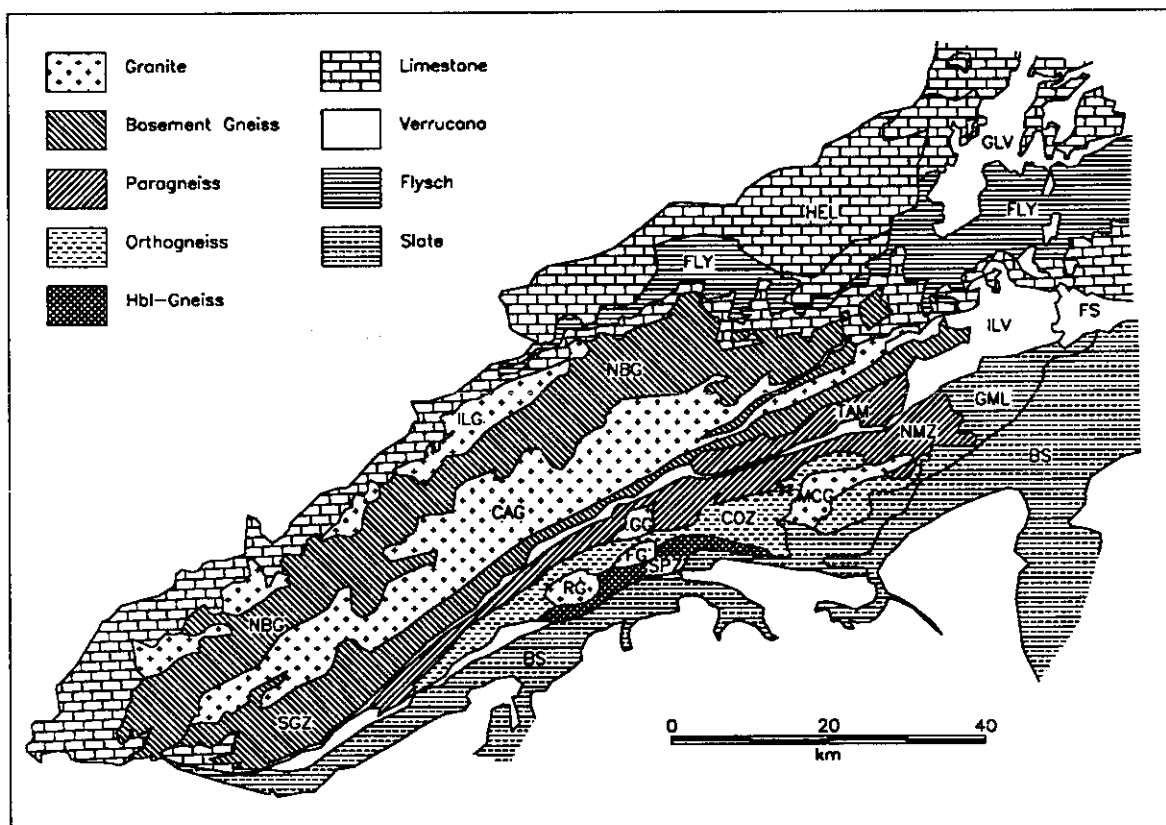


Figure 6.1: Geological map of the Central Massifs and the adjacent sediments.

In western Switzerland the Aiguilles-Rouges Massif and the Bernhard-Nappe were investigated with the survey areas "Les Marecottes" and "Verbier".

6.3.1 Aar Massif

The Aar Massif is the largest of the Central Massifs. It dips down to all sides (with exception of its southern border) like a dome and can be divided from north to south into four long stretching zones:

- The Zone of the Innertkirchen/Lauterbrunnen Granite (ILG, figure 6.1) consisting of granites interspersed with clods of gneiss.
- The Northern Basement Gneisses (NBG, figure 6.1) consisting of monotonous orthogneisses with inclusions of calc-silicate and serpentinite. Amphibolites are very common.
- The Central Aar Granite (CAG, figure 6.1) is formed by large masses of acidic, porphyritic granites. With an area of more than 550 km² it is the largest granite body of Switzerland.
- The Southern Gneiss Zone (SGZ, figure 6.1) with an important portion of "Augengneisses". Close to the village of Naters where small uranium mineralizations were found (Gilliéron, 1986).

Several smaller batholithic stocks break through the older basement rocks. One of them, the Giuv Syenite contains remarkably high amounts of thorium and uranium (Labhart and Rybach, 1971).

The Southern Gneiss Zone is covered completely by the survey area. The Northern Basement Gneisses and the Central Aar Granite were partially surveyed at the Lötschental and the Reusstal. The central part of Northern Basement Gneisses and the Innertkirchen/Lauterbrunnen Granite were not covered because of the numerous glaciers in this region.

6.3.2 Gotthard Massif/Tavetsch Massif

On its northern border the Gotthard Massif is limited by the Urseren Zone. This narrow, steeply dipping but important band of Mesozoic rocks separates the Gotthard Massif from the Aar Massif. The Gotthard Massif was strongly affected by the alpine orogenesis. Its rock units and massif borders were strongly deformed. Like the Aar Massif the Gotthard Massif can be subdivided in several parallel zones:

- The Northern Metasediment Zone (NMZ, figure 6.1) mainly formed by biotite-schists with multifarious inclusions such as calc-silicates, metaperidotites and amphibolites.
- The Central Orthogneiss Zone (COZ, figure 6.1) consisting of granitic gneisses also called "Streifengneis".
- The Southern Paragneiss Zone (SPZ, figure 6.1), with hornblende-garnet schists.

Two clusters of Hercynian granitoids can be observed in the Gotthard Massif. The first consists of the Gamsboden Granite (GG), the Fibbia Granite (FG, both strongly alpine deformed) and the younger Rotondo Granite (RG) with granitic (irregular) fabric near the Gotthard pass. The second cluster at the Lucomagno pass is formed by the Medels Granite and the Cristallina Granodiorite (MCG).

The Tavetsch Massif (TAM, figure 6.1), which thrusts between Aar and Gotthard Massif in the Vorderrhein valley, consists of paragneisses. It is separated from the Gotthard Massif by the Urseren Zone. Both Gotthard Massif and Tavetsch Massif are completely covered by the survey.

6.3.3 Aiguilles-Rouges Massif

The peripheral part of the Aiguilles-Rouges Massif consist of paragneisses with inclusions of amphibolite, quartzite and marble. The central zone of the massif is built by a narrow long stretching granitic body, the Vallorcine Granite. Unlike to the situation at the Aar Massif an actual central granite is missing. Both the basement and the Vallorcine Granite contain small uranium mineralizations near Finhaut and La Creusa (Gilliéron, 1986; Labhart et al., 1971).

6.3.4 Bernhard Nappe

The whole region of the southern Wallis between the river Rhône and the Simplon pass is covered by the Bernhard/Monte-Rosa nappes complex. The crystalline portion, the Casanna schists, is built by gneisses, metamorphic granites, gabbros, conglomerates and quartzites. All the rocks are weakly alpine metamorphic and contain small uranium mineralizations in the region of Verbier (Gilliéron, 1986).

6.4 Alps/Sediments

The Helvetic belt is situated to the north of the Central Massifs. It is composed of Permian, Mesozoic and Tertiary sediments. The latter were surveyed in the region south of the lake of Walensee. To the south of the massifs the Mesozoic sedimentary cover of the Gotthard Massif and a smaller part of Penninic units were covered (geological map see fig 6.1).

6.4.1 Helvetic belt

The Helvetic nappes cover a large homogeneous area northwest of the Central Massifs. The nappes comprise mainly Permian, Jurassic, Cretaceous and Eocene sedimentary rocks. In the eastern part, the Glarus Alps, which were covered by airborne radiometric measurements, four important lithological units can be distinguished:

- The Verrucano of the Glarus Nappe (GLV, figure 6.1). It forms a stack of 1600 m thickness and a surface of over 200 km² of red Permian conglomerates, sandstones and schists with layers of volcanics. Uranium mineralizations were discovered in the valleys of Mürtchenalp and Weisstanental (Gilliéron, 1986).
- The Ilanz Verrucano (ILV, figure 6.1) to the southeast. A second Verrucano complex, which was altered by the alpine metamorphism. Uranium mineralizations were discovered near Truns and Waltensburg (Gilliéron, 1986).

ozoic limestones (HEL, figure 6.1): The Helvetic Nappes (Mürtschen, Glarus, Säntis, Malm ,Dogger and Lias nappes) as well as the parautochthonous sediment cover of the Aar Massif consist mainly of limestones.

- Flysch (FLY, figure 6.1): Underneath the Helvetic nappes in the regions of Schächental (south of the pass of Klausen), Serrnftal, Weisstannental and near Ragaz large masses of flysch of various tectonic provenience can be found. Lithologically they consist of clay- and marl-schists with interlaced banks of sand and limestone.

6.4.2 Sediment cover of the Gotthard Massif and the Penninic nappes

The sediment cover of the Gotthard Massif ("gotthardmassivischer Lias", GML) and the Penninic nappes ("Bündnerschiefer", BS) are very similar in the survey area. They are mainly composed of recrystallised alpine epimetamorphic calcareous slates with variable quartz content.

6.5 Quaternary

Large areas of the Molasse Basin are covered by a layer of ground moraine with a thickness of up to ten meters. All important river valleys are filled with gravels. In the Alps, Quaternary was surveyed in the valleys of the Rhône and the Vorderrhein and the Flims rock slide area (FS, figure 6.1). However, in the Alps considerable portions of the bedrock are directly exposed at the surface.

7 Maps

The dose rates of the surveyed areas are compiled on three maps. For the survey area "Central Massifs" three isotope maps (K^{40} , Bi^{214} und Tl^{208}), three ratio maps (Bi^{214}/Tl^{208} , Bi^{214}/K^{40} und Tl^{208}/K^{40}) and a ternary map (see chapter 4.3) are added. To facilitate the comparison of the airborne radiometric data with geology the boundaries of the geologic units of the survey area "Central Massifs" are shown on an overlay transparency.

The presented results were calculated using the corrections described in the text. The maps are in a scale of 1:500'000 with exception of the ternary map which is at a scale of 1:200'000 . For the coordinate system the Swiss national system was chosen.

The units used are: [Bq/kg] for the isotope maps, [nSv/h] for the natural dose rate maps (excluding cosmic background) and [%] for the ratio maps. To convert the radiometrically determined activities (isotope maps) to the corresponding potassium, uranium and thorium contents the following conversion factors can be used: 311 Bq/kg K^{40} =1% potassium, 11.8 Bq/kg Bi^{214} =1ppm uranium und 4.1 Bq/kg Tl^{208} =1ppm thorium. This conversion is correct only if there is radioactive equilibrium, which is not necessary true in the case of uranium and thorium decay series. In literature the corresponding contents are therefore often quoted as eU respectively eTh (equivalent uranium, equivalent thorium). Here we present Bi^{214} and Tl^{208} activity maps.

The data are plotted using a ten color scale (blue-cyan-green-yellow-red → increasing values). To have an optimal representation of the geology the histogram of the isotope and ratio maps was equalized (see 4.3). The value range of the colors is given in the map legends.

7.1 Map captions

The map captions are intentionally kept very short. The radioactivity of the geological units however will be discussed extensively in the next chapter.

Map 1: Dose rate map of the "Central Massifs" (nSv/h)

The crystalline rocks and of the Verrucano clearly stand out from the Helvetic and Penninic sediments. The highest value is found on the Giuv Syenite (maximum value: 510 nSv/h or 4.4 mSv/a).

Map 2: Dose rate map of northwestern Switzerland (nSv/h)

The survey area "Mühleberg" in the Molasse basin shows slightly higher dose rates than the areas "Würenlingen", "Gösgen" and "Jura" (on map 3) located in the Jura mountains.

Map 3: Dose rate map of western Switzerland (nSv/h)

The two survey areas in crystalline rocks (Les Marecottes, Verbier) show the highest values on the map. The "Jura" shows clearly lower dose rates.

Map 4: K^{40} -map of the "Central Massifs" (Bq/kg)

The central zones of the Aar and the Gotthard Massifs show elevated activities. The highest activity can be found in the Glarus Verrucano on the northern border of the survey area.

Map 5: Bi^{214} -map of the "Central Massifs" (Bq/kg)

The Gotthard Massif shows with exception of the Granitoids (Rotondo, Fibbia and Gamsboden Granite) relatively low values. The rocks of the Aar Massif have generally higher activities. The maximum value is bound to the Giuv Syenite.

Map 6: Tl^{208} -map of the "Central Massifs" (Bq/kg)

High activities can be found in the Central Aar Granite and in the Rotondo Granite. The maximum value is again bound to the Giuv Syenite.

Map 7: $\text{Bi}^{214}/\text{K}^{40}$ -ratio map of the "Central Massifs" (%)

The limestones and the Southern Gneiss Zone of the Aar Massif show relatively high $\text{Bi}^{214}/\text{K}^{40}$ -ratios.

Map 8: $\text{Bi}^{214}/\text{Ti}^{208}$ -ratio map of the "Central Massifs" (%)

The $\text{Bi}^{214}/\text{Ti}^{208}$ -ratio map is very similar to map 7. Again the limestones and the Southern Gneiss Zone of the Aar Massif show the highest ratios.

Map 9: $\text{Ti}^{208}/\text{K}^{40}$ -ratio map of the "Central Massifs" (%)

The slates of the "Bündnerschiefer" and the sedimentary cover of the Gotthard Massif appear very clearly in the $\text{Ti}^{208}/\text{K}^{40}$ -ratio map.

Map 10: Ternary map of the "Central Massifs" (1:500'000)

The ternary map can almost be read like a geological map. All lithological units can be distinguished very well.

Map 11: Ternary map of the "Central Massifs" (west, 1:200'000)

See map 10.

Map 12: Ternary map of the "Central Massifs" (center, 1:200'000)

See map 10.

Map 13: Ternary map of the "Central Massifs" (east, 1:200'000)

See map 10.

Map 14: Boundaries of the geologic units of the "Central Massifs"

To facilitate the comparison of the airborne radiometric data with geology the boundaries of the geologic units of the survey area "Central Massifs" are shown on an 1:500'000 scale overlay transparency.

8 Characteristic geological settings

8.1 Jura

The Jura shows generally low radioactivity values. At such low activity levels forest areas have a disturbing effect (see 4.2) by absorbing the radiation of the ground. The forests can therefore easily be recognized by their low count rates on the maps. Furthermore areas of farming have generally higher K^{40} activities because of potassium rich fertilizers. Both effects complicate the interpretation since forests and agricultural areas are often correlated with geology in the Jura.

The airborne measurements were carried out in two small survey areas in the Aargau Jura, where marly rocks are dominating and in a survey area in the Vaud Jura where only limestones occur. As can be seen from table 8.1 the two rock types can be separated radiometrically

Table 8.1: Rock activities and dose rates of the Jura

Geological unit	Subunit	Dose rate [nSv/h]	K^{40} [Bq/kg]	Bi^{214} [Bq/kg]	Tl^{208} [Bq/kg]
Jura	Aargau Jura	66	450	31	37
	Vaud Jura	42	240	28	21

8.2 Molasse basin

The radioactivity values of the lower Freshwater Molasse are generally higher than of the Jura. This agrees with the origin of the Molasse sediments which mainly derive from crystalline primary rocks (see table 8.2).

Table 8.2: Rock activities and dose rates of the Molasse basin

Geological unit	Subunit	Dose rate [nSv/h]	K ⁴⁰ [Bq/kg]	Bi ²¹⁴ [Bq/kg]	Ti ²⁰⁸ [Bq/kg]
Molasse basin	Lower Freshwater Molasse	74	630	32	36

8.3 Alps/Crystalline units

The important geological information can easily be taken from the ternary maps (Maps 10, 11, 12 and 13). They can almost be read like a geological map. The significance of the color shades is explained in chapter 4.3; for activity relations see table 8.3.

The rocks of the Aar Massif have all a relatively bright slightly bluish or violet color. The Northern Basement Gneisses is colored by a dirty violet. The Central Aar Granite stands clearly out with its white color. The Southern Gneiss Zone marks off less clearly. It is most often somewhat darker and bluer than the Aar Granite.

The Gotthard and the Tavetsch Massif show mostly reddish colors. The northern Paragneiss Zone is with the exception of its easternmost part mostly dark violet. The Central Orthogneiss is obviously brighter and has scattered yellow spots. The Southern Paragneiss Zone shows almost no radioactivity and appears very dark. The Fibbia/Gamsboden Granite (green white) and the Rotondo Granite (blue white) clearly mark off from the surrounding rocks. The difference at the Medels/Cristallina Granite is less clear. It however contains more white color than the adjacent Orthogneiss. The Tavetsch Massif and the Northern Paragneiss Zone cannot be distinguished by airborne radiometric measurements.

The mean radionuclide contents and the corresponding dose rates of the geological units are compiled in table 8.3.

Table 8.3: Rock activities and dose rates of the Alps/Crystalline units

Geological unit	Subunit	Dose rate [nSv/h]	K ⁴⁰ [Bq/kg]	Bi ²¹⁴ [Bq/kg]	Ti ²⁰⁸ [Bq/kg]
Aar Massif	Lauterbrunnen Innertkirchen Granite	(103)	(780)	(48)	(54)
	Northern Basement Gneisses	122	825	66	63
	Central Aar Granite	160	975	88	90
	Gruv Syenite	384	1470	251	246
	Southern Gneiss Zone	133	795	79	72
Gotthard Massif	Tavetsch Massif	111	750	53	63
	Northern Paragneiss- Zone	113	840	48	63
	Central Orthogneiss Zone	128	1065	52	66
	Southern Paragneiss Zone	87	585	48	45
	Rotondo Granite	194	1125	110	111
	Fibbia/Garnsboden Granite	145	1020	84	69
	Medelser/Cristallina Granite	112	765	53	63
Aiguilles- Rouges Massif	Basement Gneiss	131	930	75	63
	Vallorcine Granite	(131)	(930)	(75)	(63)
Bernhard Nappe	Casanna schists	92	675	53	42

The Giuv Syenite shows the highest Bi^{214} and Tl^{208} activities measured in the survey. The activities determined by the airborne survey of 1470 Bq/kg K^{40} , 251 Bq/kg Bi^{214} and 246 Bq/kg Tl^{208} are in good agreement with measurements on rock samples (1520 Bq/kg K^{40} , 261 Bq/kg Bi^{214} , 271 Bq/kg Tl^{208} ; Labhart and Rybach, 1971).

The numerous uranium mineralizations known from ground measurements (Gilliéron, 1986) could not be detected by airborne measurements because of the limited extension of the mineralizations. In the Swiss Alps the uranium mineralizations are, although they partially show very high uranium concentrations, very small (some centimeters to meters). From the flight altitude of 120 m they can be regarded as point sources and are therefore only hardly detectable. A rough estimation shows that a mineralization should contain at least 100 kg of pitchblende in the uppermost 10 cm of the surface to be detectable. If a small mineralization is not accompanied by a regional elevation of the average uranium concentration (which is apparently not the case in the Swiss Alps) it can not be traced by the airborne survey.

8.4 Alps/Sediments

The ternary maps show less contrast in the sedimentary milieu because of the relatively low radioactivity of sediments. Nevertheless some lithologies can be distinguished on the ternary maps.

The Helvetic sediments normally show in dark shades of color. An exception is the Verrucano. The Glarus Verrucano clearly marks off with a white violet color. The Illanz Verrucano contains less radioisotopes and appears in greenish to yellowish colors to the north and in brown to the south. The Mesozoic limestones are black or dark green. The Flysch shows in black violet color shades. The sedimentary cover of the Gotthard Massif and the "Bündnerschiefer" are black blue on the map.

The mean radionuclide contents and the corresponding dose rates of the geological units are compiled in table 8.4.

Table 8.4: Rock activities and dose rates of the Alps/Sediments

Geological unit	Subunit	Dose rate [nSv/h]	K ⁴⁰ [Bq/kg]	B ²¹⁴ [Bq/kg]	Tl ²⁰⁸ [Bq/kg]
Helvetic Sediments	Glarus Verrucano	105	720	57	54
	Ilanz Verrucano	108	690	66	54
	Mesozoic limestones	76	450	53	36
	Flysch	75	510	40	39
Sediments of the Gotthard massif and the Penninic Nappes	"Gotthardmassivischer Lias"	102	525	75	51
	"Bündnerschiefer"	99	555	70	48

The previously known uranium mineralizations in the Glarus and Ilanz Verrucano could not be detected by means of the airborne measurements for the same reasons as explained in chapter 8.3.

8.5 Quaternary

Normally no difference between the Quaternary deposits and the surrounding bedrock can be seen. The Ilanz Verrucano on the right side of the valley of the Vorderrhein is an exception. It is mostly covered by detritus of the Gotthard massif and shows its values. Furthermore the Quaternary fillings of the valleys of the rivers of the Alps (particularly Vorderrhein and Rhône) show slightly elevated values, possibly due to heavy mineral accumulation.

9 Concluding remarks

The projects have shown that commonly used calibration and reduction procedures following the specifications of the U.S. National Uranium Resource Evaluation (NURE) program can only be used with several modifications and additional correction steps in the extreme topographic conditions of the Swiss Alps. Furthermore the NURE calibration procedure requires large concrete calibration pads with accurately known uranium, thorium and potassium concentrations, to determine the spectral stripping correction factors and the detector sensitivity. Because no calibration facility of this kind exists in central Europe, both parameters have been determined with point sources and mathematically corrected for the differing source geometry.

It is impossible to maintain the desired survey altitude constant in the Swiss Alps because of the limited flight capabilities of the aircraft. Furthermore the measurements are strongly influenced by ground topography. Processing of data acquired in areas with high topographic relief is therefore very difficult. In order to estimate the influence of topographic irregularities, the gamma-ray field above real topography has been modelled in both two and three dimensions. The calculations have shown a strong increase of the count rates especially in narrow valleys. The correction procedure for topography and flight altitude variations is based on the same method as used for the model calculations (Schwarz et al., 1992). Knowing the effect of ground geometry from modelling, the count rate can then be reduced to flat geometry and constant flight altitude.

The methods developed for processing and correction allow a routine treatment of airborne radiometric data acquired even in areas with high topographic relief. The results for the areas processed so far show a very good fit with geology and can be used for geological overview mapping.

The airborne radiometric survey conducted so far covers about ten percent of the area of Switzerland. The results of the survey allow to describe the mean radioactivity level in Switzerland and its variation in broad outline. Together with in-situ-gammaspectrometric ground measurements and data from rock samples the air-

borne survey can serve as a good base for the compilation of a radiometric (dose rate) map of whole Switzerland including the contributions of artificial isotopes and cosmic radiation.

10 References

- ABRAMOWITZ, M., STEGUN, I.A., 1972: Handbook of mathematical functions. Dover Publications Inc., New York.
- ADAMS, J.A.S., GASPARINI, P., 1970: Gamma-Ray Spectrometry of Rocks. Elsevier Publishing Company, Amsterdam/London/New York.
- DARNLEY, A.G., GRASTY, R.L., 1970: Mapping from the air by gamma-ray spectrometry. Proc. 3rd International Geochemical Symposium Toronto (Can), Can. Inst. Min. Metall., Special Volume 11; 485-500.
- EAFV, 1988: Schweizerisches Landesforstinventar; Ergebnisse der Erstaufnahme 1982-1986. Berichte der Eidgenössischen Anstalt für the forstliche Versuchswesen (EAFV), Birmensdorf.
- EG&G GEOMETRICS, 1980: Aerial gamma ray and magnetic survey Montrose detail projects Colorado: Final report. EG&G Geometrics, Sunnyvale (California).
- EG&G GEOMETRICS, 1985: Operating and Maintenance Manual for Models GR-800, GR-900, G-714 and DET-1024. EG&G Geometrics, Sunnyvale (California).
- GILLIERON, F., 1986: Bericht über die 1966-1984 ausgeführten und mit Bundesmitteln geförderten Uranprospektions-Arbeiten in den Schweizeralpen; Bericht der Fachkommission für schweizerische Uranvorkommen. Schriftenreihe des Bundesamtes für Energiewirtschaft, Studie Nr.41, Bundesamt für Energiewirtschaft, Bern.
- GRASTY, R.L., 1975: Uranium measurements by airborne gamma-ray spectrometry. Geophysics 40, 503-519.
- GREEN, A.A., 1987: Leveling airborne gamma-radiation data using between-channel correlation information. Geophysics, 52, 1557-1562.

- HABERAECKER, P., 1985: Digitale Bildverarbeitung, Grundlagen und Anwendungen. Hanser Studienbücher, München/Wien.
- HALM, E., HERBST, W., MASTROCOLA, A., 1962: Messung des natürlichen Strahlenpegels in der Schweiz. Bulletin des Eidg. Gesundheitsamtes, Beil.B Nr.6/1962; 133-167.
- IAEA, 1979: Gamma-Ray Surveys in Uranium Exploration. IAEA Vienna, Technical Reports Series, No.186.
- KILLEEN, P.G., 1979: Gamma ray spectrometric methods in uranium exploration - application and interpretation; in Geophysics and Geochemistry in the Search for Metallic Ores. Geol. Surv. of Canada, Economic Geology Report 31; 163-229.
- KISSLING, E., 1976: Radiometrische Untersuchungen im Rotondogranit, Diplomarbeit, Institut für Geophysik ETHZ, Zürich.
- KOGAN, R.M., NAZAROV, I.M., FRIDMAN, S.D., 1969: Gamma Spectrometry of Natural Environments and Formations, Atomizdat, Moskau. (Englische Uebersetzung: Israel Program for Scientific Translations Ltd., Jerusalem, 1971, Microfiche-TT-70-50092).
- LABHART, T.P., MUELLER, W., RYBACH, L., 1971: Untersuchung der Uranvorkommen in der Umgebung von Finhaut; Bericht zuhanden des Arbeitsausschusses für die Untersuchung schweizerischer Mineralien und Gesteine auf Atombrennstoffe und seltene Elemente. Interner Bericht, Institut für Geophysik ETHZ, Zürich.
- LABHART, T.P., RYBACH, L., 1971: Abundance and distribution of uranium and thorium in the syenite of Piz Giuv (Aar-Massif, Switzerland). Chemical Geology 7, 237-251.
- LEUPIN, A., 1990: Vergleich aeroradiometrischer Messungen in der Umgebung von KKB/PSI mit In-Situ-Gamma-Spektrometrie-Messungen am Boden. Interner HSK-Bericht. Bundesamt für Energiewirtschaft.

- LØVBORG, L., BØTTER-JENSEN, L., CHRISTIANSEN, ET AL., 1975: Gamma-ray measurements in an area of high natural radioactivity. Proc. of the third international symposium on the natural radiation environment, Houston (Texas). CONF-780422, US DOE Technique Information Center.
- MURITH, C., VOELKLE, H.R., SURBECK, H., PILLER, G., BAERISWIL, L., BEURET, P., FERRERI, G., GOBET, M., GURTNER, A., RIBODRY, L., 1990: Mesures in situ - mesures aéroradiométrie dans le voisinage du PSI. Interner SUEr-Bericht. Bundesamt für Gesundheitswesen; Abteilung Strahlenschutz.
- PITKIN, J.A., DUVAL, J.S., 1980: Design parameters for aerial gamma-ray surveys. *Geophysics* 45, 1427-1439.
- PRESS, W.H., FLANNERY, B.P., TEUKOLSKY, S.A., VETTERLING, V.T., 1986: Numerical Recipes; The Art of Scientific Computing. Cambridge University Press, Cambridge (England).
- PURVANCE, D., NOVAK, E., 1983: General procedure for calibration and reduction of aerial gamma-ray measurements: Specification BFEC 1250-B. U.S. Department of Energy, Rep. GJBX-16(83) DE84004974.
- RYBACH, L., LABHART, T.P., 1973: Regelmässigkeiten der Radioaktivitätsverteilung in granitischen Gesteinskörpern (Beispiele aus den Schweizer Alpen). *Schweizerische Mineralogische und Petrographische Mitteilungen* 53, 379-385.
- SAUNDERS, D.F., TERRY, S.A., THOMPSON, C.K., 1987: Test of National Uranium Resource Evaluation gamma-ray spectral data in petroleum reconnaissance. *Geophysics* 52, 1547-1556.
- SCHAERLI, U., 1989: Geothermische Detailkartierung (1:100'000) in der zentralen Nordschweiz mit besonderer Berücksichtigung petrophysikalischer Parameter. Dissertation ETH Nr.8941, Eidgenössische Technische Hochschule, Zürich.

- SCHWARZ, G.F., 1990: GAMERO: Ein integriertes Programmpaket zur Auswertung aeroradiometrischer Daten. Interner Bericht, Institut für Geophysik ETHZ, Zürich.
- SCHWARZ, G.F., 1991: Methodische Entwicklungen zur Aerogammaspektrometrie. Beiträge zur Geologie der Schweiz, Geophysik Nr.23, Schweizerische Geophysikalische Kommission.
- SCHWARZ, G.F., KLINGELE, E.K., RYBACH, L., 1989: Aeroradiometrische Messungen in der Umgebung der schweizerischen Kernanlagen; Bericht zuhanden der Hauptabteilung für die Sicherheit der Kernanlagen. Interner Bericht, Institut für Geophysik ETHZ, Zürich.
- SCHWARZ, G.F., KLINGELE, E.K., RYBACH, L., 1990: Aeroradiometrische Messungen in der Umgebung der schweizerischen Kernanlagen; Bericht zuhanden der Hauptabteilung für die Sicherheit der Kernanlagen. Interner Bericht, Institut für Geophysik ETHZ, Zürich.
- SCHWARZ, G.F., KLINGELE, E.K., RYBACH, L., 1991: Aeroradiometrische Messungen in der Umgebung der schweizerischen Kernanlagen; Bericht zuhanden der Hauptabteilung für die Sicherheit der Kernanlagen. Interner Bericht, Institut für Geophysik ETHZ, Zürich.
- SCHWARZ, G.F., KLINGELE, E.K., RYBACH, L., 1992: How to handle rugged topography in airborne gamma-ray spectrometry surveys, First break 10, 11-17.
- SMITH, A.R., 1978: Color gamut transform pairs. Computer graphics 12.
- WARD, D.L., 1978: Construction of calibration pads facility Walker Field, Grand Junction, Colorado. Energy Res. Dev. Agency, Rep. GBJX-37(78).

Acknowledgments

We thank Prof. Dr. St. Mueller, President of the Swiss Geophysical Commission, for continuous encouragement and support. A special thank goes to the Swiss Federal Nuclear Safety Inspectorate, particularly to W. Jeschki, S. Prêtre and Dr. A. Leupin, for their unbureaucratic financing and support of the surveys in the environs of the Swiss nuclear power plants. The Branch for Radioactivity Surveillance (SUEr), the National Emergency Operation Center (NAZ) and the related commissions KUeR and KAC supported us financially and with their know how. We want particularly thank Dr. H.R. Völkle, Dr. H. Surbeck, Prof. Dr. H.H. Loosli, H.J. Knaus, Dr. D. Rauber, Dr. U. Imobersteg. The Swiss Air Force supported the project by allotting flight time and helped with the installation of the instruments.

We are particularly grateful to Chr. Bärlocher, electronics engineer (Inst. of Geophysics ETHZ) who was very engaged in the design and maintenance of the measuring instruments. Last but not least we want to thank the pilots and mechanics for the patience they had with us. Especially Mr. Arber and the employees of hangar 13 of the airport Dübendorf, Mr. Meier of Heliswiss and the pilots A. Renggli, C. Wiesmann and B. Egger.

Beiträge zur Geologie der Schweiz Matériaux pour la Géologie de la Suisse Contributions to Geology of Switzerland

Geophysik — Géophysique — Geophysics

No.		Fr.
1	H. Röhllsberger. Zur seismischen und petrographischen Charakterisierung einiger Molassegesteine, einschliesslich der Beschreibung von Methoden der Korngrössenbestimmung in festmaterial. 91 Seiten, 31 Figuren. 1957.....	14.-
2	O. Friedenreich. Eine grossräumige Widerstandskartierung nordwestlich von Zürich und ihre geologische Deutung. 47 Seiten, 22 Textfiguren, 9 Karten. 1959.....	20.-
3	F. Gassmann. Schweremessungen in der Umgebung von Zürich. 70 Seiten, 24 Textfiguren, 2 Tafeln. 1962.....	24.-
4	E. Poldini. Les Anomalies gravifiques du canton de Genève. Avec 63 pages, 25 figures et 3 planches. 1963.....	24.-
5	L. Rybach. Refraktionsseismische Untersuchungen im Raum Aare-, Limmat- und Surbtal. 49 Seiten, 42 Figuren. 1962.....	14.-
6	O. Gonet. Etude gravimétrique de la plaine du Rhône. Région Saint-Maurice—Lac Léman. 50 pages, 30 figures, 2 planches. 1965.....	14.-
7	C. Meyer de Stadelhofen. Carte des résistivités de la plaine du Rhône. 8 pages, 2 figures, 2 planches. 1966.....	8.-
8	O. Gonet. Etude gravimétrique du lac Léman à bord du mésoscaphe <i>Auguste Picard</i> . 50 pages, 8 figures, 1 planche. 1969.....	8.-
9	J.-J. Wagner. Elaboration d'une carte d'anomalie de Bouguer. Etude de la vallée du Rhône de Saint-Maurice à Saxon (Suisse). 91 pages, 32 figures, 2 planches. 1970.....	22.-
10	H. Lazreg. Etude géophysique, géologique et hydrogéologique de la région de Concise à Pompaples (pied du Jura vaudois). 51 pages, 16 figures, 2 planches. 1971.....	22.-
11	M. Petch. Contribution à l'étude hydrogéologique de la plaine de l'Orbe. 95 pages, 23 figures, 15 planches. 1970.....	22.-
12	P.-A. Gilliland. Etude géoélectrique du Klettgau (Suisse), canton de Schaffhouse. 85 pages, 47 figures, 10 annexes, 5 planches. 1970.....	22.-
13	P. Corniche. Application des méthodes géophysiques à la recherche hydrogéologique. 65 pages, 25 figures. 1973.....	22.-
14	F. Heller. Magnetische und petrographische Eigenschaften der granitischen Gesteine des Albignagebiets (Nördliches Bergeller Massiv). 66 Seiten, 24 Textfiguren. 1972.....	22.-
15	E. Klingelé. Contribution à l'étude gravimétrique de la Suisse romande et des régions avoisinantes. 94 pages, 6 figures, 35 planches. 1972.....	22.-
16	W. Sigrüst. Contribution à l'étude géophysique des fonds du lac Léman. 56 pages, 28 figures, 1 planche. 1974.....	22.-
17	R. Olivier. Elaboration d'un système de traitement gravimétrique géré par l'ordinateur. Etude gravimétrique du plateau romand de Versoix (GE) à Concise (VD). 56 pages, 21 figures, 10 planches. 1974.....	22.-
18	H. Buchli, R. Paquin, A. Donzé. Etude géoélectrique et gravimétrique du Chablais entre Asnières et Evian. 170 pages, 81 figures, 4 planches. 1976.....	32.-
19	G. Fischer, P.-A. Schnegg, J. Seslano. A new geomagnetic survey of Switzerland. 44 pages, 15 figures, 8 tables, 10 cartes. 1979.....	28.-
20	E. Klingelé, R. Olivier. La nouvelle carte gravimétrique de la Suisse (Anomalies de Bouguer). 96 pages, 9 figures, 4 tables, 1 carte. 1980.....	28.-
21	J.-J. Wagner, St. Müller. Geomagnetic and gravimetric studies of the Ivrea zone. 64 pages, 44 figures. 1984.....	32.-
22	Ph. Bodmer, L. Rybach. Geothermal map of Switzerland (Heat flow density). 48 pages, 21 figures, 6 tables. 1984.....	36.-
23	G. Schwarz. Methodische Entwicklungen zur Aerogammaspektrometrie. 160 Seiten, 56 Figuren. 1991.....	42.-
24	U. Schärli, L. Rybach. Geothermische Detailkartierung der zentralen Nordschweiz (1:100'000). 59 Seiten, 13 Figuren, 2 Karten. 1991.....	42.-

Map captions:

- Map 1: Dose rate map of the "Central Massifs" (nSv/h)**
- Map 2: Dose rate map of northwestern Switzerland (nSv/h)**
- Map 3: Dose rate map of western Switzerland (nSv/h)**
- Map 4: K^{40} -map of the "Central Massifs" (Bq/kg)**
- Map 5: Bi^{214} -map of the "Central Massifs" (Bq/kg)**
- Map 6: Tl^{208} -map of the "Central Massifs" (Bq/kg)**
- Map 7: Bi^{214}/K^{40} -ratio map of the "Central Massifs" (%)**
- Map 8: Bi^{214}/Tl^{208} -ratio map of the "Central Massifs" (%)**
- Map 9: Tl^{208}/K^{40} -ratio map of the "Central Massifs" (%)**
- Map 10: Ternary map of the "Central Massifs" (1:500'000)**
- Map 11: Ternary map of the "Central Massifs" (west, 1:200'000)**
- Map 12: Ternary map of the "Central Massifs" (center, 1:200'000)**
- Map 13: Ternary map of the "Central Massifs" (east, 1:200'000)**
- Map 14: Boundaries of the geologic units of the "Central Massifs"**

PUBLICATION N°25

AIRBORNE RADIOMETRIC MAPPING IN SWITZERLAND

By

Georg F. Schwarz
Emile Klingele
Ladislaus Rybach

MAPS

15 MAPS :

MAP 1 :	2 PAGES
MAP 2 :	2 PAGES
MAP 3 :	2 PAGES
MAP 4 :	2 PAGES
MAP 5 :	2 PAGES
MAP 6 :	2 PAGES
MAP 7 :	2 PAGES
MAP 8 :	2 PAGES
MAP 9 :	2 PAGES
MAP 10 :	2 PAGES
MAP 11 :	2 PAGES
MAP 12 :	2 PAGES
MAP 13 :	2 PAGES
MAP 14 :	1 PAGE

SG
PK

I. Geophysik
ETH-Zuerich
Hoenggerberg
8093-Zuerich




Central Massifs

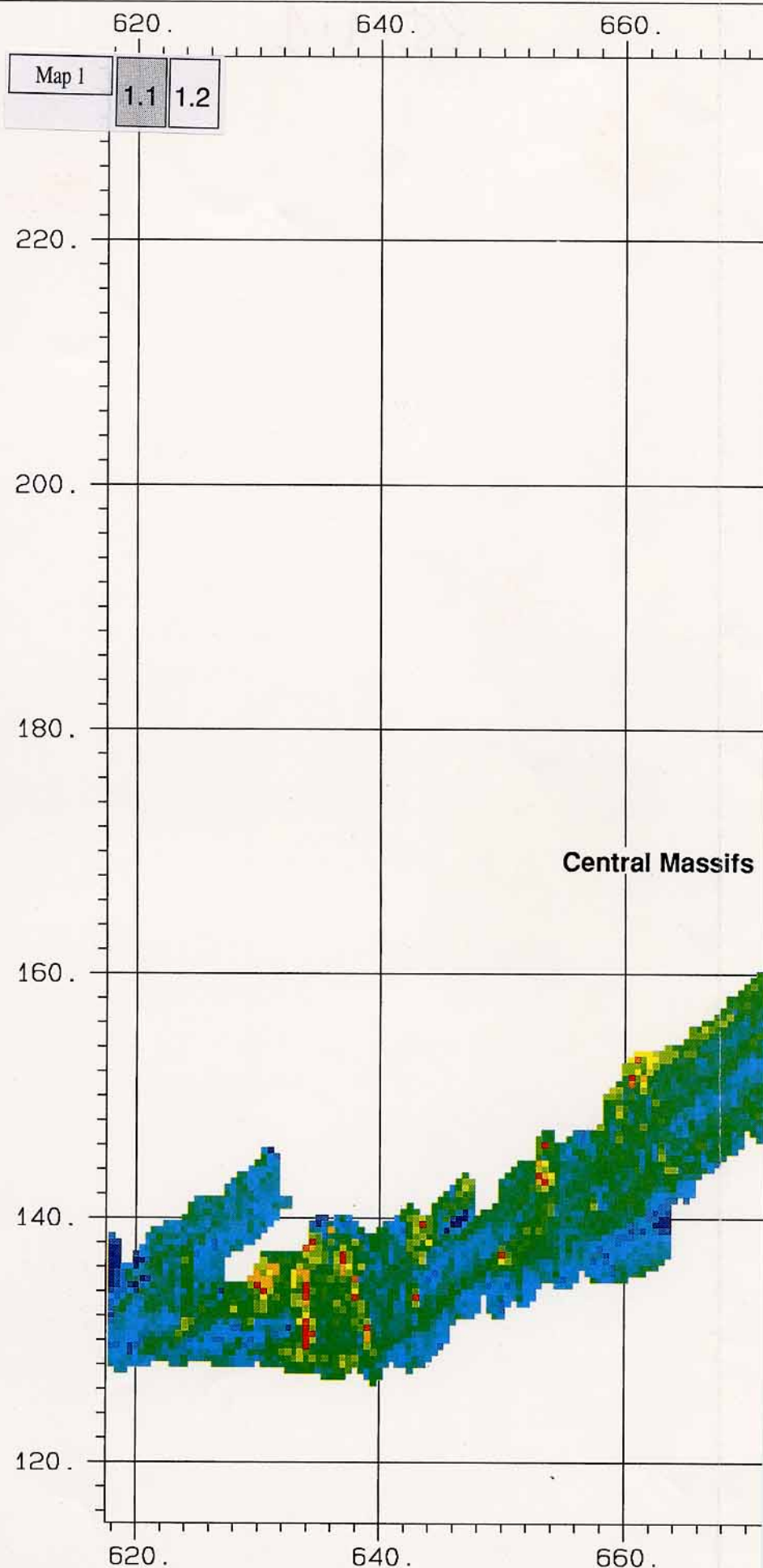
Survey	MAP92
Channel	Dose rate
Sam Int	500.
Area	2816.
Scale	500000.

Parameter

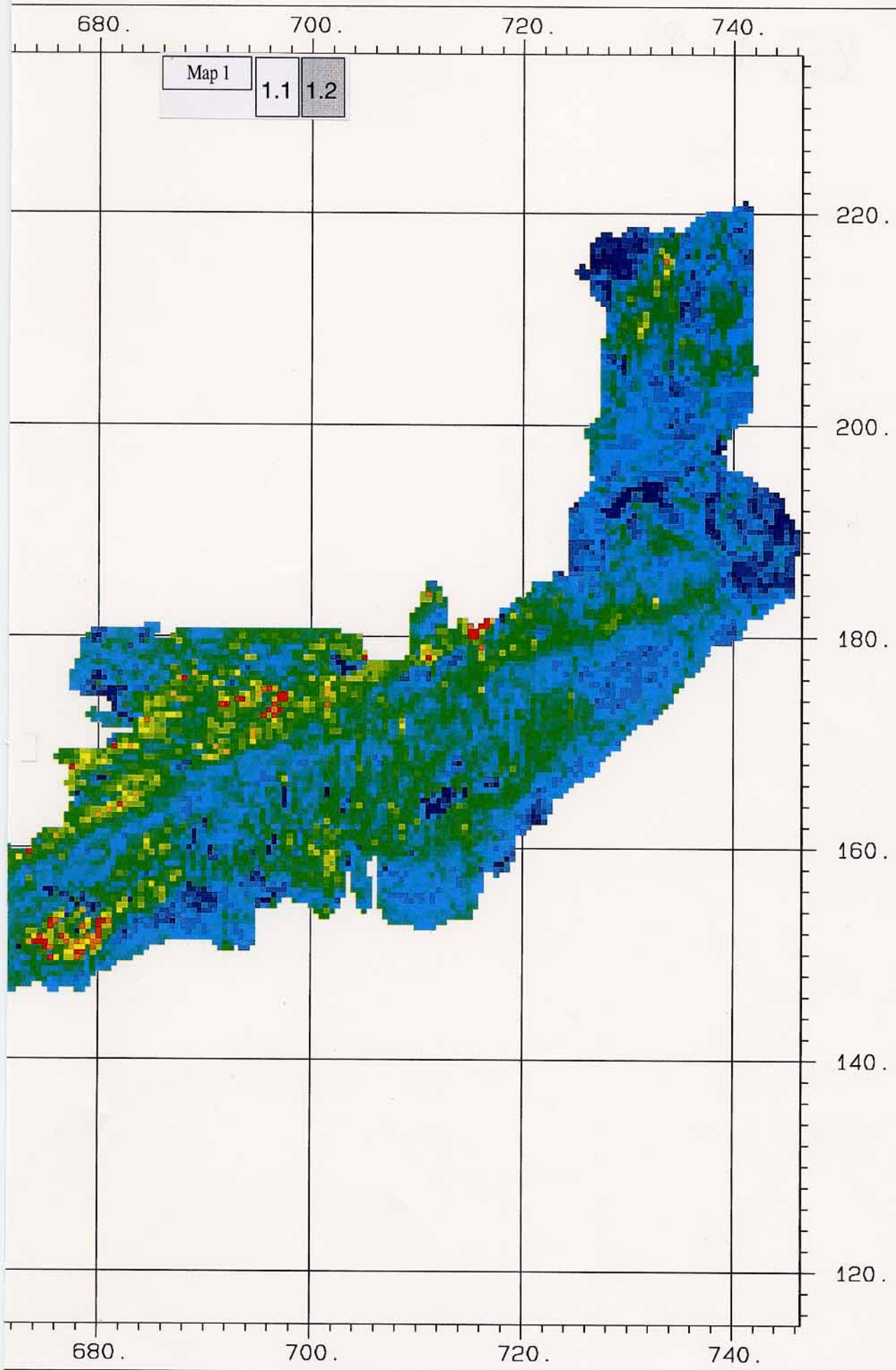
Average	113.8
Std Dev	42.4
Minimum	7.2
Maximum	512.3






Legend

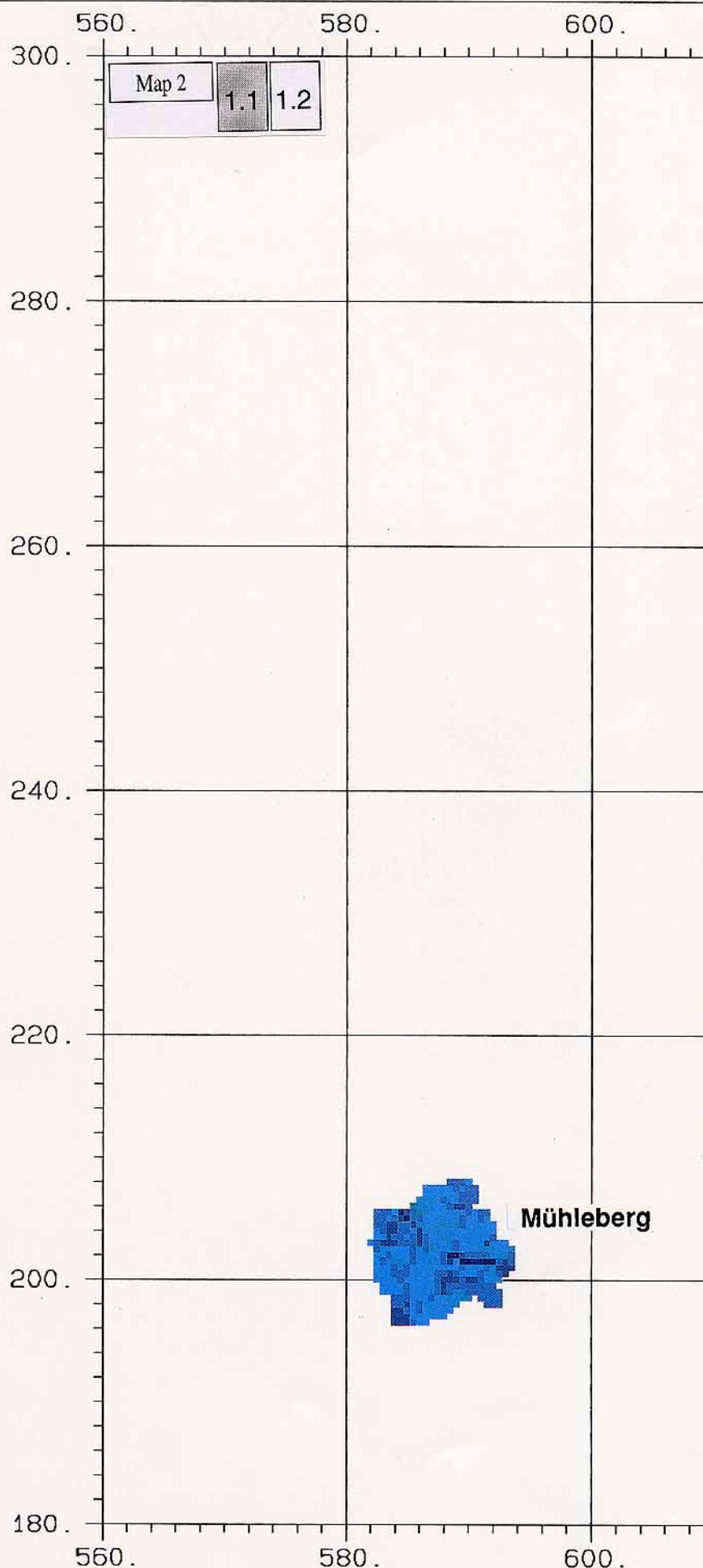
	Minimum	Maximum
	0.0	60.0
	60.0	120.0
	120.0	180.0
	180.0	240.0
	240.0	512.3



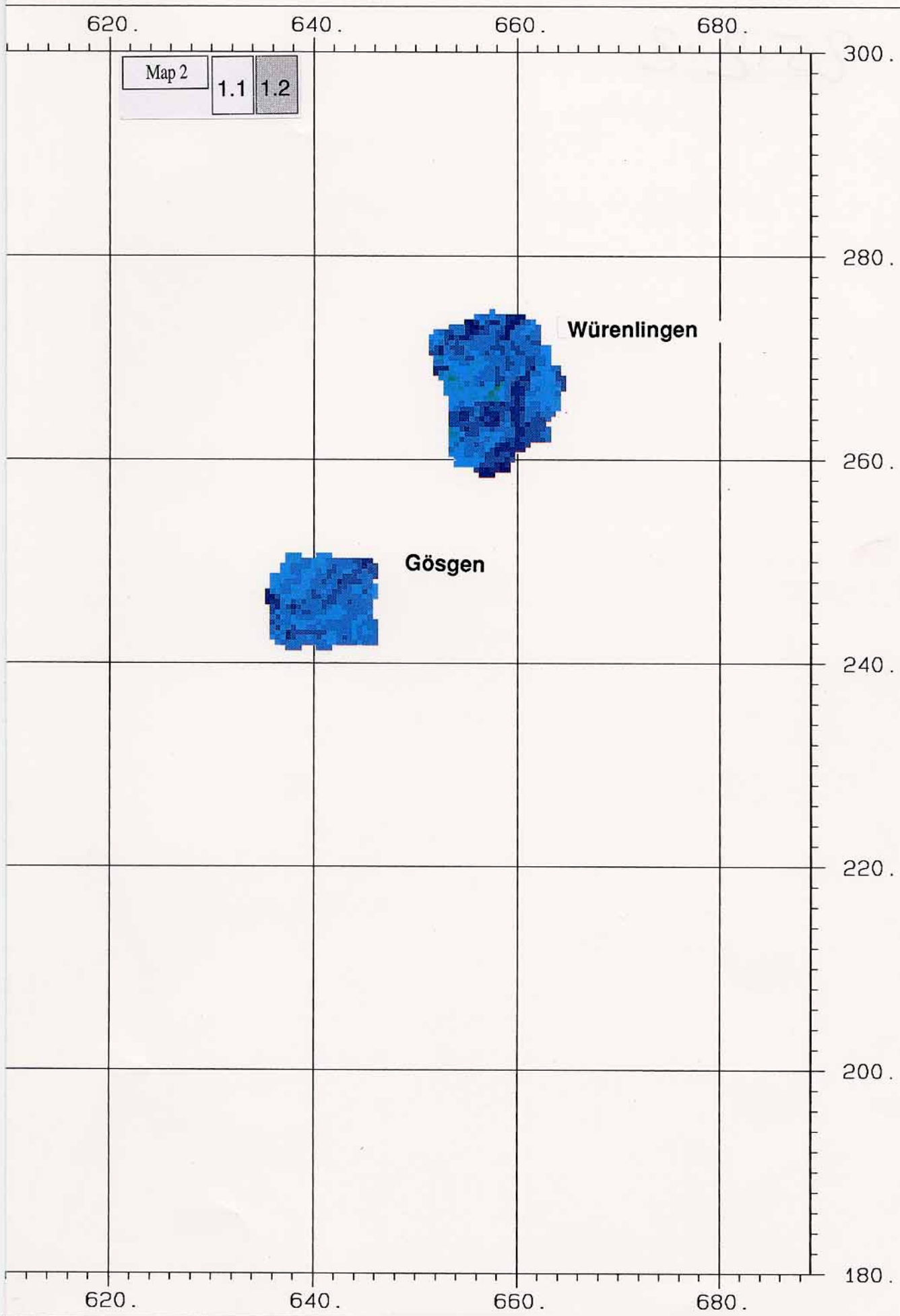
Map 1: Dose rate map of the "Central Massifs" (nSv/h)







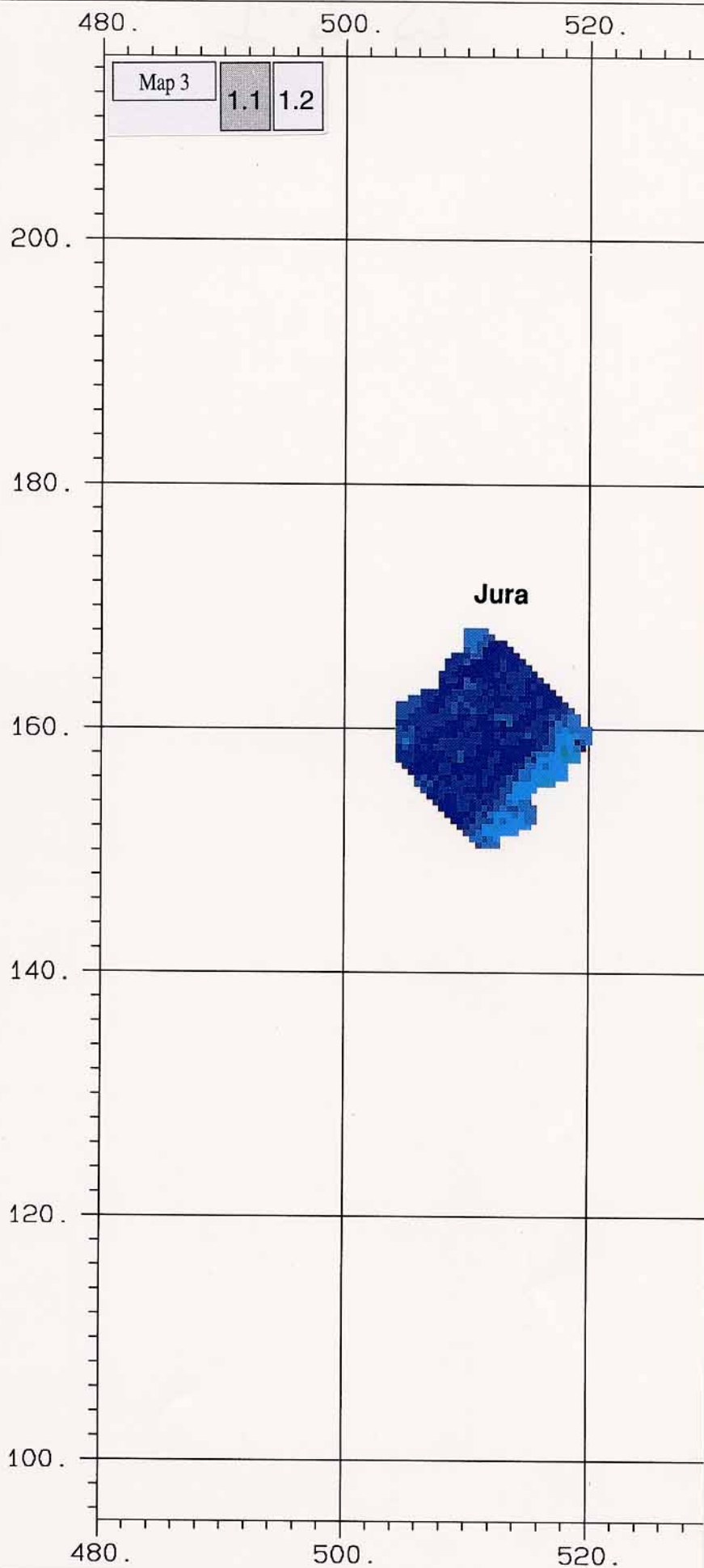
SG PK		I. Geophysik ETH-Zuerich Hoenggerberg 8093-Zuerich	
Northw. Switzerland			
Survey		NOR92	
Channel		Dose rate	
Sam Int		500.	
Area		341.	
Scale		500000.	
Parameter			
Average		67.0	
Std Dev		13.5	
Minimum		20.0	
Maximum		109.7	
Legend			
	Minimum	Maximum	
	0.0	60.0	
	60.0	120.0	
	120.0	180.0	
	180.0	240.0	
	240.0	300.0	



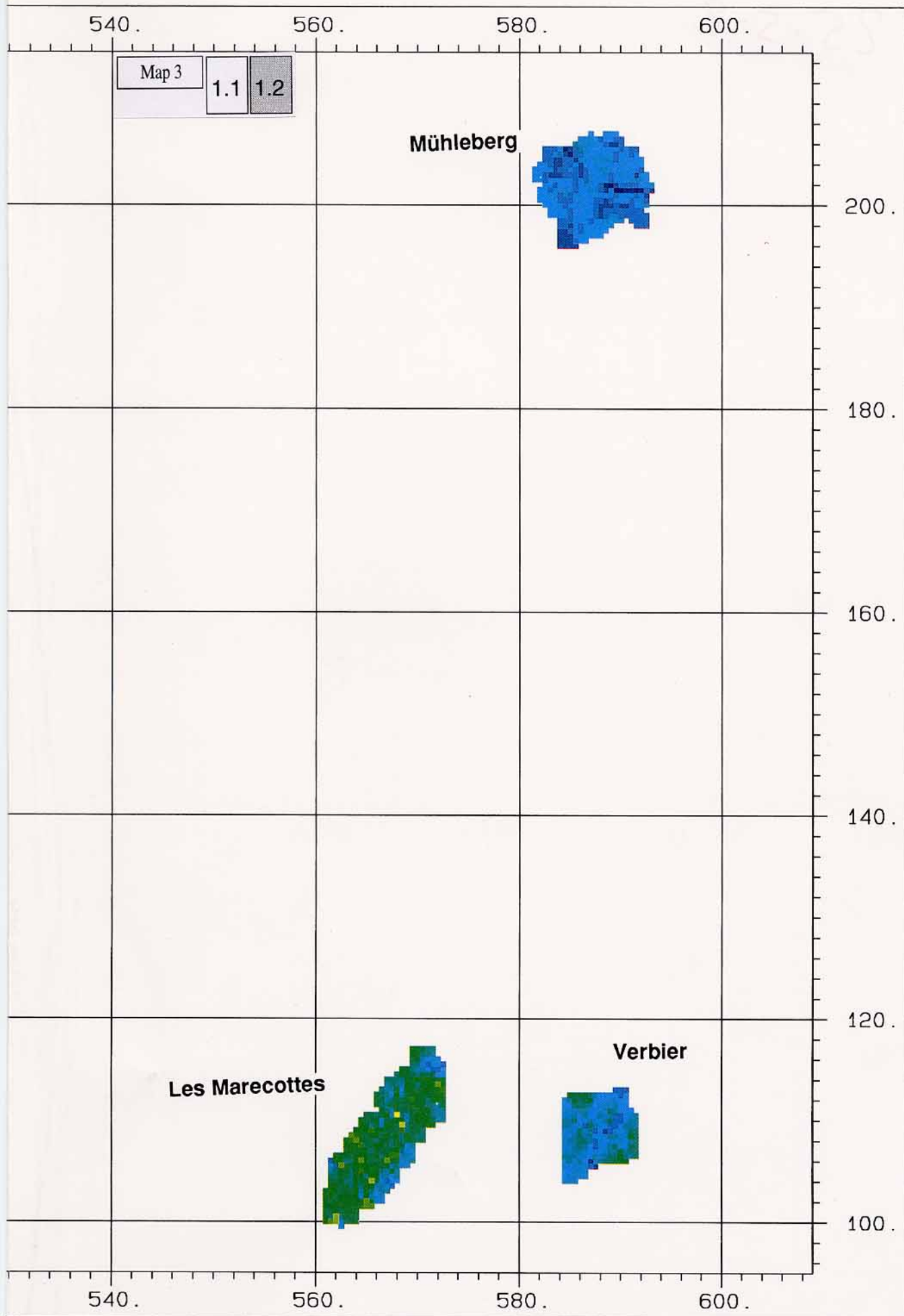
Map 2: Dose rate map of northwestern Switzerland (nSv/h)



<div>SG PK</div>		I. Geophysik ETH-Zuerich Hoenggerberg 8093-Zuerich	
Western Switzerland			
Survey		WES92	
Channel		Dose rate	
Sam Int		500.	
Area		431.	
Scale		500000.	
Parameter			
Average		77.9	
Std Dev		38.4	
Minimum		7.0	
Maximum		220.5	
Legend			
	Minimum	Maximum	
	0.0	60.0	
	60.0	120.0	
	120.0	180.0	
	180.0	240.0	
	240.0	300.0	



Map 3: Dose rate map of western Switzerland (nSv/h)



SG
PK

I. Geophysik
ETH-Zuerich
Hoenggerberg
8093-Zuerich

Central Massifs

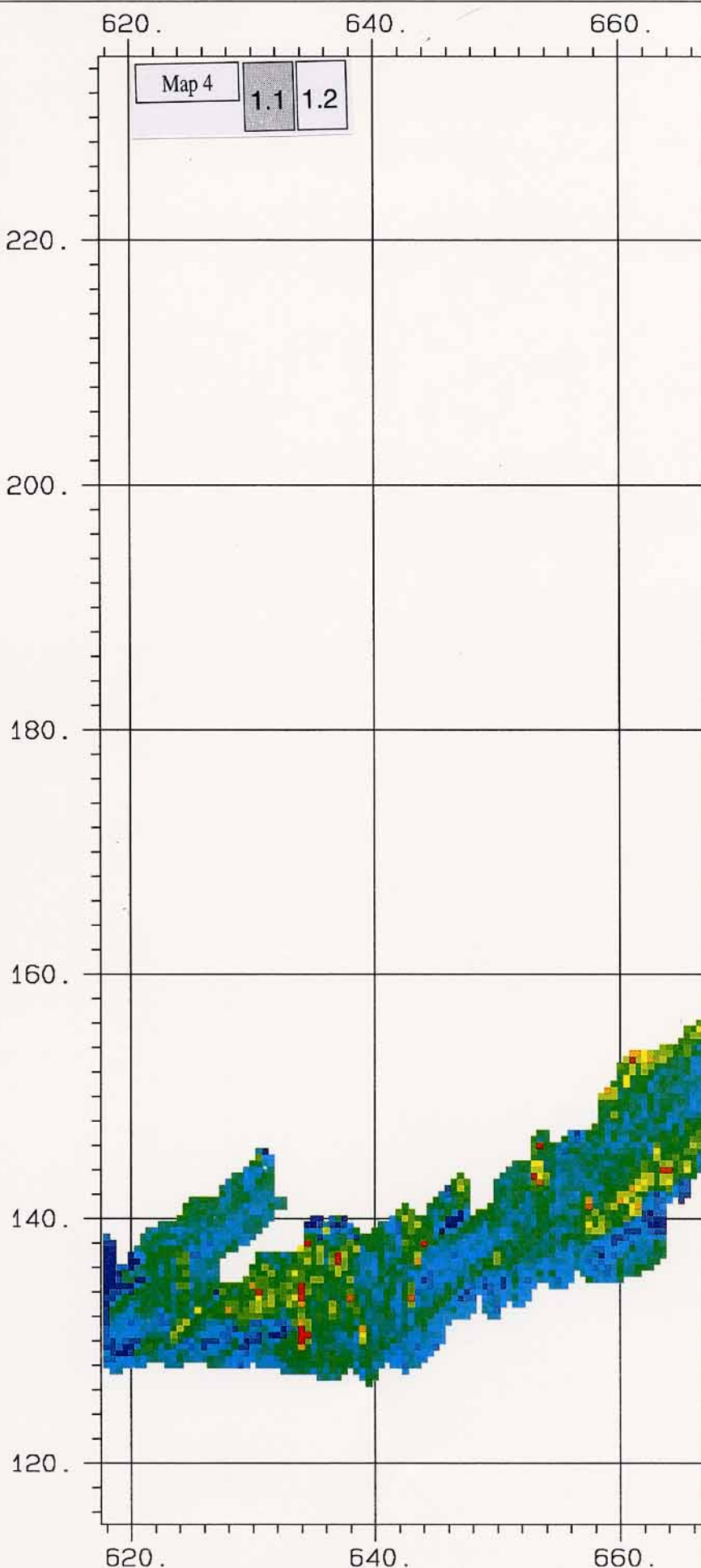
Survey	MAP92
Channel	K-40
Sam Int	500.
Area	2816.
Scale	500000.

Parameter

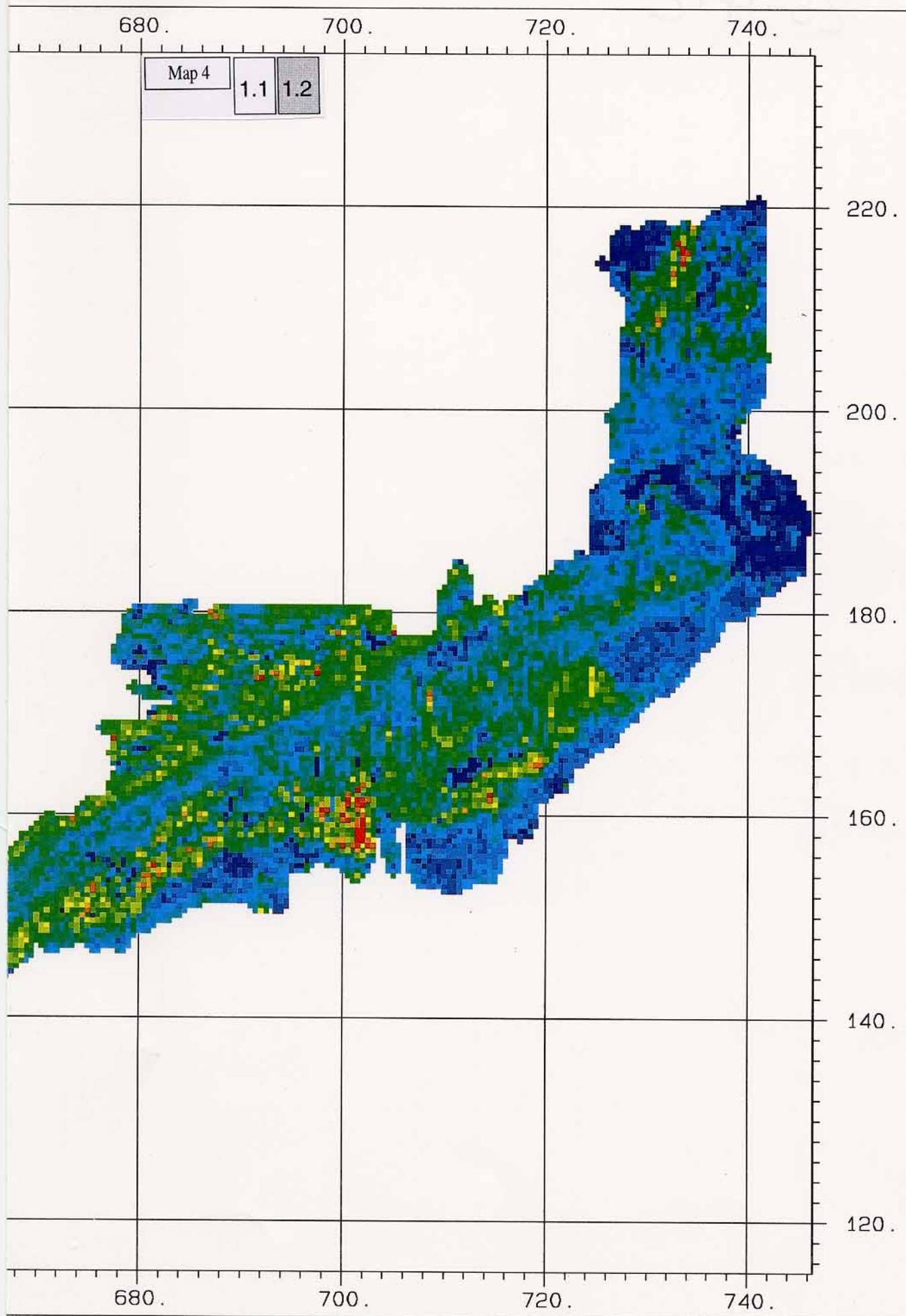
Average	744.9
Std Dev	308.6
Minimum	19.0
Maximum	2444.5

Legend

	Minimum	Maximum
	0.0	400.0
	400.0	800.0
	800.0	1200.0
	1200.0	1600.0
	1600.0	2444.5



Map 4: K⁴⁰-map of the "Central Massifs" (Bq/kg)



SG PK	I. Geophysik
	ETH-Zuerich
	Hoenggerberg
	8093-Zuerich



Central Massifs

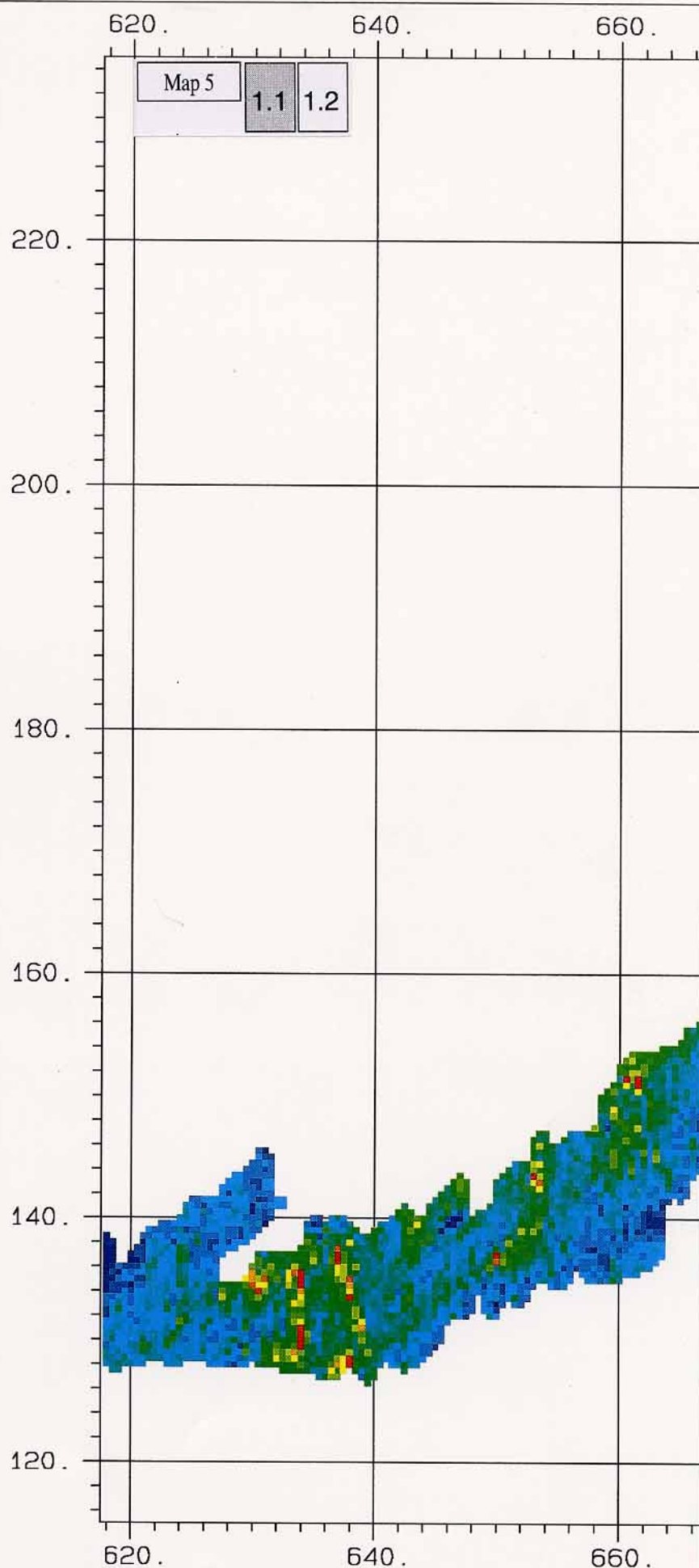
Survey	MAP92
Channel	Bi-214
Sam Int	500.
Area	2816.
Scale	500000.

Parameter

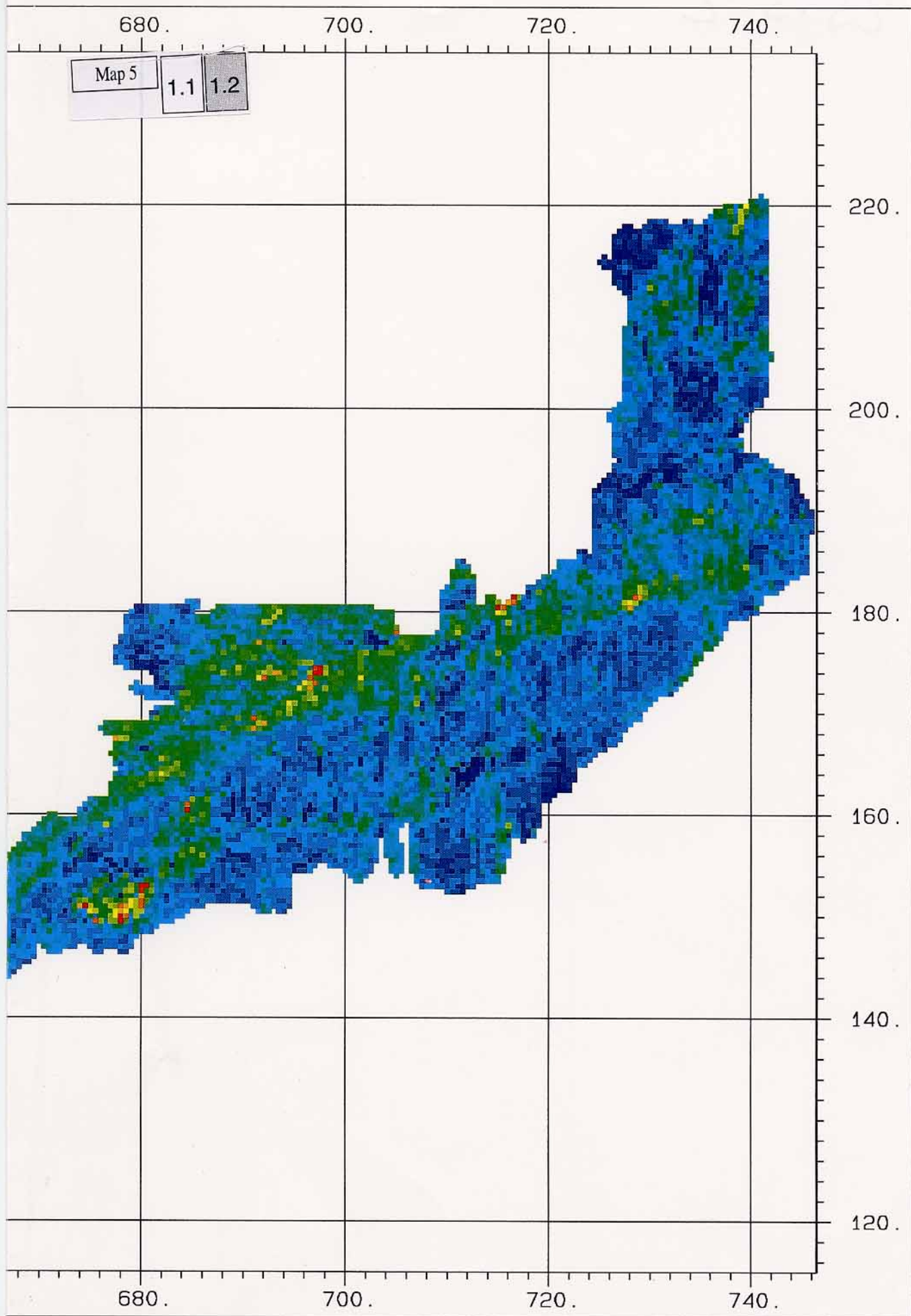
Average	61.6
Std Dev	26.0
Minimum	4.8
Maximum	344.1

Legend

	Minimum	Maximum
	0.0	40.0
	40.0	80.0
	80.0	120.0
	120.0	160.0
	160.0	344.1



Map 5: Bi²¹⁴-map of the "Central Massifs" (Bq/kg)



SG
PK

I. Geophysik
ETH-Zuerich
Hoenggerberg
8093-Zuerich






Central Massifs

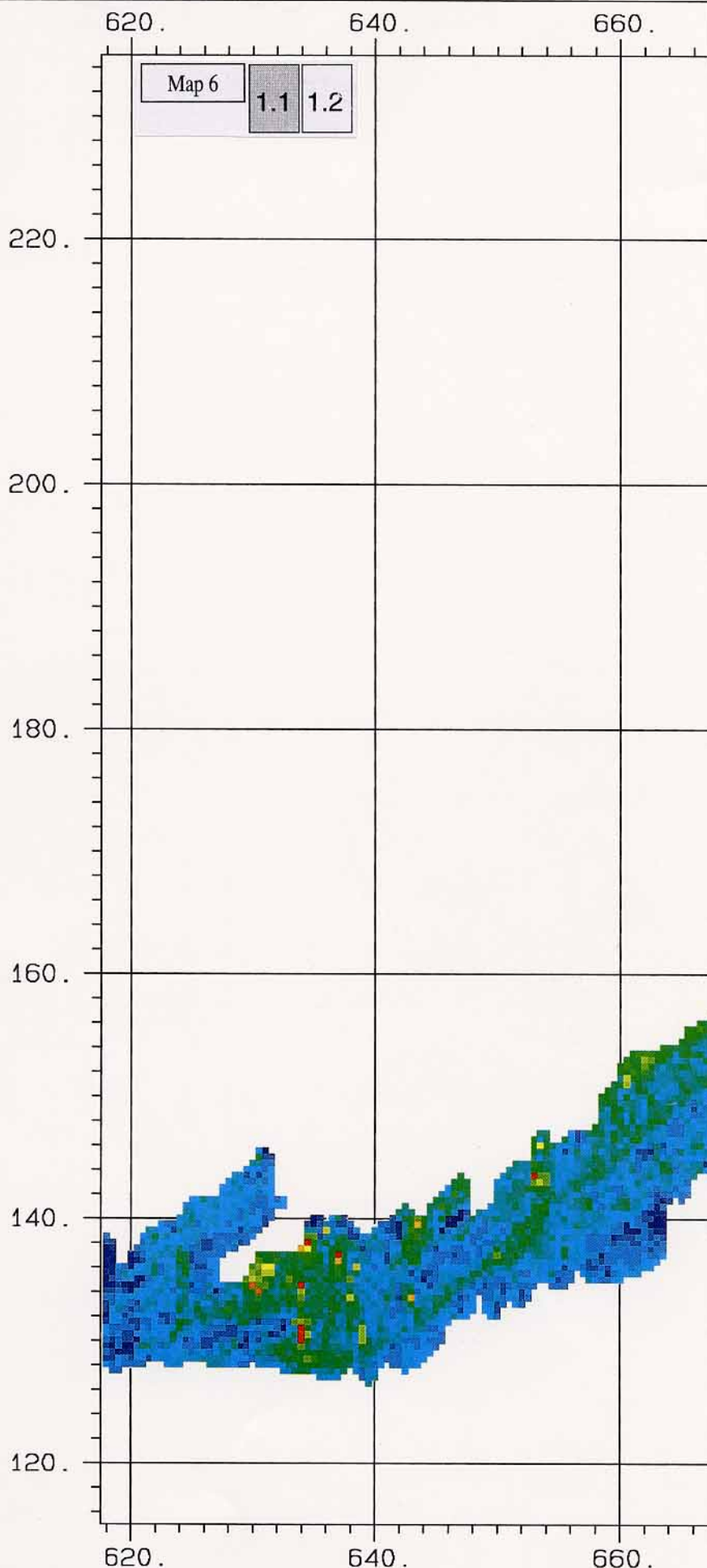
Survey	MAP92
Channel	T1-208
Sam Int	500.
Area	2816.
Scale	500000.

Parameter

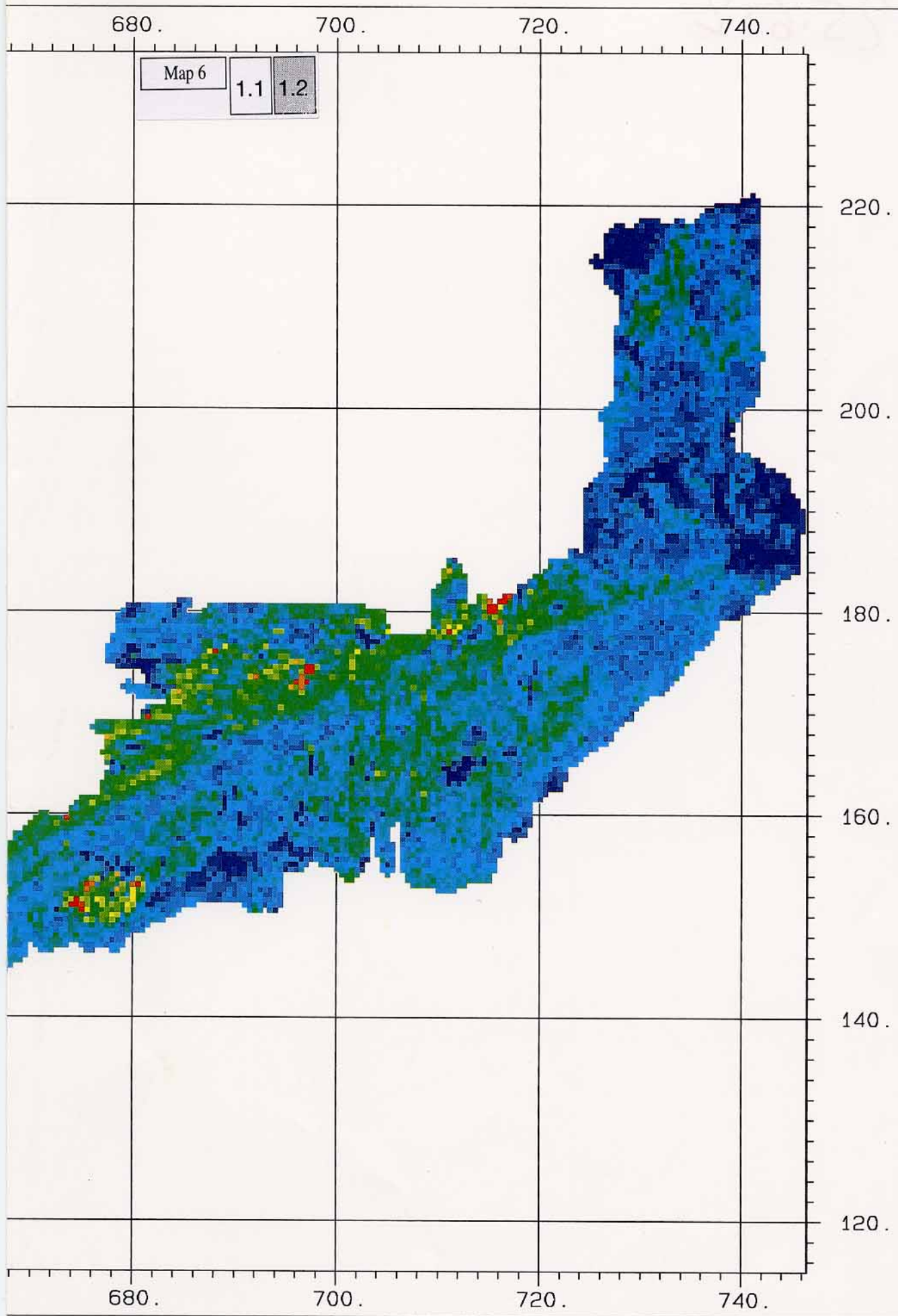
Average	60.9
Std Dev	25.4
Minimum	0.3
Maximum	328.6

Legend

	Minimum	Maximum
	0.0	40.0
	40.0	80.0
	80.0	120.0
	120.0	160.0
	160.0	328.6



Map 6: Tl²⁰⁸-map of the "Central Massifs" (Bq/kg)



SG
PK

I. Geophysik
ETH-Zuerich
Hoenggerberg
8093-Zuerich



Central Massifs

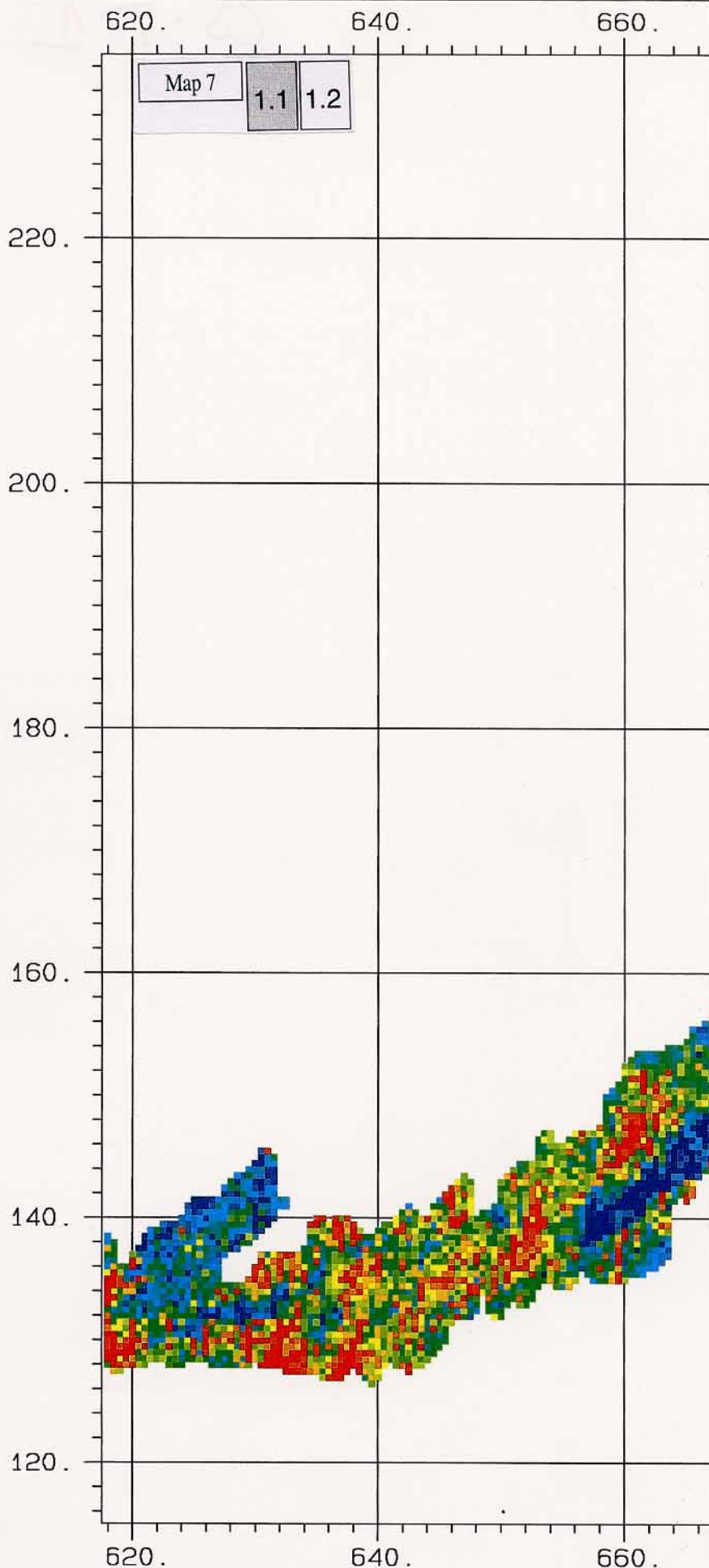
Survey	MAP92
Channel	B/K-ratio
Sam Int	500.
Area	2816.
Scale	500000.

Parameter

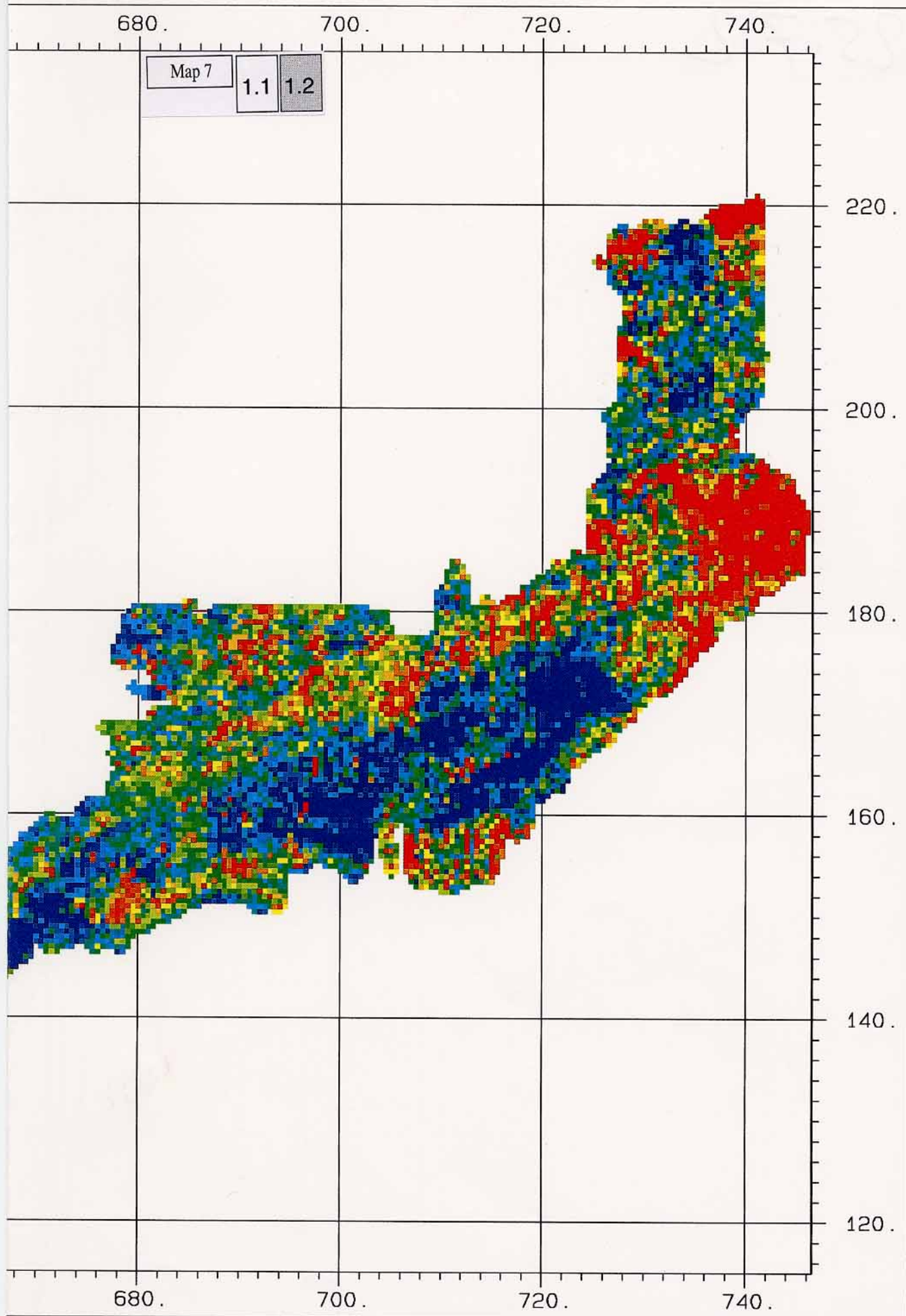
Average	9.3
Std Dev	5.3
Minimum	1.4
Maximum	88.1

Legend

	Minimum	Maximum
	1.4	6.2
	6.2	7.7
	7.7	9.1
	9.1	11.1
	11.1	88.1



Map 7: $\text{Bi}^{214}/\text{K}^{40}$ -ratio map of the "Central Massifs" (%)



SG
PKI. Geophysik
ETH-Zuerich
Hoenggerberg
8093-Zuerich



Central Massifs

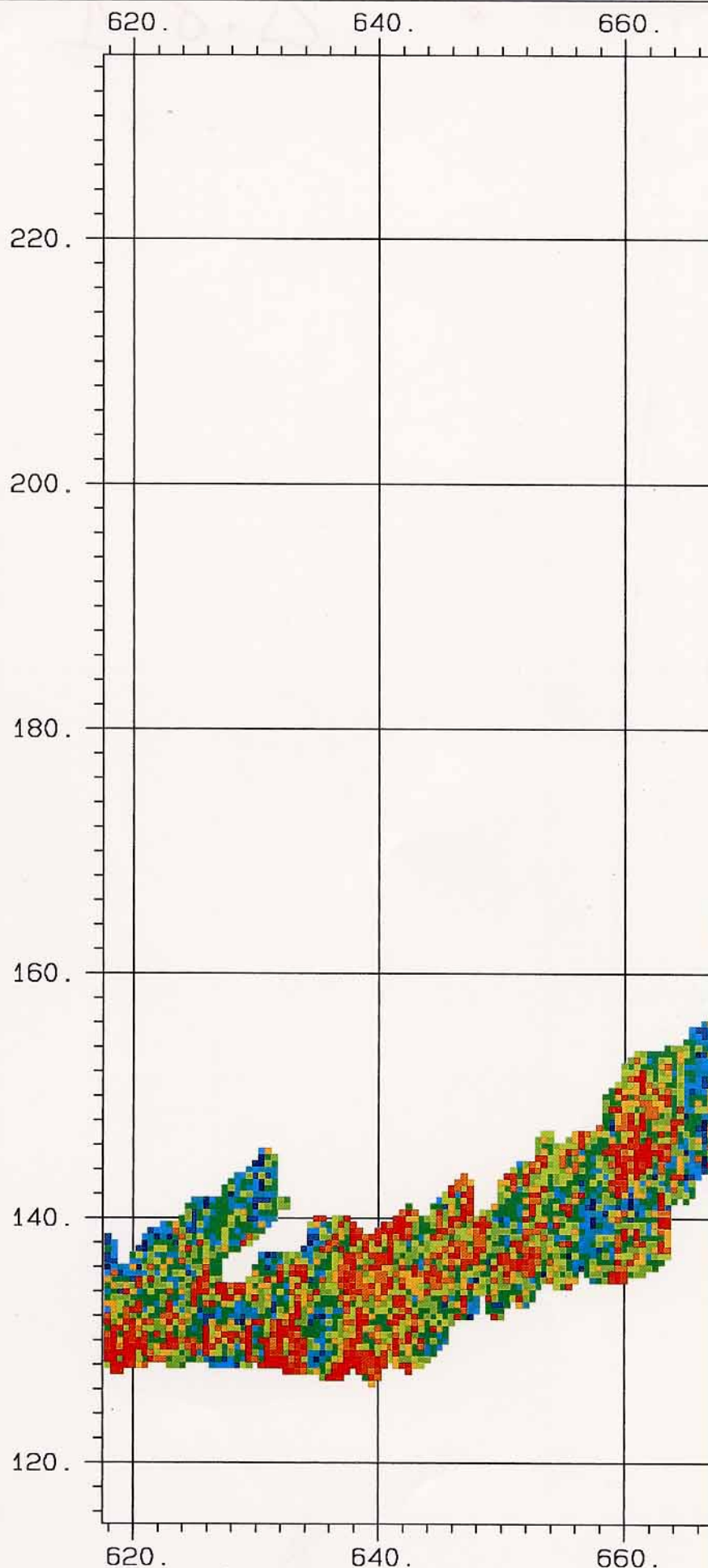
Survey	MAP92
Channel	B/T-ratio
Sam Int	500.
Area	2816.
Scale	500000.

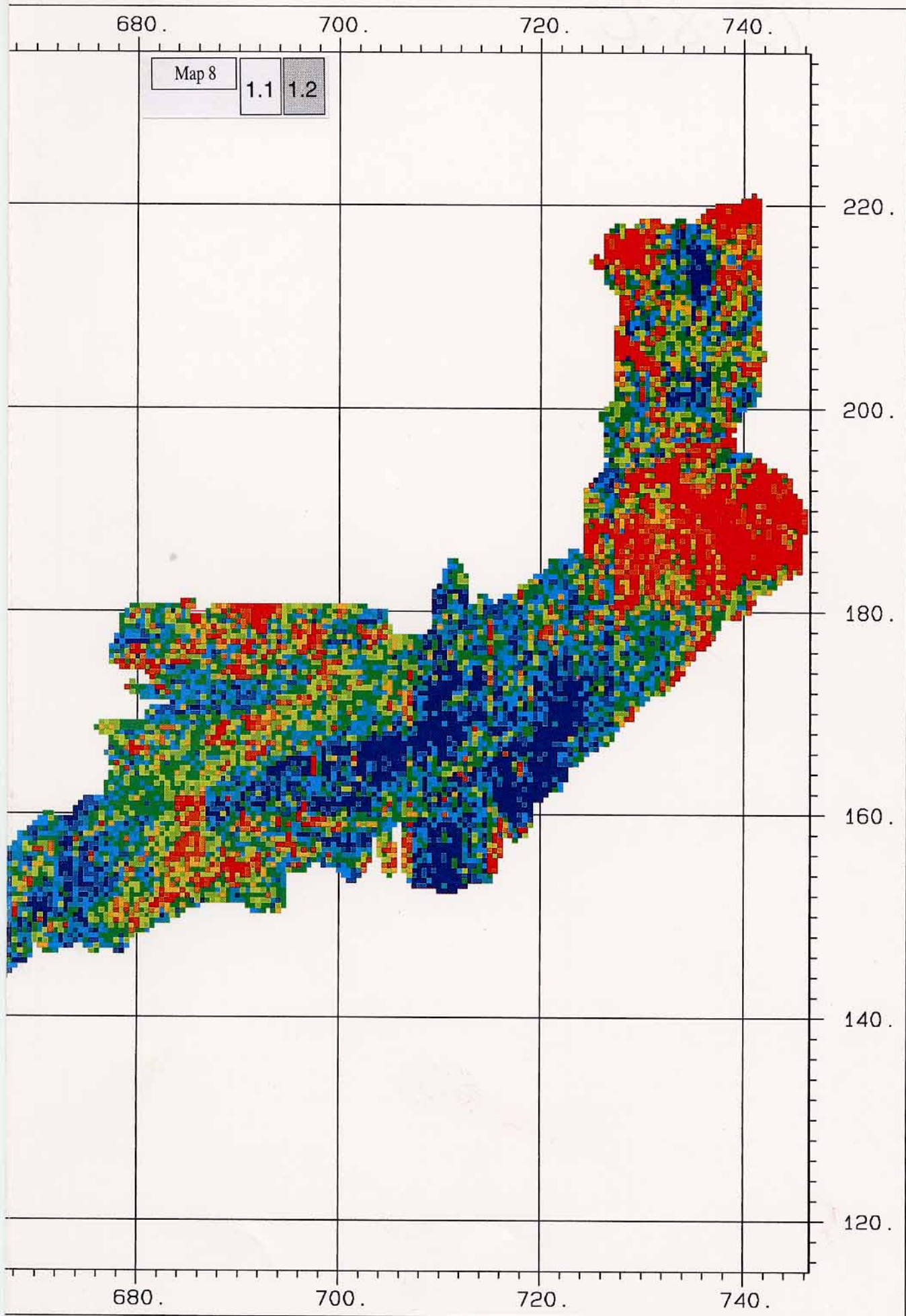
Parameter

Average	111.4
Std Dev	97.1
Minimum	22.4
Maximum	6838.2

Legend

	Minimum	Maximum
	22.4	77.0
	77.0	90.6
	90.6	104.2
	104.2	124.7
	124.7	6838.2

Map 8: $\text{Bi}^{214}/\text{Tl}^{208}$ -ratio map of the "Central Massifs" (%)



SG
PK

I. Geophysik
ETH-Zuerich
Hoenggerberg
8093-Zuerich






Central Massifs

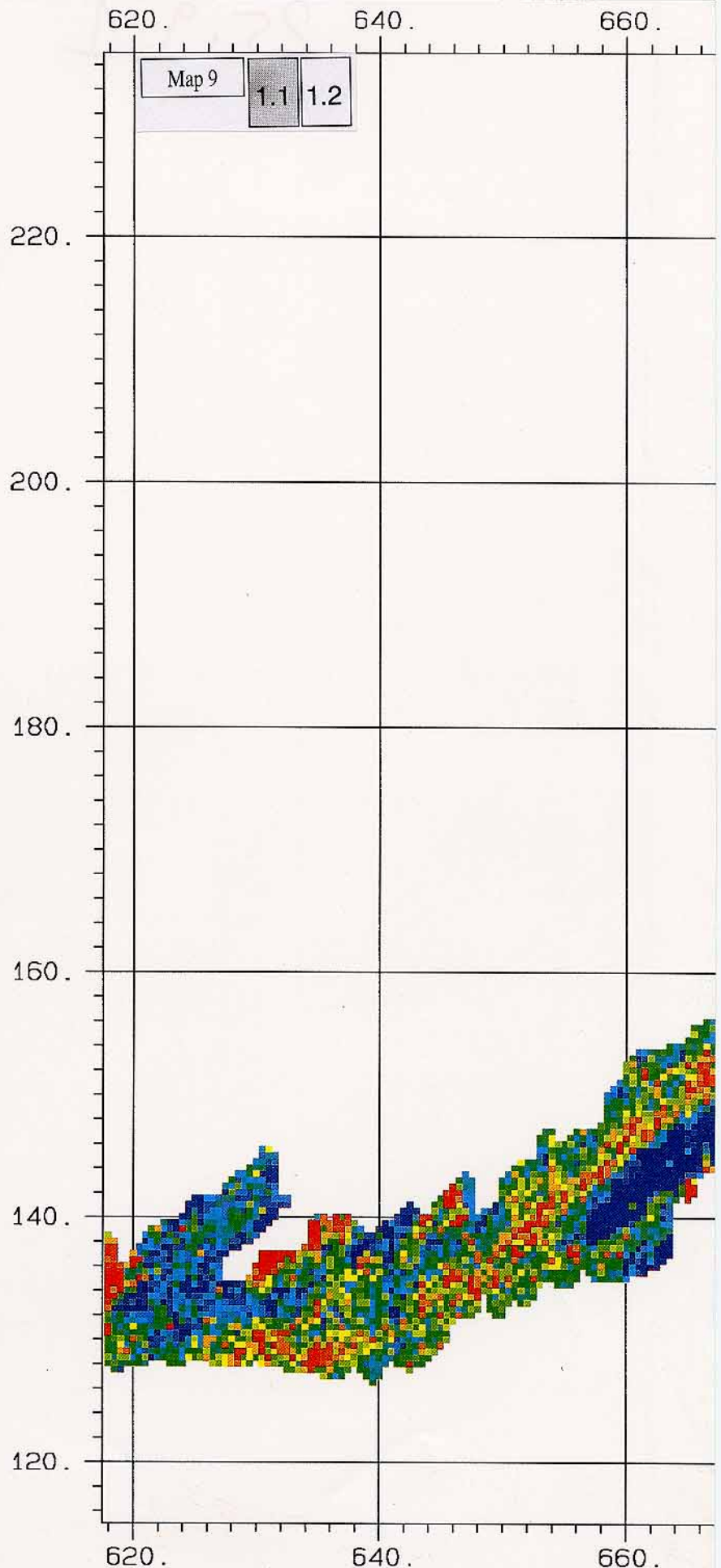
Survey	MAP92
Channel	T/K-ratio
Sam Int	500.
Area	2816.
Scale	500000.

Parameter

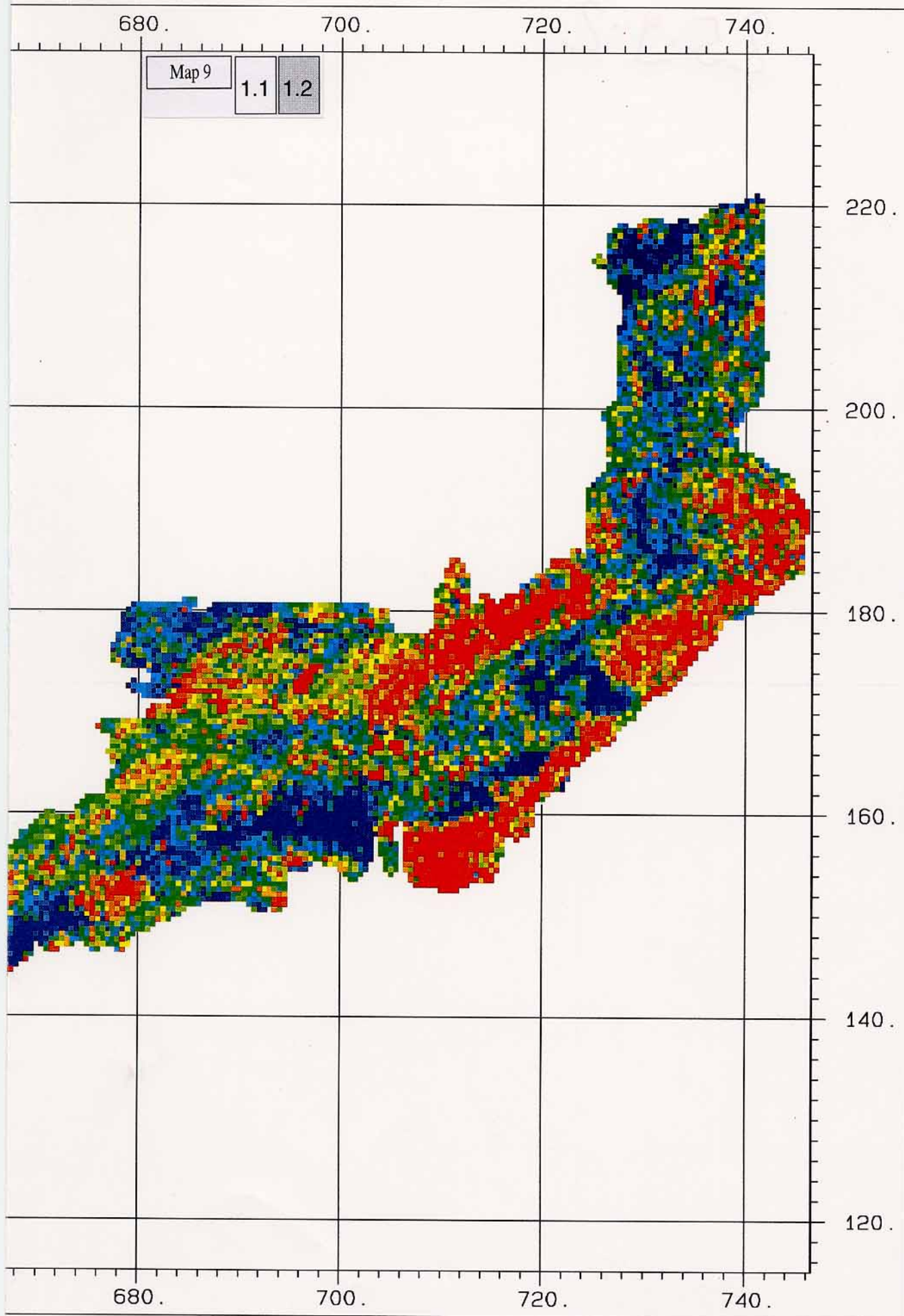
Average	8.6
Std Dev	2.4
Minimum	0.3
Maximum	37.9

Legend

	Minimum	Maximum
	0.3	6.7
	6.7	7.8
	7.8	8.7
	8.7	10.1
	10.1	37.9



Map 9: Tl^{208}/K^{40} -ratio map of the "Central Massifs" (%)


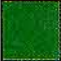



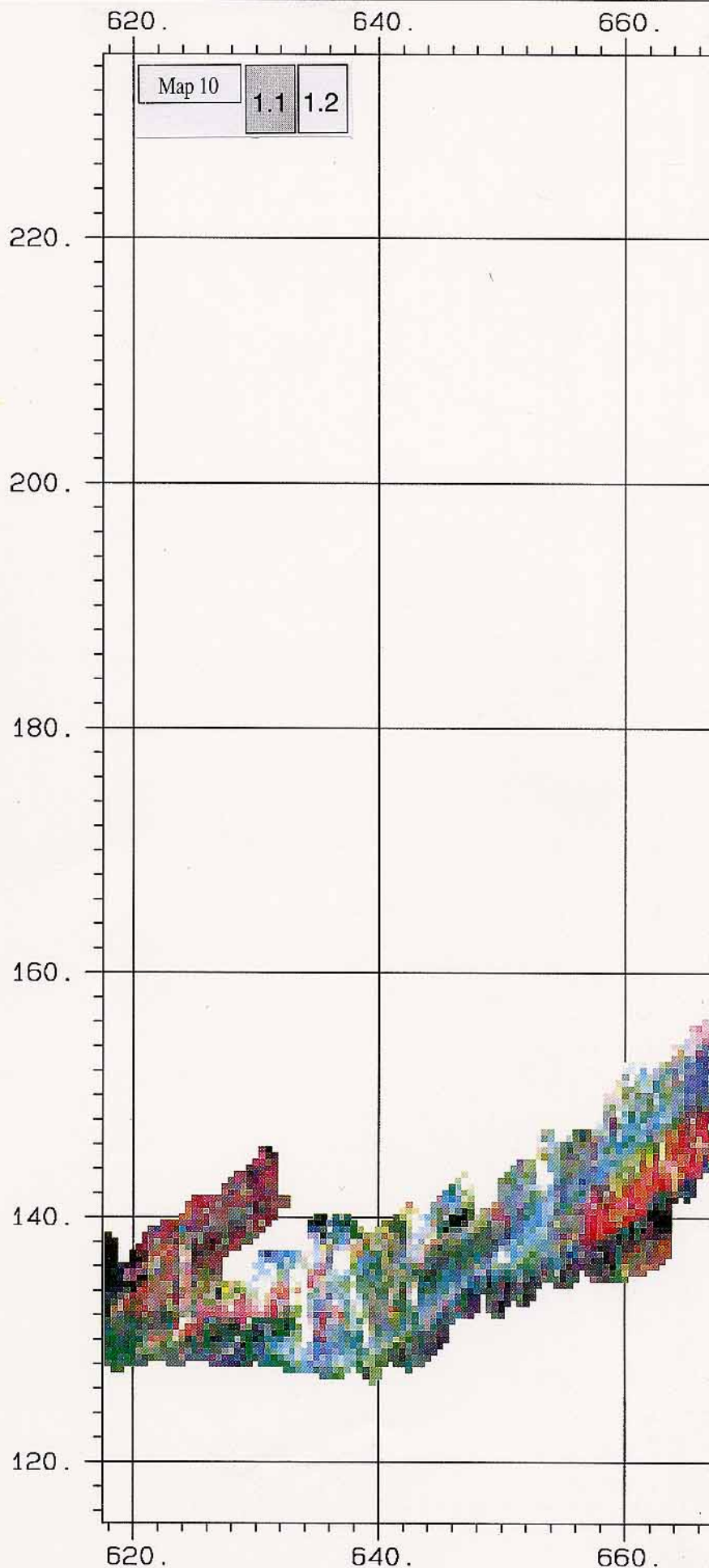
SG PK	I. Geophysik ETH-Zuerich Hoenggerberg 8093-Zuerich
----------	---

Central Massifs

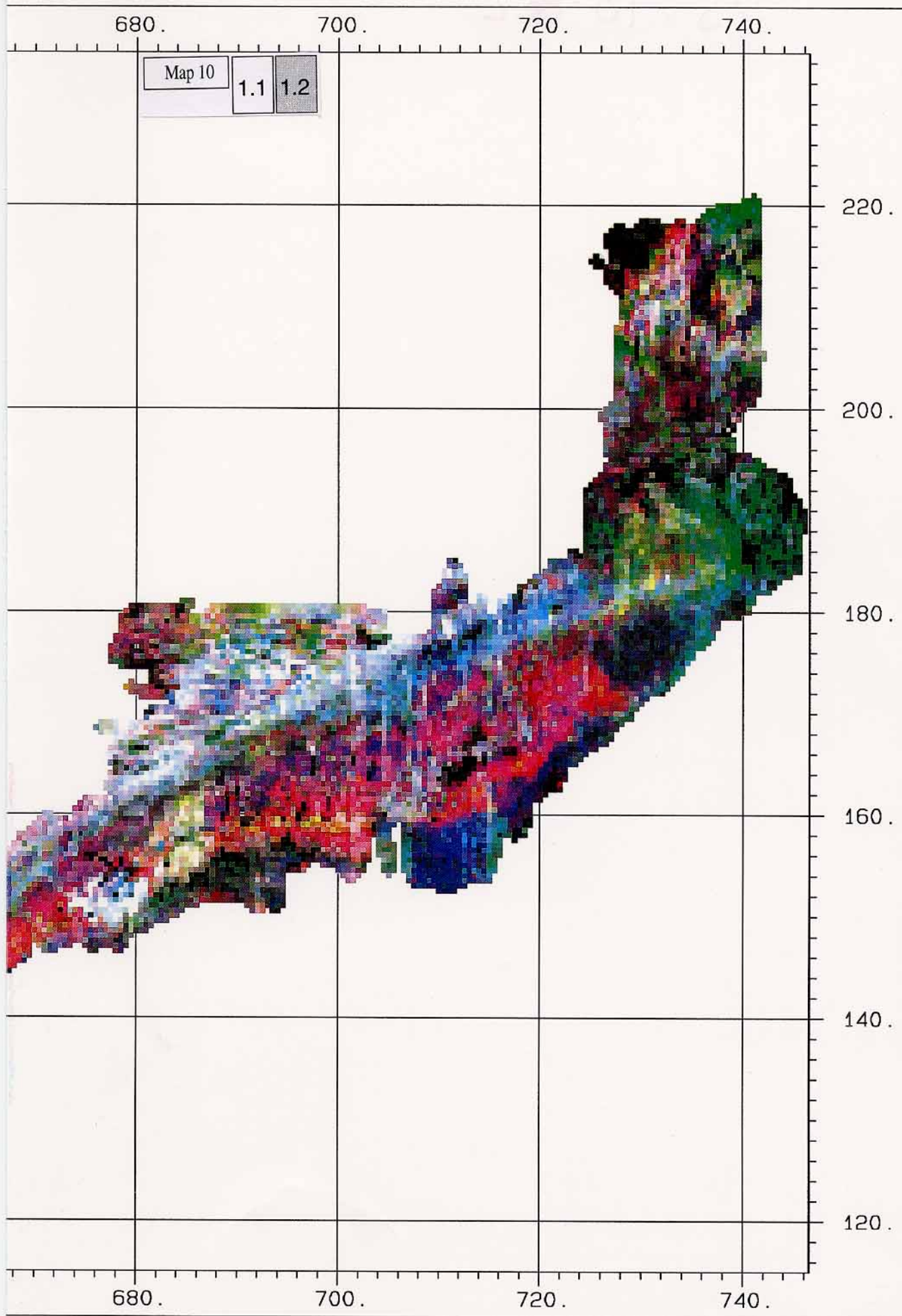
Survey	MAP92
Channels	Ternary
Sam Int	500.
Area	2816.
Scale	500000.

Legend

	Win	Min	Max
	K	19.0	2444.5
	Bi	4.8	344.1
	T1	0.3	328.6



Map 10: Ternary map of the "Central Massifs" (1:500'000)


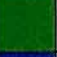



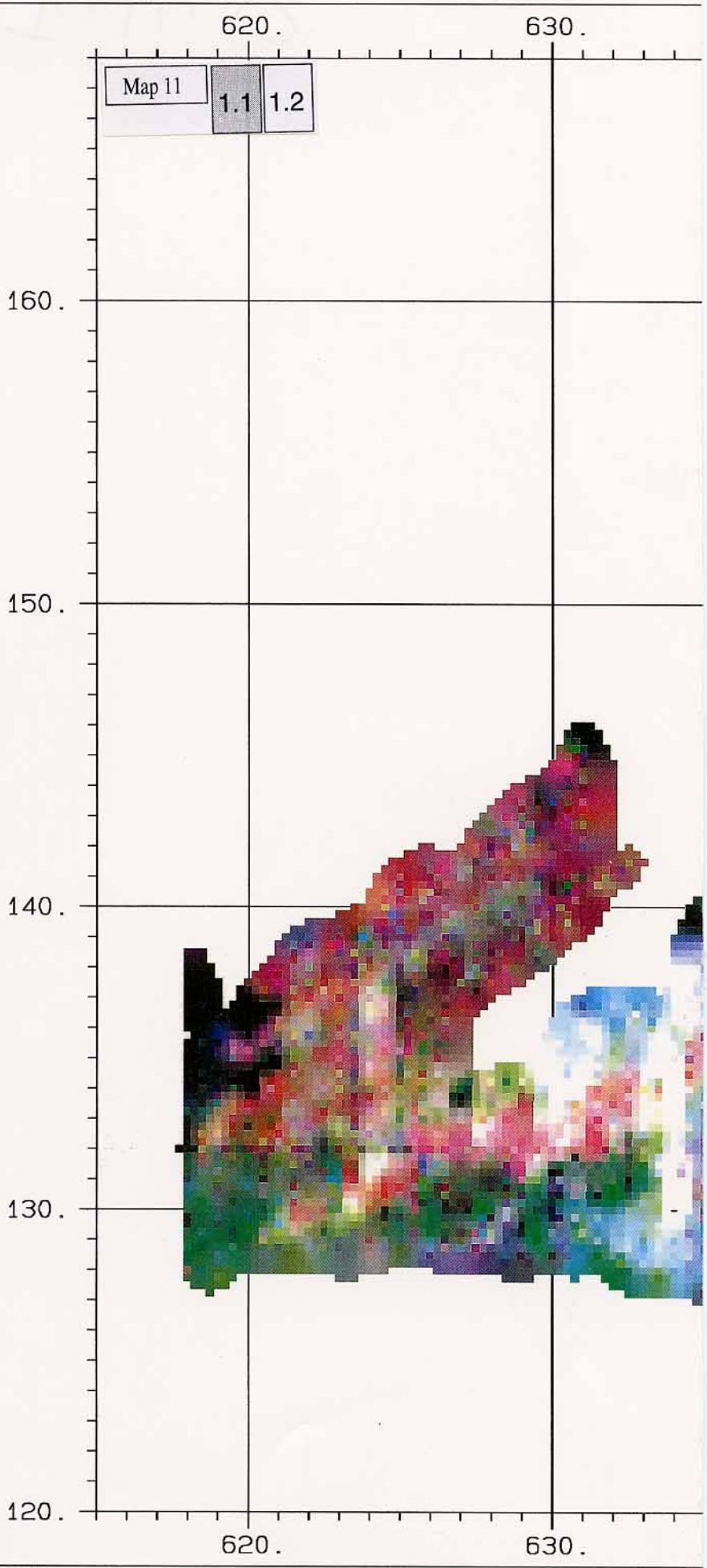
SG PK	I. Geophysik ETH-Zuerich Hoenggerberg 8093-Zuerich
----------	---

Central Massifs

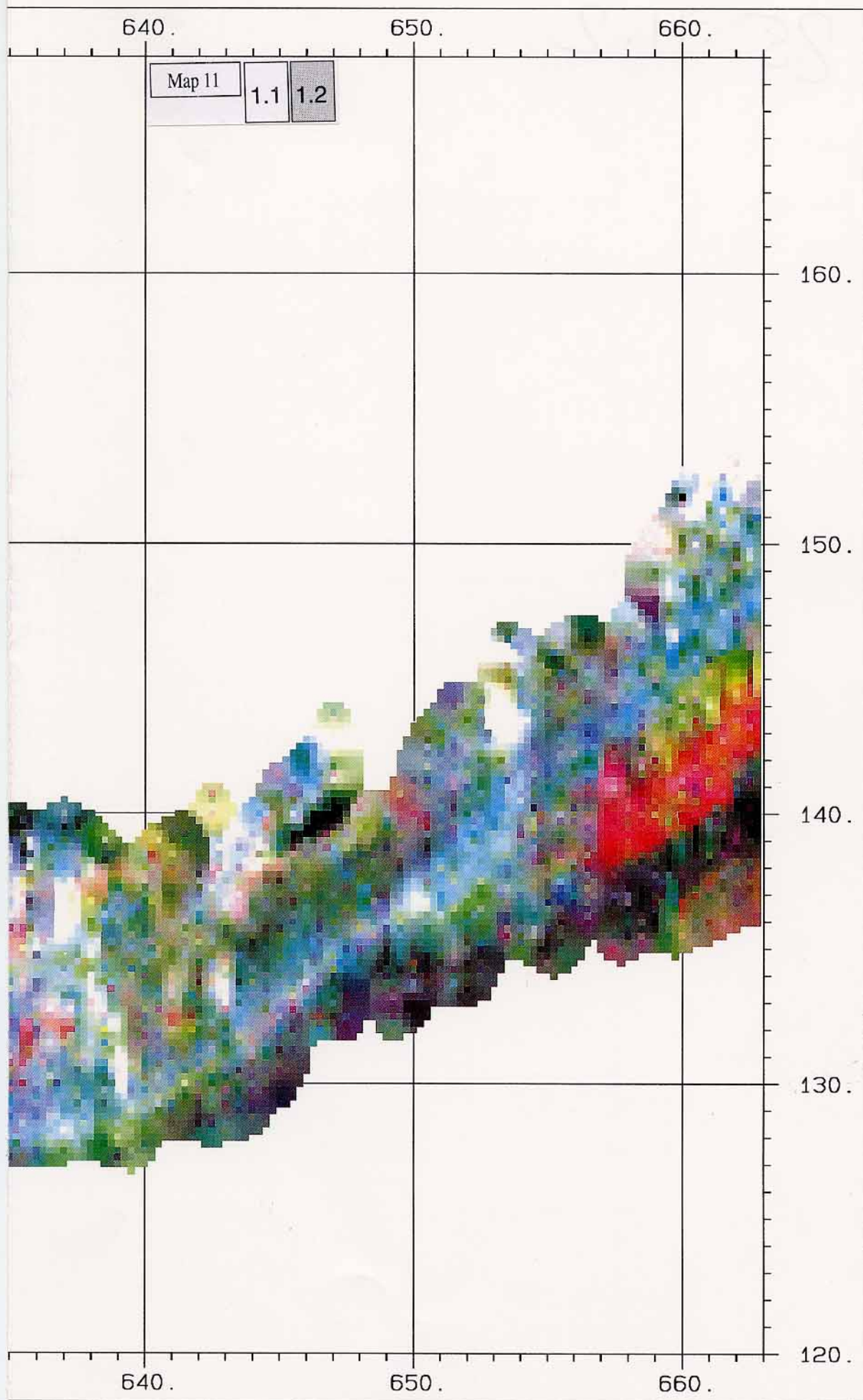
Survey	MAP01
Channels	Ternary
Sam Int	250.
Area	2902.
Scale	200000.

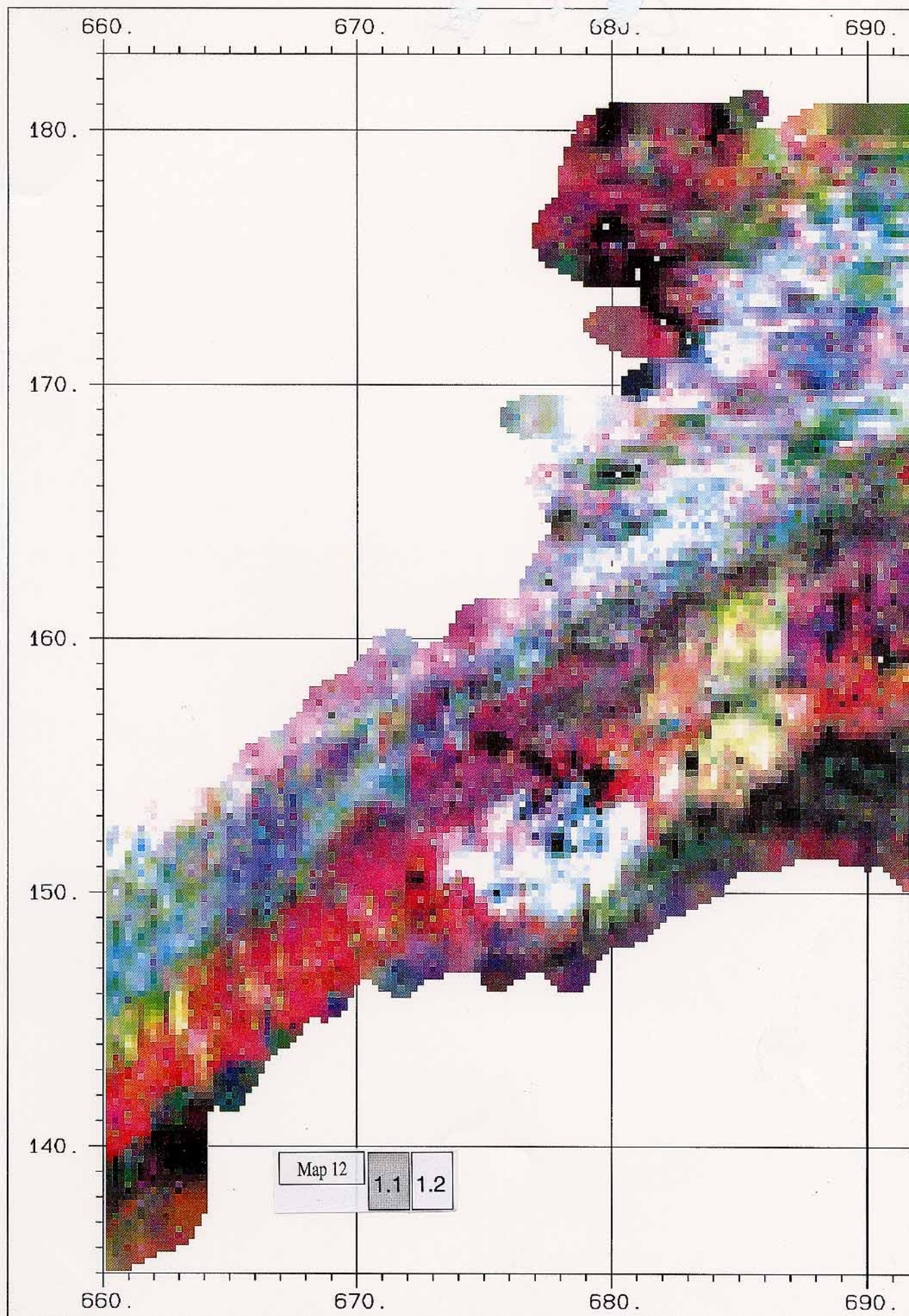
Legend

	Win	Min	Max
	K	11.5	2759.2
	Bi	1.9	379.6
	Tl	0.1	318.9

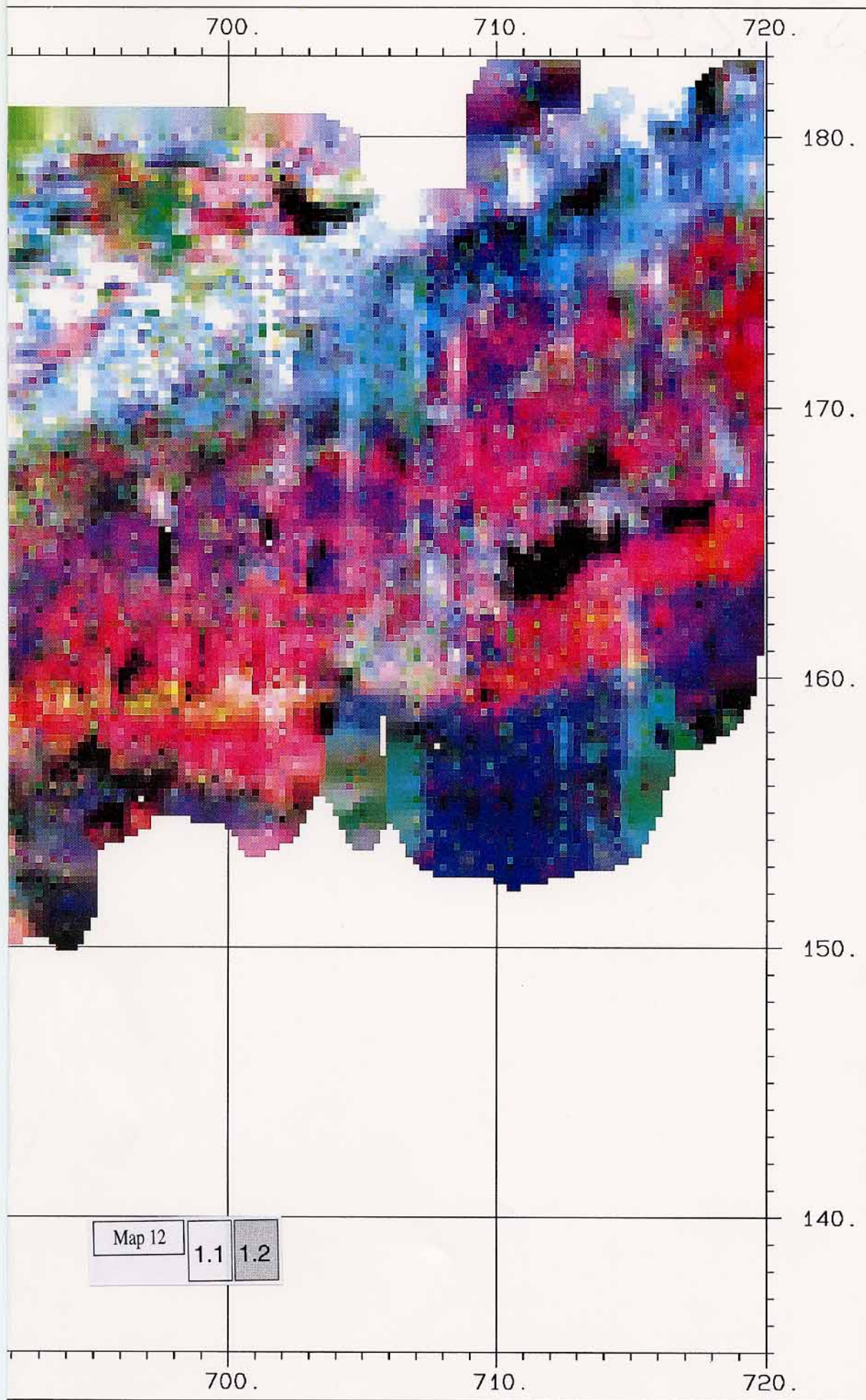


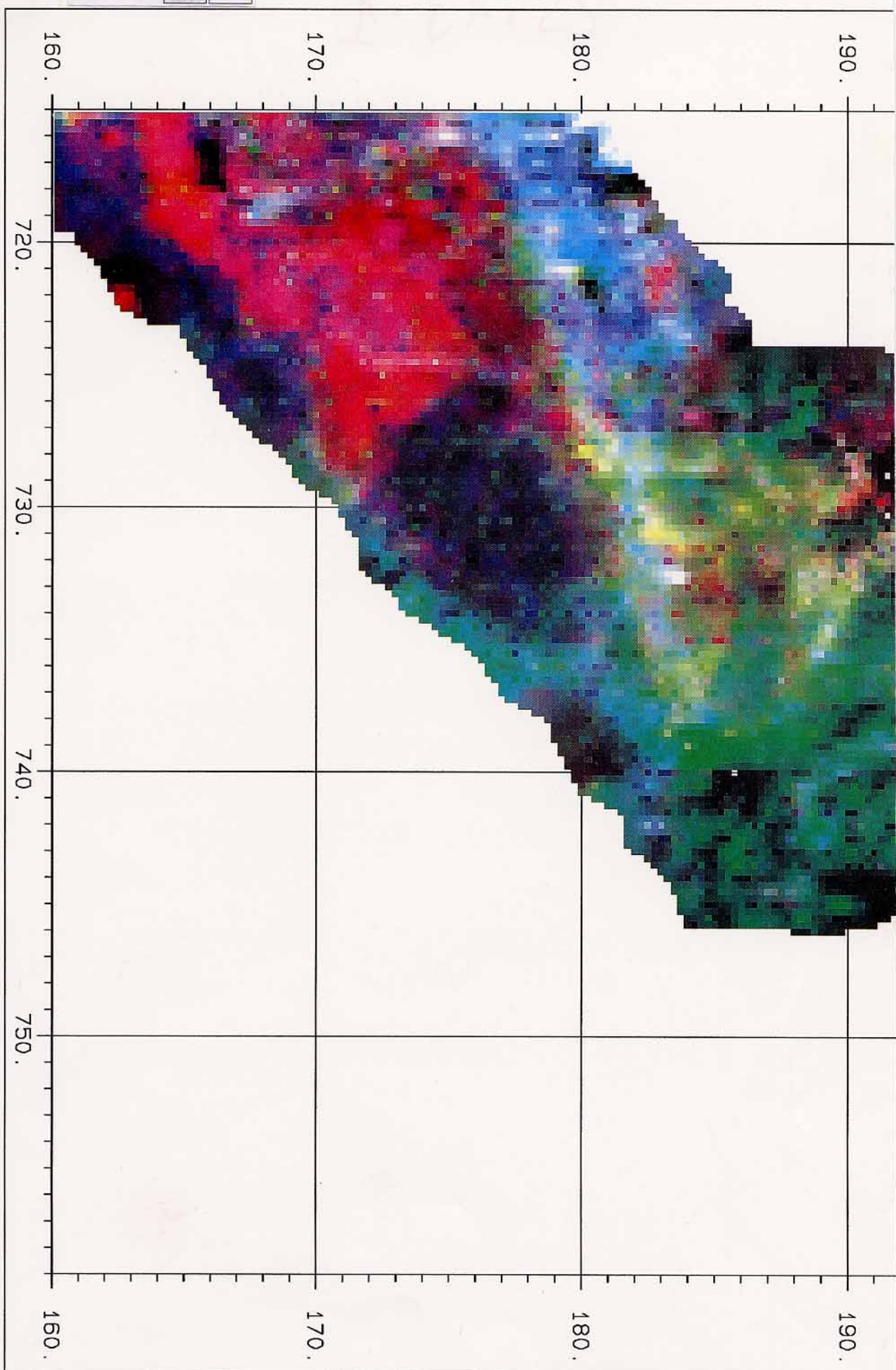
Map 11: Ternary map of the "Central Massifs" (west, 1:200'000)





Map 12: Ternary map of the "Central Massifs" (center, 1:200'000)



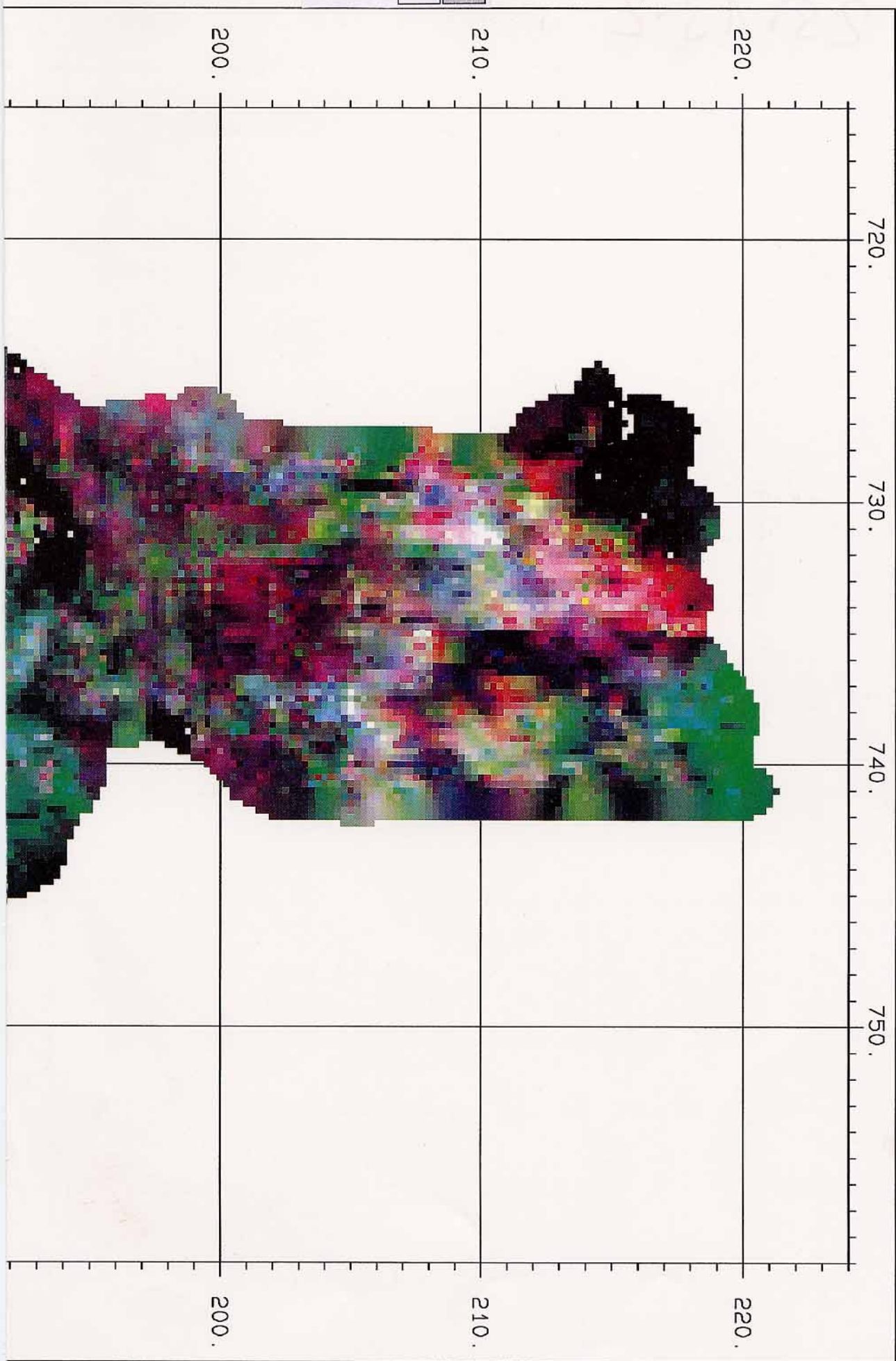


Map 13: Ternary map of the "Central Massifs" (east, 1:200'000)

Map 13

1.1

1.2



Map 14

1.1

Map 14: Boundaries of the geologic units of the "Central Massifs"

